EXPERIMENTAL AND ARTIFICIAL NEURAL NETWORK BASED MODELLING APPROACHES FOR STRENGTH PREDICTION OF CONCRETE INCORPORATING RECLAIMED ASPHALT PAVEMENT AND RICE HUSK ASH

MASTER OF SCIENCE DEGREE

MULUSEW ADERAW GETAHUN

MASTER OF SCIENCE IN CIVIL ENGINEERING

(STRUCTURAL ENGINEERING OPTION)

PAN AFRICAN UNIVERSITY INSTITUTE OF BASIC SCIENCES, TECHNOLOGY AND INNOVATION

2018

EXPERIMENTAL AND ARTIFICIAL NEURAL NETWORK BASED MODELLING APPROACHES FOR STRENGTH PREDICTION OF CONCRETE INCORPORATING RECLAIMED ASPHALT PAVEMENT AND RICE HUSK ASH

MULUSEW ADERAW GETAHUN

CE300-0004/17

A Thesis submitted to Pan African University Institute of Basic Sciences, Technology and Innovation in partial fulfilment of the requirement for the award of the degree of Master of Science in Civil Engineering (Structural Engineering Option)

2018

DECLARATION AND RECOMMENDATION

I, Mulusew Aderaw hereby declare that this Thesis is my original work and it has not been presented for the award of a degree in any other University.

Signature: ………………..   **Date**: ………………..

Mulusew Aderaw Getahun

CE300-0004/17

This Thesis has been submitted with our approval as University supervisors.

Signature: ………………..   **Date**: ………………..

Prof. (Eng.) Stanley Muse Shitote

Deputy Vice-Chancellor

Rongo University, Kenya

Signature: ………………..   **Date**: ………………..

Prof. (Eng.) Z. Abiero Gariy

Dean School of Civil, Environmental and Geospatial Engineering

JKUAT, Kenya

DEDICATION

Dedicated to my family for their love, prayers, support, and sacrifice along the path of my academic pursuits.

ACKNOWLEDGEMENT

ABSTRACT

Construction industry is exhausting natural resources thereby posing environmental problems. On the other hand, solid waste generation from agricultural and construction industries is growing at an upsetting rate that causes a heavy burden on landfill facilities. For these reasons, there is a pressing need for reusing and recycling waste materials for use in concrete production. This study assesses the potential use of rice husk ash (RHA) and reclaimed asphalt pavement (RAP) which are originating from agro-industry and road sector respectively as promising construction materials. To this end, the study characterizes these materials and investigates their effects on the fresh and hardened properties of concrete. An effort has been also made to develop an artificial neural network (ANN) model for predicting the 28th-day compressive and tensile splitting strengths of concrete containing RHA and RAP. The materials were characterized in terms of gradation, fineness modulus, water absorption, specific gravity, bulk density, void space between aggregate particles, chemical analysis, aggregate crushing and impact values. The wet and hardened concrete properties were assessed by partially replacing cement and virgin aggregates with RHA and RAP, up to 20% (by mass of cement) and 50% (by mass of aggregates), respectively. A total of 22 mixes were prepared and studied, twelve of which were devoted to studying the collective effects of RHA and RAP on the properties of concrete. ANN model was then developed in MATLAB version R2017a using the predetermined attributes of concrete constituent materials. The study results show that RHA and RAP decrease slump, compacting factor, density, absorption and sorptivity. RHA increases compressive and tensile splitting strength, whereas RAP decreases compressive and tensile splitting strength. Comparable strength, favourable absorption and sorptivity

values were obtained when 15% RHA was combined with up to 20% RAP in the concrete mixes. The developed ANN model predicted the compressive and tensile splitting strength with prediction error values of 0.648 and 0.072 MPa respectively. The compressive strength (f_c) was overpredicted on average by 0.123 MPa, whereas the model underpredicted the tensile splitting strength (f_{ts}) by 0.019 MPa. The predicted compressive and tensile splitting strength deviated on average by 2.088 and 2.905 % respectively from experimental results. The ANN model was successful in predicting the compressive and tensile splitting strength results accurately. On this basis, it is recommended to use RHA and RAP inclusive concrete for general concreting works. Further research could be undertaken to evaluate economic, social and environmental benefits of using RHA and RAP as concrete ingredients.

TABLE OF CONTENTS

LIST OF TABLES

LIST OF FIGURES

LIST OF ABBREVIATIONS AND ACRONYMS

ACV	Aggregate Crushing Value
AD	Apparent Density
AE	Average Error
AIV	Aggregate Impact Value
ANN	Artificial Neural Network
ASTM	American Society for Testing Materials
BDI	Bulk Density After Immersion
BDIB	Bulk Density After Immersion and Boiling
BS	British Standard
BS EN	British Standard European Norm
CFM	Composite Fineness Modulus
CRAP	Coarse Reclaimed Asphalt Pavement
CS	Compressive Strength
CSG	Composite Specific Gravity
CT	Curing Temperature
CVA	Coarse Virgin Aggregate
CWA	Composite Water Absorption
DBD	Dry Bulk Density
FAO	Food and Agriculture Organization
FM	Fineness Modulus
FRAP	Fine Reclaimed Asphalt Pavement
FVA	Fine Virgin Aggregate

GAs	Genetic Algorithms
GDP	Growth Domestic Product
HMA	Hot Mix Asphalt
HPC	High-Performance Concrete
IF	Influence Factor
IS	Indian Standard
LOI	Loss on Ignition
MAPE	Mean Absolute Percentage Error
MLP	Multi-Layer Perceptron
MPa	Mega Pascal
MSE	Mean of Squared Errors
NAS	Nominal Aggregate Size
OPC	Ordinary Portland Cement
PCC	Portland Cement Concrete
RAP	Reclaimed Asphalt Pavement
RHA	Rice Husk Ash
RMSE	Root Mean Square Error
TSS	Tensile Splitting Strength

LIST OF SYMBOLS

a	Actual value
f_c	Compressive strength
f_{cf}	Flexural strength
f_{ts}	Tensile splitting strength
F	Maximum load at failure
l	Span length
I	Commutative water absorption
δ	Error gradient
d	Desired response
g	Activation function
K	Sorptivity
p	Predicted value
v	Permeable void spaces
o	Output unit
η	Learning rate
w	Connection weight
i	Input unit
C_3S	Tricalcium silicate
C_2S	Dicalcium silicate
C_3A	Tricalcium aluminate
C_4AF	Tetracalcium aluminoferrite
C-S-H	Calcium-silicate-hydrate

DEFINITION OF TERMS

Concrete is a mixture of aggregates either gravel or crushed stone, held together by a binder of cementitious paste.

Conventional Concrete is a concrete produced by mixing virgin fine and coarse aggregates, cement, water and with/without additives in a certain prescribed proportion.

Multilayer Perceptron is a feedforward neural network with one or more hidden layers.

Reclaimed Asphalt Pavement is the recycled pavement materials obtained during rehabilitation of old flexible pavement that contains both degraded bituminous material and aggregate particles.

Rice Husk Ash is an agricultural waste, which is produced in millions of tons by burning of the rice husk obtained from rice milling factories.

CHAPTER ONE

INTRODUCTION

1.1 Background

Portland cement concrete is the most widely consumed construction material in the world due to its versatility and durability (Meyer, 2009). Concrete finds applications in a variety of structures from massive dams to elegant reinforced bridges, buildings and pavements. It is the second most consumed material in the world next to water (Smith & Maillard, 2007). The strive for economic growth, urbanization and industrial development is significantly snowballing the demand for concrete. Consequently, the global annual production of Portland cement concrete is estimated to be more than 10 billion tons (Kosmatka, 2011).

Concrete is a mixture of cement paste and aggregates, which can be cast into any practical shape and dimension of the desired structures (Dolan, 2010). Cement is the most expensive and active ingredients of concrete used as a binding agent. The high demand for concrete has increased both cement production and aggregate extractions. As a result, about 1.89 billion tons of cement is produced every year worldwide (Suhendro, 2014). The cement production is both resource and energy intensive. Every ton of cement production consumes about 4 GJ of energy and 1.7 tons of raw materials and is responsible for the release of about 0.73 - 0.99 ton of CO_2 (Benhelal, Zahedi, Shamsaei, & Bahadori, 2013; Khan et al., 2012).

In addition, Portland cement concrete production consumes about 8-12 billion tons of aggregate every year (Naderpour, Hossein, & Fakharian, 2018). In Portland cement concrete, 60% to 75% of the volume and 79% to 85% of the weight are made

1

up of aggregates (Michael & John, 2011). The demand for aggregates in concrete production continues reducing natural stone deposits drastically (Ismail, Wai, & Ramli, 2013) thereby posing a huge impact to the environment (Adom, 2013; Lun, 2015).

On the other hand, solid waste generation from agricultural and construction industries is growing at an alarming rate that causes a heavy burden on landfill facilities (Aprianti, Shafigh, Bahri, & Nodeh, 2015; Ismail et al., 2013). One of those construction areas is the road sector. According to the African Union forecast (African Union, 2012), by the year 2040, the transport volume alone has to be increased up to 14 folds for some landlocked countries. Consequently, the road sector is expected to implement massive highway investments and maintain existing road networks in years to come. Road maintenance and rehabilitation activities have been generating a substantial amount of valuable asphalt pavement waste materials that are either discarded along the generation point or hauled off to the disposal site therein consuming landfill facilities and posing threats to the surrounding fertile land (Bida, Danraka, & Ma'ali, 2016).

Moreover, the food insecurity problem has led to an increase in agricultural activities across the world due to the strategic planning policies for food security. According to the Food and Agriculture Organization 2017 report, the global paddy production in the year 2017 was forecasted to amount to 756.7 million tons (FAO, 2017). Assuming annual rice production remains the same, 254.5 million tons of rice husk is available for disposal every year worldwide. Thus, agro-industrial solid waste disposal is another serious concern (Alex, Dhanalakshmi, & Ambedkar, 2016) unless

we find a preferred alternative use. Therefore, the cement and concrete industry can be an ideal home for the construction and agro-industrial solid wastes.

The concrete industry is exploring ways to utilize alternative materials for concrete production that minimize environmental impact and achieve sustainable development (Abraham, & Ransinchung, 2018; Bida et al., 2016; Jain, Garg, & Minocha, 2015;Modarres & Hosseini, 2014; Singh, Ransinchung, & Kumar, 2017). Agro-industry and construction wastes are among the potential alternatives which have been utilized to supplement cement and aggregate aiming to produce cheaper concrete. This approach can contribute to natural resources preservation and solid waste management (Juenger & Siddique, 2015; Madurwar, Ralegaonkar, & Mandavgane, 2013).

Recycled asphalt pavement (RAP) and rice husk ash (RHA) are among the construction and agro-industrial wastes which can be used as potential aggregate and cement supplements respectively. Thus, utilizing RAP in combination with RHA for concrete production may contribute to engineering benefits, economic savings, solid waste management and environmental protection.

Conventional concrete is an assortment of cement, water and aggregates (coarse and/or fine) (Duan, Kou, & Poon, 2013). The properties of concrete are influenced by lots of parameters such as quality and quantity of aggregates, cement type, water content, water to cement ratio (Chopra, Sharma, & Kumar, 2016). The traditional approach used in modelling the effects of these parameters on mechanical properties of concrete starts with an assumed form of analytical equation (Chopra, 2014). This

3

approach fails to grasp the actual scenario when some of the concrete constituents are not the conventional materials and when the assumption is wrong. The concrete incorporating RHA and RAP is noticeably different in composition and properties compared with conventional concrete, making it hard to predict its performance using the traditional approach. This is likely to hinder attempts to use such kinds of materials as alternatives for concrete production.

Recently, many studies have been using various methods such as analytical modelling, mechanical modelling, statistical methods and artificial intelligence (Siraj, 2015; Zhen, 2013) for predicting the strength of concrete incorporating various constituents. One of the areas in artificial intelligence that has grown fast and gained popular engineering applications is an artificial neural network (ANN) (Ming, 2003; Silva, 2004). ANN has been employed in many civil engineering applications like detection of structural damage, structural system identification, material behaviour modelling, groundwater monitoring, foundation settlement prediction, concrete mix proportioning and concrete strength prediction (Ling, 2011; Naderpour, Kheyroddin, & Amiri, 2010; Zhen & Shi, 2013).

In reference to the growing demand for construction materials and a substantial amount of solid waste generated from construction and agro-industries, there is a concerning need for recycling and reusing solid waste materials for use as aggregate and cement substitutes in general construction and pavements among other works. This study investigates the potential use of agro-industrial waste (RHA) and construction waste (RAP) as promising construction materials aimed at reducing environmental impact and cost of concrete production. An effort has been also made

to develop the ANN model for predicting the 28th-day strength of concrete containing RHA and RAP.

The results of this study provide evidence on the viability of utilizing RHA and RAP as partial cement and aggregate replacements respectively in concrete production. The study results further indicate that the ANN is an efficient model to be used as a tool for predicting the compressive and tensile strengths of concrete incorporating RHA and RAP.

1.2   Problem Statement

The construction industry touches the daily lives of everyone, as the quality of life is heavily influenced by the built milieu surrounding people. Every economic value creation occurs within or by means constructed assets. However, the construction industry consumes about 40% of the global energy; is the largest global consumer of raw materials; and is also responsible for 25–40% of the world's total CO_2 emissions and 28% of solid waste in the form of construction debris (World Economic Forum, 2016). A study by Pacheco and Labrincha (2013) shows that during the last century, materials consumption increased eight-fold thereby humanity currently consumes almost 60 billion tons of materials every year. The construction industry alone consumes almost 50% by weight compared to any other economic activity that makes it unsustainable.

The growing demand for infrastructure has led to a radical increase in the cost of concrete production over the past two decades. In excess of 10 billion tons of Portland cement concrete is produced each year around the world. Such volumes involve

5

consumption of large amounts of natural resources and a substantial amount of energy. Consequently, more than 8 billion tons of aggregates have been exploited each year for concrete production (Khan et al., 2012). In addition, every ton of cement production consumes about 4 GJ of energy and 1.7 tons of raw materials and releases approximately 0.73–0.99 ton of CO_2 (Benhelal et al., 2013; Suhendro, 2014).

The aggregate extraction for use in concrete production continues reducing natural stone deposits drastically (Ismail et al, 2013) thereby posing a huge impact on the environment (Adom, 2013; Lun, 2015). As such, natural resource utilization is not sustainable thereby compromising the environment. Climate change and depletion of natural resources are the two environmental issues that pose a challenge on the construction industry. Environmentally speaking, the virgin aggregate is mined from the earth either dug out of pits or blasted out of quarries. The process of virgin aggregate extraction creates pits or quarries that involves the removal of virtually all natural vegetation, topsoil and subsoil to reach the aggregate underneath lead to loss of biodiversity as plants and aquatic habitats are destroyed. In addition, adjacent eco-systems are influenced by noise, dust, pollution and contaminated water. The noise and dust created by several dump trucks hauling aggregates also have serious effects on the health of individuals living adjacent. Moreover, most old pits and quarries are not being properly rehabilitated thereby create ponds and eventually turn in to mosquito habitats leading to the loss of innocent lives.

On the other hand, solid waste generation from agricultural and construction industries is growing at an upsetting rate that causes a heavy burden on landfill facilities (Aprianti et al., 2015). The road sector is one of the construction areas that

generate vast amounts of waste materials during rehabilitation and maintenance activities (Bida, et al.; 2016). Similarly, the agricultural industry is responsible for more than 254.5 million tons of rice husk that is available for disposal every year worldwide, causing a heavy burden on landfill facilities (FAO, 2017). Subsequently, the discarded construction and agro-industrial wastes lead to air, land and water pollution thereby make the construction industry unfit in the contemporary picture of a sustainable industry.

Furthermore, the traditional approaches used for predicting the compressive strength of concrete have not considered supplementary cementitious materials and uncommon aggregates. Consequently, these current approaches fail to grasp the actual scenario when some of the concrete constituents are not conventional materials and when the assumptions are wrong. Concrete incorporating RAP and RHA is noticeably different from the conventional concrete both in composition and properties making it hard to predict its strength using the usual analytical and statistical modelling approaches. The analytical approaches are usually limited by problem complexity and are either too difficult to be constructed or useless due to unrealistic assumptions. Statistical models also use predetermined forms and parameterization.

1.3 Objective

1.3.1 General Objective

The general objective of this study is to assess experimental and artificial neural network based modeling approaches for strength prediction of concrete incorporating reclaimed asphalt pavement and rice husk ash.

1.3.2 Specific Objectives

The specific objectives of this study include:

i. to characterize the concrete ingredients;

ii. to determine the effect of rice husk ash and reclaimed asphalt pavement on the wet and dry concrete properties;

iii. to develop Artificial Neural Network model for predicting the concrete strength.

1.4 Justification

Road sectors have worked for years to meet Africa's urgent infrastructure needs for economic prosperity and sustainable development. This growing infrastructure demand involves not only consuming a substantial amount of natural resources but also generating vast amounts of asphalt pavement materials during road maintenance and rehabilitation activities.

Regional infrastructure development will not move forward without a sharper focus on resource preservation and environmental protection. The best way to address these challenges is recycling and reusing construction and agricultural solid wastes as building materials. This calls for a study to assessing reclaimed asphalt pavement

waste (RAP) and rice husk ash (RHA) for use as partial replacements of virgin aggregates and cement respectively.

The three primary factors of using RAP and RHA are economic savings, engineering benefits and environmental welfare. Incorporating RAP and RHA in the production of cheaper concrete may play an important role to reverse earth's capacity from the verge of exhaustion, minimise environmental pollution and ease solid waste management.

Besides, it is worthy to apply artificial neural network (ANN) for predicting the performance of concrete because ANN can generate results to problems even when input signals comprise errors and are incomplete due to its capability to learn and generalize from instances and experience.

1.5   Scope of the Study

Fine virgin aggregate (FVA) and coarse virgin aggregates (VCA) were purchased from Masinga and Molongo districts of Kenya respectively. Reclaimed asphalt pavement (RAP) was obtained from an old distressed flexible pavement, Ruaka-Banana-Limuru Road (D407), sampled at the section near Tigoni, Kiambu County of Kenya. The road was constructed about 21 years ago and has served without major rehabilitation. Rice husk ash (RHA) was collected from the dump site of Mwea Rice Milling Factory, Kenya

The study on concrete ingredient materials was limited to physical, mechanical and chemical properties determined using relevant standards and X-Ray Fluorescence

Spectrometer method. The engineering properties of concrete incorporating RAP and RHA as partial substitutes of virgin aggregates and cement respectively were evaluated in terms of fresh (workability and fresh density) and hardened (absorption, sorptivity, hardened density, compressive, flexural and tensile strengths) properties of concrete. The compressive strength of concrete was assessed at 7 and 28 days of curing, whereas flexural and tensile splitting strengths were monitored at 28 days of curing. Finally, the compressive and tensile splitting strengths of concrete were predicted by using multilayer perceptron. The 70, 15, 15% random dataset portioning was applied for training, validating and testing the ANN model.

1.6   Limitations

There were some practical difficulties that I encountered. One of the challenges was to place the sorptivity test specimens in an environmental chamber that allows for air circulation and enable to maintain a temperature of 50 °C and a relative humidity at 80 %. Alternatively, the test specimens were placed in a desiccator inside an oven at a temperature of 50°C for 3 days. The other challenge was to determine the total CaO content of RHA by XRF due to the exists of CaO in multiple bound and free states in the RHA. The X-ray diffraction on the RHA could be performed to determine CaO in crystalline phases. In addition, a complexometric titration with hot ethylene glycol extraction would allow quantifying the actual free lime content of the RHA.

The reclaimed asphalt pavement was collected from one source due to time and financial shortcomings. Likewise, rice husk ash was sampled from a single source.

Furthermore, the reclaimed asphalt pavement and rice husk ash generated in Africa have not been quantified due to luck of registered statistical datasets.

1.7 Note on Publications

Two journal papers have been produced from this research work and published in international, scientific, peer-reviewed, open access journals. The copies of these papers are attached in Appendix D.

(i) The first article entitled "Artificial neural network-based modelling approach for strength prediction of concrete incorporating agricultural and construction wastes" has been published in **Construction and Building Materials (ISSN: 0950-0618)-Elsevier**. This paper can be cited as shown below:

Getahun, M., Shitote, S., & Gariy, Z. (2018). Artificial neural network-based modelling approach for strength prediction of concrete incorporating agricultural and construction wastes. Construction and Building Materials, 190, 517–525. https://doi.org/10.1016/j.conbuildmat.2018.09.097

(ii) The second article entitled "Experimental investigation on engineering properties of concrete incorporating reclaimed asphalt and rice husk ash" has been published in **Buildings (ISSN: 2075-5309)-MDPI**. This paper can be cited as shown below:

Getahun, M., Shitote, S., & Gariy, Z. (2018). Experimental investigation on engineering properties of concrete incorporating reclaimed asphalt and rice husk ash. Buildings, 8(9), 24. https://doi.org/10.3390/buildings8090115

1.8   Organization of the Thesis

This thesis is divided into five chapters as follows: Chapter 1 introduces sufficient background information to conceptualize circumstances prevailing in the sphere of construction material consumption patterns and the challenges of construction and agro-industrial wastes that motivated this study. Chapter 2 is dedicated to reviewing theoretical and empirical literature related to the present study. It is organized starting with theoretical literature followed by empirical literature review. Chapter 3 is devoted to providing clear and detailed information about the materials and methodologies used to achieve the objectives of the study. Chapter 4 focuses on the discussion of results obtained from experimental investigation and ANN model simulations. Finally, the conclusion and recommendation for future work are highlighted in chapter 5.

CHAPTER TWO

LITERATURE REVIEW

2.1 Introduction

This chapter is dedicated to reviewing theoretical and empirical literature related to the present study. It is organised starting with theoretical literature followed by empirical literature review. From these concepts and theories, the theoretical basis for the current study was formulated. Finally, it also tries to summarize the gaps that were addressed by this study.

2.2 Theoretical Review

2.2.1 Concrete

The word "concrete" is originated from the Latin word *concretus*, meaning "to grow together" (Li, 2011). Concrete is composed of aggregates and cement paste. Cement and water form a paste or matrix that fills the voids of aggregates, coats the surface of aggregates and binds them together. The matrix is usually 25-35% of the total volume of concrete and aggregates generally occupy 65% to 75% of the concrete mix (Duggal, 2008).

On the basis of the type of cement used, different concrete types are produced. However, Portland cement concrete is so predominant that the term concrete is always presumed to mean Portland cement concrete unless otherwise stated. Portland cement concrete is widely used building material in the world. The significance of concrete in our everyday lives cannot be overstated. It is used in structures such as buildings, bridges, tunnels, dams, factories, pavements, playgrounds and so on (John, 2011).

13

The performance of concrete is related to workmanship, mix proportions, material characteristics and adequacy of curing (Mamlouk, 2011). Good quality concrete has well-defined and accepted requirements. Requirements for freshly mixed concrete are consistency, workability, finishability, uniformity and stability. Concrete should be workable but segregation or excessive bleeding should be avoided.

Satisfactory strength (compressive, flexural, tensile, torsion and shear), durability, appearance and economy are the primary requirements of hardened concrete. The strength of concrete is often considered the most important property and is used as a basis to determine the quality of concrete. This is vital since it is the element ultimately considered in structural design (Wilson, 2011).

The progress made in the concrete technology brought about the advancement of other options to ordinary concrete such as self-consolidating concrete, lightweight concrete, high-strength concrete, polymer concrete, fibre-reinforced concrete, roller compacted concrete and among others (John, 2011).

Self-consolidated concrete is profoundly flowable, non-segregating concrete that can spread into place, fill the form and encapsulate the reinforcement with no mechanical exertion. Stability and flowability are the two important properties specific to self-compacting concrete in its plastic state (Li, 2011).

Roller-compacted concrete is a non-slump concrete that is placed and compacted with the help of equipment. It was developed based on the unique requirements for mass concrete to be used for dam construction. This material uses a relatively low cement

factor, relaxed graduation requirements and water content selected for construction considerations rather than strength (John, 2011).

A concrete with an airdried unit weight less than 2000 kg/m^3 is referred to as lightweight concrete. It offers design flexibility and substantial cost savings. Lightweight concrete offers less dead load, improves seismic structural response, longer spans, better fire ratings, thinner sections, decreases story height, smaller size structural members, less reinforcing steel and lower foundation costs (Li, 2011).

Heavy-weight concrete is a brilliant shielding material used to construct some special structures such as hospital examination rooms, laboratories and nuclear plant where the radioactive shield is needed to minimalize its effect on people's wellbeing (Li, 2011). Biological shielding used for nuclear power plants, medical units and atomic research and test facilities requires massive walls to contain radiation (John, 2011).

A concrete having compressive strength value above 40 MPa is considered to be high-strength concrete. Producing a concrete with more than 40 MPa compressive strength requires care in the proportioning of the components and in quality control during mixing (Duggal, 2008).

A concrete incorporating fibres that improve its structural integrity is said to be fibre-reinforced concrete. The brittle nature of concrete is due to the rapid propagation of microcracking under applied stress. Fibre-reinforced concrete can sustain load after initial cracking. This effectively improves the toughness of the material. Additionally, the flexural strength of the concrete is enhanced by up to 30% (John, 2011).

2.2.2 Constituents of Concrete

As a composite material, concrete is composed of different graded aggregates or fillers embedded in a hardened matrix of cementitious material. Aggregates, cementitious materials, water and admixtures are the main ingredients of concrete. Understanding the properties of concrete constituents is vital to better learn the properties and performance of concrete.

a) Cementitious material

Cementitious materials comprise traditional Portland cement and others such as blast furnace slag, fly ash, ground granulated, silica fume, limestone fines and natural pozzolans. These materials are either combined at the cement works or at the concrete mixer when the concrete is being produced (John, 2011).

Cement is an adhesive building material which is capable of binding together particles of aggregates into a solid compacted durable mass. It is classified as hydraulic and non-hydraulic cement. The hydraulic cement set and harden in water and gives stable product under water. Portland cement is one such. Non-hydraulic cement does not set and harden in water that is not stable underwater (Duggal, 2008).

Joseph Aspdin discovered Portland cement in 1824 and got a patent for his invention that he named Portland cement as in its final state, it resembles the colour of the normal limestone quarried on the Isle of Portland (Kosmatka, 2011). The basic raw materials that are used for producing Portland cement are alumina, silica, iron oxide and lime. These materials interact in the kiln to produce complex chemical compounds, as shown

in Table 2.1. The roles of these principal compounds in Portland cement are presented in Table 2.2.

Table 2.1 Major components of Portland cement

Compound	Formula		Percentage (%) by Weight
	Chemical	Common	
Tricalcium Silicate	$3\,CaO\,SiO_2$	C_3S	45-60
Dicalcium Silicate	$2\,CaO\,SiO_2$	C_2S	15-30
Tricalcium Aluminate	$3\,CaO\,Al_2O_3$	C_3A	6-12
Tetracalcium Aluminoferrite	$4\,CaO.Al_2O_3\,Fe_2O_3$	C_4AF	6-8

Source: Mamlouk (2011)

Table 2.2 Roles of principal mineral compounds in Portland cement

Compound	Role
C_3S	Increase resistance to freezing and thawing, early hardness and strength and high heat due to rapid hydration.
C_2S	Slow hydration, add long-term strength and resistance to chemical attack.
C_3A	Cause flash set of the finely grounded clicker.
C_4AF	Early setting, high heat of hydration and volume changes causing cracking.

Source (Duggal, 2008)

Hydration is the chemical reaction between cement particles and water. It starts at the surface of cement particles. The finer the cement particles, the larger the surface area and the quicker the hydration process. Thus, finer material leads to quicker strength development and a higher initial heat of hydration. The properties of fresh concrete such as setting and hardening are the direct results of hydration. The hydration of tricalcium silicate (C_3S) gives 61% calcium-silicate-hydrate (C-S-H) and 39% calcium hydroxide. The hydration of dicalcium silicate (C_2S) results in 82% C-S-H and 18%

calcium hydroxide. In fact, up to 15% of the weight of Portland cement is hydrated lime (John, 2011).

The maximum size of the cement particle is 0.09 mm. Most of the cement particles (85% to 95%) are smaller than 0.045 mm and the average diameter is 0.01 mm (Mamlouk, 2011). The particle density of Portland cement is about 3.15. The density of bulk cement differs substantially depending on how it is handled and kept. Thus, cement quantities are specified and measured by weight rather than volume.

Rice husk ash (RHA) is one of the natural pozzolans. Through the rice milling process, about 22% of the weight of paddy is obtained as rice husk (Rao, Kumar, & Singh, 2014). The burning of the rice husk found from rice mills yields the largest amount of ash with about 93% silica that gives it pozzolanic properties. RHA has a very high specific surface area (5×10^5 - 10×10^5 cm^2/g) (Duggal, 2008).

RHA reacts with the calcium hydroxide (by-product formed during cement hydration) to produce extra cementing complex that holds the concrete together (ASTM C595, 2003; Saravanan & Sivaraja, 2016) thereby offers an opportunity to alter the free lime (Calcium hydroxide) to a C-S-H gel which makes the concrete strong (Jamil, Kaish, Raman, & Zain, 2013). This chemical reaction between RHA's siliceous material and calcium hydroxide ($Ca(OH)_2$) results in a reduction of $Ca(OH)_2$ content. The reduction of $Ca(OH)_2$ improves the durability of cement paste by making the paste dense and impervious (Ephraim, Akeke, & Ukpata, 2012).

b) Aggregate

About three-quarters of the volume of conventional concrete is occupied by aggregate. Aggregates are usually regarded as inert materials in the cement paste. Aggregates influence significantly the wet and dry concrete properties, mixture proportions and economy. The properties of concrete such as fluidity, cohesiveness and rheological behaviours are largely influenced by the amount, type, surface texture, size and gradation of the aggregate. Hardened density, strength, thermal properties, bond and wear resistance are some of the hardened concrete properties largely influenced by aggregate qualities (Li, 2011).

Fine aggregate usually comprises of normal sand or crushed stone with particle sizes smaller than 5 mm. Coarse aggregate particles are bigger than 5 mm and usually between 9.5 and 37.5 mm (Kosmatka, 2011).

Reclaimed Asphalt Pavement (RAP) is a recycled aggregate. Typical RAP material contains both coarse and fine aggregates. It is obtained by milling and crushing the old flexible asphalt pavement that mostly comprises aggregates partially or fully covered by aged asphalt films. The surface of RAP aggregates is usually coated by asphalt film with a thickness between 6 to 9 microns (Huang, Shu, and Li, 2013). The properties of RAP rely upon the state of asphalt pavement from where it is reclaimed. There can be critical variation in the RAP material because of the kind of blend, total quality and size and asphalt mix consistency.

The most important qualities of aggregates include gradation, specific gravity, shape, texture and soundness. The weight volume characteristics of aggregates are not

significant indicators of aggregate quality, but they are important for concrete mix design. The density of an aggregate mix is a function of its particle size distribution (Mamlouk, 2011).

c) Mixing Water

Water is an important ingredient of concrete. Properly designed concrete mixture contains about 15 to 25% water by volume so that the concrete possesses the required workability for wet concrete and the desired durability and strength for hardened concrete. The total amount of water in concrete and the water to cement ratio may be the most significant factors in the production of good quality concrete. Too much water reduces concrete strength, while too little water makes the concrete unworkable (Mc Cormac, 2013).

When water mixes with Portland cement, cement paste is produced that binds the aggregates together. Water play key role to the harden the concrete through hydration process. Water needs to be of suitable quality for use in concrete so as not to adversely affect the desired properties of concrete (John, 2011). The water used for concrete should be clean, free from dirt and organic matter. Water comprising even small amounts of acid can have a serious harmful effect on concrete. The existence of oil will result in slowing the set and reducing the strength. Generally, water should be potable for producing good quality concrete (Kett, 2010).

d) Admixtures

Admixtures are constituents other than cement, water and aggregates that might be incorporated into concrete in order to impart a specific quality to either the plastic (fresh) mix or the hardened concrete. Chemical admixtures are classified as air

entrainers, water reducers, retarders, hydration controller admixtures and accelerators (Mamlouk, 2011).

2.2.3 Wet and Hardened Concrete Properties

Freshly mixed concrete before the set is known as wet concrete, while after setting and hardening it is said to be hardened concrete. Fresh/wet concrete is demarcated as a fully mixed concrete in a rheological state which has not lost its plasticity. The plastic state of fresh concrete offers a time period for transportation, placing, compaction and surface finishing. The effort required to place a concrete depends on the rheological properties of the cement paste and the inner friction between the aggregate particles (Kosmatka, 2011).

Slump, Vebe and Compaction factor tests are the most widely used test methods for determining the workability of concrete. Slump test is suitable for the concrete of high workability. The compacting factor is suitable for the concrete of medium to high workability. The Vebe test is more suitable for mixtures with low consistency (Mamlouk, 2011).

Concrete will change from a fluid to a plastic state and then to a solid hardened state due to hydration. The most vital properties of hardened concrete include various strengths (compressive, flexural, tensile, torsion and shear), stress-strain relationship, moduli and Poisson's ratio and durability (Li, 2011).

2.2.4 Artificial Neural Networks

Artificial neural networks are computational networks that were developed based on the desires for solving large-scale complex problems (Graupe, 2007). They are composed of massively parallel, highly interconnected nonlinear processing elements which are similar in purpose to human neurons and are tied together with connection weights corresponding to brain synapses. Parallelism and nonlinearity are the two crucial requirements in developing solution methods for many practical problems due to the complexity involved and the needs for processing massive amounts of information in real time. The root of fixing many engineering issues lies in the modelling and assessment of the relationship between a set of input and output variables. (Silva, 2004).

The two basic modelling approaches are analytical and empirical models. Analytical modelling approaches are commonly mathematical models developed primarily based on first principles. Even though an analytical approach may give exact solutions, it is frequently limited by problem complexity. Conversely, the empirical approach develops models based on input and output data collected through experiment. It estimates the unknown relationship between input and output features by investigating imperative characteristics embedded in the data. Empirical methods can be further divided into statistical models and artificial neural networks. Statistical models use a predefined form (e.g., logarithmic form) and they are fixed in parametric form. On the other hand, artificial neural networks use a network of interconnected "neurons" (computing units) that can learn the input/output relationship of a system through proper training with sampled data (Ming, 2003).

ANNs are capable of learning and generalizing from instances and experience to produce accurate solutions to problems even when input features contain errors and are incomplete. ANN can reveal astonishing capability in modelling the human brain (Duan & Kou, 2013). This makes ANNs a powerful instrument for solving some of the complex engineering problems. The processing elements of a neural network are similar to the neuron in the brain, which consists of many simple computational elements arranged in layers (Chopra, 2014).

Koivo (2008) highlighted the multilayer feedforward ANN architectures as the most successful application for predicting and forecasting. A multilayer perceptron is composed of a set of massively parallel and distributed processing units (neurons) as shown in Figure 2.1. Each node is fully connected to the other through connection weights and receives input signals from neurons linked to it. The successive layers of nodes receive input from the previous layers; the outputs of nodes in each layer are inputs to nodes in the next layer. The first layer is the source/input layer. The last layer is called the output layer. Layers between the input and output layers are known as hidden layers (Jamalaldin, Hakim, Noorzaei, Jaafar, & Jameel, 2011a).
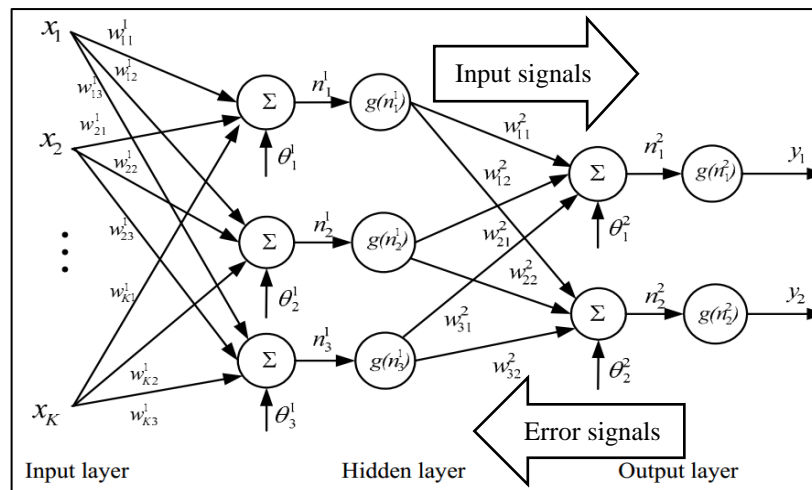
Figure 2.1 Multilayer Perceptron (Koivo 2008)

In order for the ANN to achieve the required task, the network should be trained with data regarding the problem. Backpropagation is a frequently used training algorithm. Apart from the input, hidden and output neurons, activation function is an important factor that affects the ANN performance (Suba, 2009). Tan-sigmoid and Log-sigmoid are most commonly used activation functions (Shmueli, Bruce, Stephens, & Patel, 2017).

Input signals are multiplied by connection weights and summed up together with the constant bias term. The result is then input to the activation function. The popular approach to estimate weights involves using the errors iteratively. In particular, the error for the output node/neurons is distributed across all the hidden nodes/neurons so that each node is assigned "responsibility" for part of the error (Shmueli et al., 2017).

The most popular method for using model errors to update weights is backpropagation of errors. A backpropagation algorithm trains network layer by layer doing forward and backward computations (Koivo, 2008).

2.3 Empirical Review

2.3.1 Characteristics of Concrete Constituent Materials

Su and Chen (2012) reported that RAP is usually finer than natural aggregate due to fragmentations of particles during the recycling process. According to the study, the most significant difference between natural aggregate and RAP was that RAP usually contains a substantial amount of attached asphalt films. Duan and Kou (2013) tried to compare RAP with natural aggregate and their findings revealed that lower bulk and

saturated surface dry densities, lower water absorption, inferior strength, the presence of contaminants and lower resistance to mechanical and chemical actions were the primary features of RAP.

Brand, Roesler and Al-qadi (2014) also assessed the gradation, unit weight, specific gravity and water absorption of RAP. Based on their findings, RAP had lower unit weight, specific gravity and water absorption than that of virgin aggregate. A study by Shi, Mukhopadhyay and Liu (2017) shows that RAP materials exhibited lower dry rodded unit weight, specific gravity and absorption than those of virgin aggregates.

According to a study by Surender, Ransinchung, Debbarma and Kumar (2017), fine reclaimed asphalt pavements were categorised as well graded aggregates but coarser when compared with the natural fine aggregates. The specific gravity and bulk density of CRAP and FRAP aggregates were found to be lower than natural coarse and fine aggregates respectively. A study by Abraham and Ransinchung (2018) also exhibited that the particle size distribution of RAP aggregates satisfied the grading requirements. However, specific gravity and density of RAP materials were lower than those of virgin aggregates, whereas the percent voids in RAP materials were higher than those of virgin aggregates.

The lower the specific gravity and bulk density of RAP materials might have potential influences on the wet and hardened concrete properties such as density and strength of concrete. The fresh and hardened density as well as the strength of hardened concrete usually decrease when lower specific gravity aggregates are incorporated in the concrete mixes (Ryu & Monteiro, 2002). The higher the void spaces in aggregates

indicate the cement paste requirements of the aggregates to produce a good quality concrete (John, 2011).

Jaya, Bakar, Azmi and Johari (2011) investigated the physical and chemical properties of RHA. According to the study, the specific surface area and loss of ignition (LOI) of the RHA were 11770 m^2/kg and 3.03% respectively. The CaO and SiO_2 contents of the RHA were 0.46 and 90% by mass respectively. Khan et al (2012) assessed the effects of the cooling process on the chemical and LOI contents of RHA. Based on the results, the study asserts that the amount of silica content in rapid cooled RHA was less than that of the slow cooled RHA. However, there was no any significant difference in terms of LOI contents in both the rapid cooled and slow cooled RHA ash. Ephraim et al (2012) investigated the properties of RHA. The specific gravity of RHA was found to be 1.55.

According to a study by Nair, Sivaraman and Thomas (2013) the specific gravity and specific surface area of RHA reported were 2.04 and 38398 m^2/kg respectively. A study by Khassaf, Jasim and Mahdi (2014) also reported the specific gravity value of RHA as 2.30 as well as the specific surface area value of 97750 m^2/kg.

Lakra and Gupta (2016) investigated the influence of burning temperature on the chemical contents of RHA. Their study exhibited that the silica content in the RHA increases with increasing burning temperature. According to the study, RHA produced by burning rice husk between 600 and 700°C temperatures for 2 hours contains 90-95% SiO_2, 1-3% K_2O and less than 5% unburnt carbon. The study also reported the

specific gravity and bulk density values of rice husk ash as 2.10 and is 0.781 g/cc

respectively.

A study by Nathen and Ravi (2017) shows that the properties of RHA are reliant on

the soil chemistry, paddy diversity, fertilizers applied during rice cultivation and

climate situations. The chemical composition of RHA from a study by Nathen and

Ravi (2017) is shown in Table 2.3.

Table 2.3 Chemical properties of rice husk ash

| Constituent | Location | | | |
	India	Malaysia	Brazil	Netherland
SiO_2	90.90	93.01	92.90	86.90
Al_2O_3	2.90	0.21	0.18	0.84
Fe_2O_3	0.30	021	0.43	0.73
CaO	0.89	0.41	1.03	1.4
K_2O	0.56	2.31	0.72	2.46
MgO	0.96	1.59	0.35	0.57
Na_2O	0.10	-	0.02	0.11
SO_3	0.20	-	0.10	-
LOI	4.0	2.36	-	5.14

Source: Nathen and Ravi (2017)

The physical properties of rice husk ash as reported by a few researchers are given in

Table 2.4.

Table 2.4 Physical properties of rice husk ash

| Property | Values | | | | |
	Philips et al.,(2018)	Huang.et al.,(2017)	Khan et al.,(2012)	Chao et al.,(2011)	Naji et al.,(2010)
Specific gravity	1.77	2.19	2.10	2.06	-
Mean particle size(mm)	0.150	0.095	0.075	0.087	0.095

Generally, RHA has lower specific gravity and higher unburnt carbon content

compared to that of cement. The lower the specific gravity may result in reducing the

wet and hardened density of concrete. The higher the unburnt carbon content may

increase the water demand of the concrete mixtures. The combustion of rice husk yields the largest quantity RHA with more than 85 percent silica content which gives it pozzolanic properties (Duggal, 2008).

2.3.2 Reclaimed Asphalt Pavement in Concrete

Hossiney, Tia and Bergin (2010) studied the performance of RAP concrete used in a rigid pavement application. In their study, four concrete mixtures incorporating 0, 10, 20, and 40% RAP aggregate were assessed in a laboratory setup. Typical ASTM tests were carried out on the wet concrete and in the cured state. The study showed that the compressive, tensile splitting and flexural strengths of the hardened concrete were inversely related to the amount of RAP content in the mix. The study also noticed that the coefficient of thermal expansion was unaffected by the addition of reclaimed asphalt pavement in the concrete mixture and shrinkage tendencies of the material decreased as the RAP content increased.

Huang, Shu and Li (2013) expanded the available information on concrete containing RAP. The aim of their study was to improve the toughness of concrete and decrease its chances of brittle failure. The study realized that the fine layer of asphalt coating protects the particles from breakage and facilitates the dissipation of energy in the event of a crack. Accordingly, the study concluded that the use of RAP aggregate in concrete would arrest crack. Their test data further indicated that coarse RAP had a greater positive effect to increase toughness compared to fine RAP.

Berry, Stephens, Bermel and Hagel (2013) investigated RAP used in concrete pavement. In the study, the virgin coarse aggregate was partially replaced by RAP with

0, 20, 35, and 50%. The study outlined that compressive and tensile strengths and elastic moduli decreased with increasing RAP content, whereas shrinkage was relatively unaffected by RAP content. Overall, the research recommends that a concrete containing up to 50 percent coarse RAP replacement as suitable for low to medium strength concretes.

Brand et al (2014) assessed the use of fractionated coarse RAP as a partial replacement (at 0%, 20%, 35% and 50%) of natural coarse aggregate in a ternary blend concrete incorporating slag. The results show that the unit weight, compressive, tensile splitting and flexural strength, elastic and dynamic moduli decrease as the percentage of RAP increases. The study further recommends that up to 50 percent coarse RAP may be suitable to meet the strength and durability requirements for paving applications.

Solanki and Dash (2015) studied RAP as a partial replacement (at 0, 10, 20, and 40%) of virgin coarse and fine aggregates in a concrete containing class C fly ash. Aggregate substitution with RAP was found to decrease both compressive and tensile splitting strength of concrete. The study noted that the reduction in strength was reliant on the content of aggregate replacement with RAP screenings, amount of cement replacement with fly ash and type of aggregate being replaced (coarse or fine).

Mufti and Fried (2016) studied RAP concrete during early age to establish the effects of replacing 20 mm gravel with 20 mm RAP in concretes made by varying water to cement ratios in the mix. Concrete mixtures with water to cement ratios of 0.4, 0.5, 0 .6, and 0.7 were made and tested using gravel and RAP aggregates. The compressive strength test results show that the RAP concrete strength increases with a reduction in

water to cement ratio throughout testing ages. Strength data collected through the laboratory testing further show that the replacement of 20 mm gravel with RAP has resulted in a significant reduction in porosity of concrete ($p < .0001$). Accordingly, the study concluded that RAP concrete is less porous than natural aggregate concrete. This would favour its application where the requirement might be for a more durable rather than a strong concrete.

Bida et al (2016) investigated the possibility of recycling RAP material in concrete specimens as partial replacement of fine aggregate. The mix design of 1:2.07:3.11 for cement, fine and coarse aggregate respectively and water to cement ratio of 0.5 was used. Based on the results obtained, the study recommends up to 40% RAP content replacement of virgin fine aggregate.

Shi, Mukhopadhyay and, Liu (2017) assessed the effect of RAP on Portland cement paving mixtures by replacing virgin coarse aggregate with coarse RAP at 20 and 40%. The study observed a higher reduction rate in compressive strength than the flexural and splitting tensile strengths. The decrement in flexural strength was 5–28% less than the corresponding reduction in compressive strength. The study results also show that the inclusion of small amounts of RAP could possibly improve the concrete's splitting tensile strength.

Studies conducted by Brand et al. (2014); Mufti et al (2016) and Shi et al., (2017) were limited to replacing the coarse portion of virgin aggregates by coarse reclaimed asphalt aggregates. Mufti and Fried (2016) made an effort to assess the effects of replacing a particular coarse aggregate size .i.e. 20mm. On the other hand, Bida et al (2016)

investigated the possibility of recycling only fine RAP material in concrete as a partial replacement of fine aggregate. Solanki and Dash (2015) studied the effects of replacing coarse aggregate with coarse RAP and fine aggregate with fine RAP leaving out the combined effects of both fine and coarse RAPs. Thus, the study did not capture the combined effects of both coarse and fine RAPs on the concrete properties.

2.3.3   Rice Husk Ash in Concrete

Nair, Sivaraman and Thomas (2013) studied the mechanical properties of high strength concrete containing 0, 5, 15, and 25% RHA. The study exhibited that the compressive strength of concrete improved as the replacement levels increased up to 25 percent, but the maximum compressive strength was attained at 25% RHA content. Kulkarni, Mirgal, Bodhale and Tande (2014) reported that replacing cement by 10% RHA showed a 16% increase in compressive strength when compared to the control mix. When 20% RHA was added to the concrete mix, the compressive strength increased by 8%. The study also noted insignificant difference in compressive strength when 30% RHA was added to the concrete mix relative to normal concrete.

Singh and Pareek (2015) examined the compressive strength and tensile splitting strength of concrete containing 5%, 10%, and 15% of RHA and plastic fibre in different amounts. The study exhibited that concrete samples incorporating RHA and plastic fibres resulted in better strength as compared to control concrete specimens. Saravanan and Sivaraja (2016) investigated the mechanical properties of concrete with w/c ratio of 0.45 containing 10%, 20% and 30% RHA. Based on their test results, the study recommends 20% as optimum replacement quantity of RHA.

Chinnaraj, Sivaranjani, Arthi and Dhamodharan (2017) investigated 10 and 15% replacement of cement by RHA. The study results show that 15% replacement of RHA by mass of cement increased the compressive strength of concrete, but the tensile splitting and flexural strengths were decreased. However, 10% placement of cement by RHA increased the compressive, tensile splitting and flexural strengths.

Huang et al (2017) investigated the influence of RHA on the strength and permeability of ultra-high-performance concrete. Compressive strength, permeability and flowability were evaluated. The results of the study show that the addition of RHA decreased the fluidity of fresh mixture, improved the compressive strength and impermeability of concrete.

A study by Lam, Bulgakov, Aleksandrova, Larsen and Ngoc (2018) primarily focuses on determining the dependence of the compressive strength of high-performance concrete on the quantity of RHA and fly ash by using the central composite design. The result of this study come up with the second-order regression equation that shows the relationship between RHA content and compressive strength. The study reported 12.51 percent as an optimum RHA content to obtain 76.72 MPa compressive strength after 28 days of curing.

2.3.4 Concrete Strength Prediction by ANN Model

Several studies used ANNs for predicting the strength of different types of concrete. Jamalaldin, Hakim, Noorzaei, Jaafar and Jameel (2011) made an effort to predict the compressive strength of high strength concrete using ANN. The study assessed a total

of 30 ANN architectures of which the 8-10-6-1 was found to be the best possible architecture and their ANN model was able to mimic experimental data accurately.

Duan and Kou (2013) also developed ANN strength predictive model with one hidden layer. The model predicted the compressive strength of recycled aggregate concrete accurately. Omran and Chen (2014) investigated the application of ANN to forecast the compressive strength of concrete made with alternative materials such as fly ash, lightweight aggregate and Portland cement. A feed-forward Multilayer Perceptron ANN was employed for this purpose. The accuracy and flexibility of the ANN model were tested using relative and numerical input methods. The study results exhibited that MLP with one hidden layer was effective in predicting the compressive strength. It was also observed that both relative and numerical input methods gave satisfactory accuracy.

A study by Saif and Alquzweeni (2015) applied the ANN-based method to predict the mechanical properties of high-performance concrete. The study developed a backpropagation ANN that was trained and tested using actual datasets obtained from a laboratory experiment. The results of the study show that ANN is an accurate tool for predicting the compressive strength of high-performance concrete.

Chopra, Sharma and Kumar (2016) applied ANNs as strength prediction model. Based on study results, it was reported that the ANN model with the Levenberg-Marquardt training function and tan-sigmoid activation function was the best prediction tool. Kalra and Joseph (2016) created 5-10-1 multilayer feedforward ANN architecture for predicting the compressive strength of concrete. According to the study, the best

validation performance was found at epoch 40 with root mean squared error value of 3.31 MPa.

Bharathi, Manju and Premalatha (2017) created the ANN model for forecasting the wet and hardened properties of self-compacting concrete containing fly ash as partial replacement of cement. Heidari, Hashempour and Tavakoli (2017) also applied the ANN model for predicting the compressive strength of concrete. The study noted that the predicted results of the ANN model were accurate and closer to the actual values. Hosein et al. (2018) predicted the recycled aggregate concrete compressive strength accurately using ANN predictive model.

Studies by Duan and Kou (2013), Chopra et al. (2016), Kalra and Joseph (2016), Bharathi et al. (2017), Heidari et al (2017) and Behfarnia et al (2017) were focused on studying single ANN architecture to predict the compressive strength of concrete. However, several ANN architectures should have been examined by varying the number of hidden layers, number of neurons in each hidden layer and type of activation functions in order to arrive at optimum activation function and select the best possible architecture. In addition, their ANN model performances were not assessed and checked for overfitting. This implies that their networks were probably unstable and oscillatory. The probability of networks entrapment in local minima was also very high.

2.3.5 Summary of Literature Review and Research Gaps

From the literature survey, it is understood that RAP is a useful alternative to virgin aggregates and can replace aggregates up to 40% that leads to a significant reduction

in the cost of concrete production (Bida et al., 2016; Bolden et al., 2013; Brand et al., 2012; Huang et al., 2013; Berryet al., 2013; Shi et al., 2017; Solanki & Dash, 2015). Likewise, RHA has been proven suitable in the production of strong and durable concrete as partial replacement of cement up to 20% (Kumar et al., 2016; Chinnaraj, 2017; Gupta & Wayal, 2015; Gupta et al., 2015; Jamil & Karimc, 2014; Kene et al., 2015; Lakra & Gupta, 2016; Lun, 2015; Nathen & Ravi, 2017; Singh & Pareek, 2015).

However, limited research was done to examine the potential of incorporating wastes such as RAP and RHA into concrete. Most relevant materials research efforts were wasted on materials with a toxic profile and are still excessively focused on their mechanical properties with minor environmental concerns (Jin & Chen, 2013; Pacheco & Labrincha, 2013). Very few (10% of the published papers) were in some degree related to environmental concerns (Pacheco & Labrincha, 2013).

In addition, the combined effects of both RAP and RHA on wet and hardened properties of concrete have not been studied so far. Therefore, more research works are required to assess the properties of concrete containing RAP and RHA. Hence, this study focuses to capture the combined effects of RAP and RHA on wet and hardened properties of concrete.

Furthermore, in the recent years, prediction of mechanical properties of construction materials, in particular, the 28th-day compressive strength of concrete, has gained a pronounced attention amongst the material scientists (Siraj, 2015; Duan & Kou, 2013). Some research works were found in the literature that focused on the prediction of the 28th-day compressive strength of different types of concretes (Behfarnia & Khademi,

2017; Bharathi et al., 2017; Chopra et al., 2016; Faruqi, et al, 2015; Heidari et al., 2017; Kalra & Joseph, 2016; Sahoo, & Sarkar, 2016; Saif & Alquzweeni, 2015).

The current equations presented in codes and standards for forecasting the strength of concrete have not considered supplementary cementitious materials and non conventional aggregates (Jamalaldin et al., 2011; Noorzaei et al., 2007). Consequently, the traditional approach can hardly be applied when some of the concrete constituents are not the conventional materials. Thus, this research also applied the ANN model for predicting the compressive and tensile splitting strength of concrete incorporating both RHA and RAP.

2.4 Conceptual Framework

The blueprint of this study that explains achieved study objectives, key factors, concepts, variables and presumed relationship among them is shown diagrammatically in Figure 2.2.

INDEPENDENT VARIABLES

Material properties

- Physical (specific gravity, voids in aggregates, water absorption, density, gradation, etc.)
- Chemical (CaO, SiO_2, Al_2O_3, Fe_2O_3 & others)
- Mechanical (aggregate impact and crashing values)

Concrete trial mixes

- RHA-inclusive concrete (0% RHA, 5% RHA, 10% RHA, 15% RHA and 20% RHA)
- RAP-inclusive concrete (0 % RAP, 10% RAP, 20% RAP, 30% RAP, 40% RAP, and 50% RAP)
- RHA- and RAP-inclusive concrete (5% RHA + 10%RAP, 5% RHA + 20%RAP, 5% RHA + 30%RAP, 10% RHA + 10%RAP, 10% RHA + 20%RAP, 10% RHA + 30%RAP, 15% RHA + 10% RAP, 15% RHA + 20% RAP, 15% RHA + 30% RAP, 20% RHA + 10% RAP, 20% RHA + 20% RAP, and 20% RHA + 30% RAP)

PROCESSES

- Material preparation and characterization
- Mixing, casting, curing, testing and analyzing
- Network design, training, evaluating and analyzing

DEPENDENT VARIABLES

Wet and hardened concrete properties

- Fresh concrete (density & workability)
- Hardened concrete (sorptivity, voids in concrete, water absorption, tensile, compressive, and flexural strengths)

Strength prediction by ANN model

- 28th-day tensile splitting strength
- 28th-day compressive strength

Figure 2.2 Conceptual framework

CHAPTER THREE

MATERIALS AND METHODS

3.1 Introduction

This chapter is devoted to providing clear and detailed information about the materials and methodologies used to achieve the objectives specified in chapter one. The research designs adopted were an experimental investigation and computer simulation. Experimental research design is the most frequently used design to obtain information about mechanical and physical characteristics of materials from experimental setup. Computer simulation is used to imitate or mimic the logical relationships among the model input features and desired outputs.

3.2 Characteristics of Concrete Constituent Materials

3.2.1 Source of Data

The study required both primary and secondary data. Data collected through experimental laboratory setup served as primary sources of data for scientific analysis and interpretation. All the data obtained from published materials such as books, journals and articles used as secondary data sources.

3.2.2 Materials

Materials used for this study were fine reclaimed asphalt pavement (FRAP), coarse reclaimed asphalt pavement (CRAP), fine virgin aggregate (FVA), coarse virgin aggregate (CVA), ordinary Portland cement (OPC) type I (42.5 N), rice husk ash (RHA), water, Sika ViscoCrete 3088 superplasticizer (SVCSP) and Sikament NNG

superplasticizer (SNNGSP). SNNGSP was used in order to enhance the workability of fresh RHA inclusive concrete mixes, whereas SVCSP was used in both RHA and RAP inclusive concrete mixtures. Figure 3.1 depicts aggregates (CRAP, CVA, FRAP, and FVA) and cementitious materials (cement and RHA) used in the study. All materials were obtained from different parts of Kenya. FVA (river sand) and CVA were procured from Masinga and Molongo districts of Kenya respectively. The RAP was obtained from an old distressed flexible pavement, Ruaka-Banana-Limuru Road (D407), sampled at the section near Tigoni, Kiambu County of Kenya. The road was constructed about 21 years ago that served without major rehabilitation and has been under reconstruction since April 2016. RHA was collected from the dump site of Mwea Rice Milling Factory. Cement and superplasticizers were purchased from Bamburi Cement factory and Sika Kenya Limited in Kenya respectively. Tap water was used for both mixing and curing of concrete specimens.
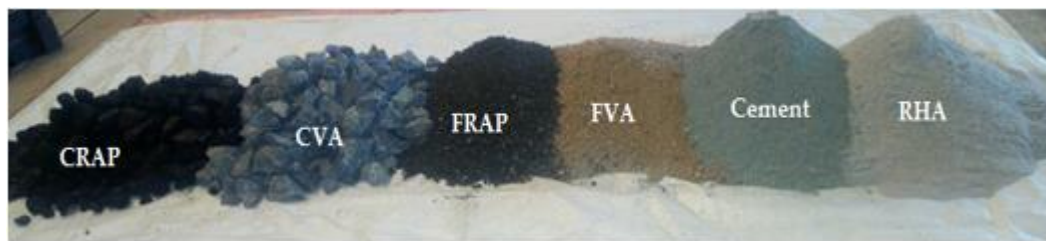
Figure 3.1 Materials

3.2.3   Methods for Material Characterization

Sampling of aggregates was carried out in accordance with BS EN 932-1 (1997) provisions to obtain a sample that is representative of the average properties of the batch. Grading of the aggregates was determined in accordance with BS EN 933-1 (2012) using test sieves of the sizes complying with BS ISO 3310-2 (2013)

39

requirements. The RAP material was obtained through ripping and milling of old flexible existing pavements and then crushed manually and finally sieved using 5 mm sieve in order to separate into FRAP (size < 5 mm) and CRAP (size > 5 mm). The specific gravity and water absorption of coarse and fine aggregates were determined as per BS EN 1097-6 (2013) testing method. Bulk density and voids in aggregates were determined in line with the procedures defined in ASTM C29 / C29M (2003). Aggregate crushing and impact tests were performed according to the procedures specified in IS 2386: Part IV (2002). Natural RHA was sieved using 0.10 mm sieve. The chemical analysis of cement and RHA were conducted as per BS EN 196-2 (2013) test method. The specific gravities of cement and RHA were performed in accordance with ASTM C188 (2016) provisions using Le-Chatelier apparatus. The most important test methods adopted for characterizing materials are summarised in Table 3.1.

Table 3.1 Test methods adopted for material characterization

Characteristics of Materials	Methodology Adopted
Gradation and Fineness modulus	BS EN 933-1 (2012)
Water absorption and specific gravity	BS EN 1097-6 (2013)
Density and voids in aggregates	ASTM C29 (2003)
Aggregate crushing and impact values	IS 2386-IV (2002)
Cement and RHA specific gravity	ASTM C188 (2016)
Chemical analysis	BS EN 196-2 (2013

3.2.4 Data Processing and Analysis

Data processing and analysis were done in accordance with the respective standards listed in Table 3.1. Excel 2016 (spreadsheet) was used as a computational tool to generate graphs, tables and figures for making contemplated comparisons, interpretation and conclusion. The particle size distribution of aggregates was plotted

using a spreadsheet. Detailed analysis of material characterization is presented in Appendix A.

3.3 Fresh and Hardened Concrete Properties

3.3.1 Concrete Mix Design and Mixing Procedures

The mix design for 25 MPa (characteristic cube strength) Portland cement concrete was done in accordance with BS EN 206 (2014) and its complementary standard BS 8500-2 (2012) provisions. A total of 22 mixtures were prepared and studied. Table 3.2 shows the particulars of studied mixture proportions. Sample calculation for mix design is given in Table B1, Appendix B. In all the mixtures, 254 kg/m^3 of water and water to cementitious material ratio of 0.65 were kept constant.

The first phase of the study was to assess the effect of RHA on wet and hardened properties of concrete by replacing cement with 5, 10, 15 and 20% RHA (by weight of cement). In the second phase, FVA and CVA were replaced by 10, 20, 30, 40 and 50% FRAP and CRAP (by weights of FVA and CVA) respectively to ascertain the influence of RAP on the properties of concrete. The third phase was to investigate the combined effects of RHA and RAP on wet and dry properties of concrete.

SNNGSP was used at 0.5, 0.85, 2 and 2.75% (by weight of cementitious material) for 5, 10, 15, and 20% RHA content respectively. SVCSP (more powerful than SNNGSP) was used at 0.5, 0.7, 0.9 and 1.1% (by weight of cementitious material) for RHA and RAP combined mixtures. Manual mixing was performed as per BS 1881-125 (2013) provisions with a control mechanism to prevent the loss of water and cementitious materials quantified during mixture proportioning.

Table 3.2 Concrete mix proportions

Mix Description	Cement (kg/m^3)	RHA (kg/m^3)	FVA (kg/m^3)	FRAP (kg/m^3)	CVA (kg/m^3)	CRAP (kg/m^3)
Control	390	0	712	0	1593	0
5% RHA	371	20	712	0	1593	0
10% RHA	351	39	712	0	1593	0
15% RHA	332	59	712	0	1593	0
20% RHA	312	78	712	0	1593	0
10% RAP	390	0	641	71	1434	159
20% RAP	390	0	570	142	1274	319
30% RAP	390	0	498	214	1115	478
40% RAP	390	0	427	285	956	637
50% RAP	390	0	356	356	797	797
5% RHA + 10% RAP	371	20	641	71	1434	159
5% RHA + 20% RAP	371	20	570	142	1274	319
5% RHA + 30% RAP	371	20	498	214	1115	478
10% RHA + 10% RAP	351	39	641	71	1434	159
10% RHA + 20% RAP	351	39	570	142	1274	319
10% RHA + 30% RAP	351	39	498	214	1115	478
15% RHA + 10% RAP	332	59	641	71	1434	159
15% RHA + 20% RAP	332	59	570	142	1274	319
15% RHA + 30% RAP	332	59	498	214	1115	478
20% RHA + 10% RAP	312	78	641	71	1434	159
20% RHA + 20% RAP	312	78	570	142	1274	319
20% RHA + 30% RAP	312	78	498	214	1115	478

3.3.2 Test Methods for Fresh and Hardened Concrete Properties

Fresh concrete was assessed by conducting slump, compacting factor and fresh density tests. Sampling for testing was done in accordance with the procedures stipulated in BS EN 12350-1(2009). Methods specified in BS EN 12350-2 (2009) were followed to

determine the slump. The fresh concrete was compacted into a frustum of cone of size 100 mm x 200 mm x 300 mm in three layers and then the cone was withdrawn upwards. The distance the concrete had slumped provides a measure of the consistency of the concrete.

Compacting factor was determined in accordance BS 1881-103 (1993) provisions using compaction factor apparatus shown in Figure 3.2. The fresh concrete sample was placed in the top hopper up to the rim. Then, the trap door was unlocked so as to the concrete fall into the bottom hopper. Next, the trap-door of the bottom hopper was opened to enable the concrete to fall into the cylinder. After the excess concrete was trimmed off using plane blades, it was weighed to obtain the weight of partially compacted concrete. The cylinder was then filled with new concrete sample and vibrated to attain a fully compacted weight of concrete. The compaction factor is then the ratio of weights of partially compacted to fully compacted concrete.
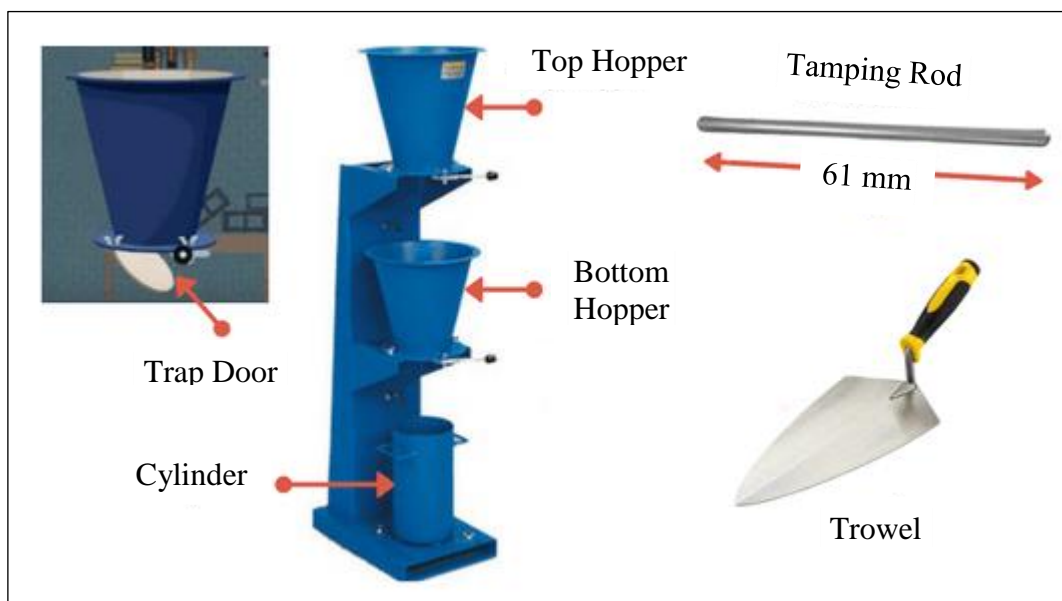
Figure 3.2 Compaction factor apparatus

Cubes of dimensions 100 mm x 100 mm x 100 mm, prisms of dimensions 150 mm x 150 mm x 500 mm and cylinders with a diameter of 100 mm and 200 mm long conforming to BS EN 12390-1 (2012) requirements were used to make concrete test specimens for compressive, flexural and tensile splitting strength tests respectively. A total of 132 cube, 9 beam and 66 cylinder specimens were made and cured in accordance with the methods specified in BS EN 12390-2 (2009) for compressive, flexural and tensile splitting strength tests respectively. Compressive, flexural and tensile splitting strengths of concrete were determined according to BS EN 12390-3 (2009), BS EN 12390-5 (2009) and BS EN 12390-6 (2009) test methods respectively.

Specimens were loaded to failure in a compression testing machine conforming to BS EN 12390-4 (2000), shown in Figure 3.3. The two-point method of loading was used for the flexural strength test. The maximum load sustained by the specimen was recorded and the compressive, flexural and tensile splitting strengths of the concrete were calculated by using Equations (3.1), (3.2) and (3.3) respectively.

$$f_c = \frac{F}{A_c} \qquad (3.1)$$

$$f_{cf} = \frac{Fl}{bh^2} \qquad (3.2)$$

$$f_{ts} = \frac{2F}{\pi Ld} \qquad (3.3)$$

Where: f_c is the compressive strength, in MPa; f_{cf} is the flexural strength, in MPa; f_{ts} is the tensile splitting strength, in MPa; F is the maximum load at failure, in N; l is the the span of the beam, in mm; L is the length of the line of contact of the specimen, in mm; b is the width of cross-section, in mm; h is the height of failed crosssections, in

mm, d is the designated cross-sectional dimension, in mm, A_c is the cross-sectional area of the specimen on which the compressive force acts.

| Compression Test | Tensile Test | Flexural Test |

Figure 3.3 Compression, tensile and flexural testing setups

Density, water absorption and voids in concrete by immersion and boiling were determined in accordance with ASTM C642 (2013) provisions. A total of 66 cubes of dimensions 100 mm x 100 mm x 100 mm were made and cured for 28 days. The specimens were dried in an oven for 72 hours at a temperature of 110 °C until the change in mass was less than 0.5 % of the lowest value obtained. Then, the specimens were immersed in water at an average temperature of 21.5 °C for about 72 hours until the increase in saturated surface-dried mass was less than 0.5 % of the larger value obtained. Finally, the specimens were placed in a receptacle, covered with tap water and boiled for 5 hours and then cooled by natural loss of heat for 15 hours to a final average temperature of 22 °C. After immersion and boiling, specimens were suspended by a wire and the apparent masses in water were determined. Using the values determined in accordance with the procedures described above, the following calculations were made as presented in Equations (3.4) - (3.10).

$$w_i = \frac{(B - A)}{A} \times 100 \tag{3.4}$$

$$w_{i\&b} = \frac{(C - A)}{A} \times 100 \tag{3.5}$$

$$\rho_{dry} = \frac{A}{(C - D)} \rho_w \tag{3.6}$$

$$\rho_i = \frac{B}{(C - D)} \rho_w \tag{3.7}$$

$$\rho_{i\&b} = \frac{C}{(C - D)} \rho_w \tag{3.8}$$

$$\rho_{app} = \frac{A}{(A - D)} \rho_w \tag{3.9}$$

$$v = \frac{(\rho_{app} - \rho_{dry})}{\rho_{app}} \times 100 \tag{3.10}$$

Where: w_i is absorption after immersion, in %; $w_{i\&b}$ is absorption after immersion and boiling, in %; A is the mass of oven-dried sample in air, in grams; B is the mass of surface-dry sample in air after immersion, in grams; C is the mass of surface-dry sample in air after immersion and boiling, in grams; D is the apparent mass of sample in water after immersion and boiling, in grams; ρ_{dry} is dry bulk density, in g/cm^3; ρ_{app} is apparent density, in g/cm^3; ρ_w is density of water, in g/cm^3 and v is the volume of permeable pore space, in %.

Sorptivity by the concrete specimens was determined in accordance with ASTM C1585 (2013) test methods. A total of 66 cubes of dimensions 100 mm x 100 mm x 100 mm were made and cured for 28 days for the sorptivity test. The specimens were dried in an oven at 110 °C temperature for 24 hours and then remained in an oven at a temperature of 50°C for 3 days. After the 3 days, each specimen was placed inside a sealable container and stored at 22°C for 15 days before the start of the absorption procedure. The specimens were removed from the storage container and the five faces

of the specimens were sealed properly using box sealing tape to hinder the entrance of moisture while the opposite face was left open and exposed to water (see Figure 3.4). The initial weight of the specimens was recorded after sealing and submerged in water about 3 mm above the bottom face (see Figure 3.4). The weight gain due to sorption was determined by weighing the submerged specimen at a definite interval of time 5, 10, 30 min, 1, 2, 3, 4, 5, and 6 hours. The absorption, I, and sorptivity, K were calculated by using Equations (3.11) and (3.12) respectively. Sorptivity was obtained from linear regression analysis of the plot of I versus square root of time at which sorption was observed (see Figures B1-B6, Appendix B).

$$I = \frac{\Delta m_t}{A\rho_w} \tag{3.11}$$

$$K = \frac{I}{\sqrt{t}} \tag{3.12}$$

Where: I is the absorption, in mm; K is sorptivity, in mm/h$^{1/2}$; Δm_t is the change in specimen mass, in grams at the time t; A is the exposed surface area of the specimen, in mm^2; ρ_w is the density of water, in g/cm^3; and t is the time, in hours at which the submerged weight was determined.
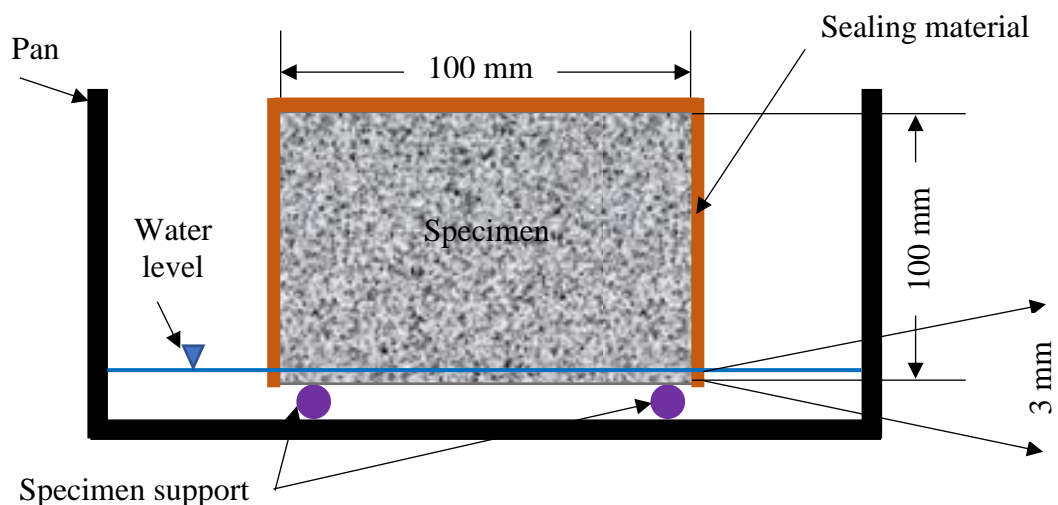
Figure 3.4 Schematic of the sorptivity procedure

Test methods adopted for determining the fresh and hardened properties of concrete are summarised in Table 3.3.

Table 3.3 Test methods for fresh and hardened concrete properties

Fresh and Hardened Properties	Methodology Adopted
Fresh Density	EN 12350-6 (2009)
Slump	BS EN 12350-2 (2009)
Compacting factor	BS 1881-103 (1993)
Compressive strength	BS EN12390-3 (2009)
Splitting tensile strength	BS EN 12390-6 (2009)
Flexural strength	BS EN 12390-5 (2009)
Hardened density & water absorption	ASTM C642 (2013)
void spaces in hardened concrete	ASTM C642 (2013)
Sorptivity	ASTM C1585 (2013)

3.3.3   Data Processing and Analysis

Data processing and analysis were done in accordance with the respective standards listed in Table 3.3. Excel 2016 was used as an analysis tool to obtain descriptive statistics such as graphs, tables, figures and inferential statistics for making anticipated comparisons and evaluating the relationship among variables. Relationships between RHA and RAP contents, and compressive strength, flexural strength, density, sorptivity, water absorption, compacting factor and slump were determined using multiple regression and ANOVA. All the figures were plotted with the help of a spreadsheet.

3.4 Development of ANN Model for Predicting Concrete Strength

3.4.1 Designing the Architecture of ANN

A three-layer perceptron was created using MATLAB version R2017a. A total of 33 Artificial networks were created using 132 experimental data sets obtained from 22 laboratory concrete mixtures. The network was composed of source neurons (input layer), computational neurons (hidden layer) and an output layer.

Fifteen input signals/parameters were used namely mass of water (W), cement (C), RHA, FVA, FRAP, CVA, CRAP, water to cement ratio (W/C), composite fineness modulus of fine aggregates (CFM_{fa}), composite water absorption of fine aggregates (CWA_{fa}), composite water absorption of coarse aggregates (CWA_{ca}), composite specific gravity of fine aggregates (CSG_{fa}), composite specific gravity of coarse aggregates (CSG_{ca}), nominal maximum size of aggregate (NAS) and average curing temperature (CT_{av}). The compressive and tensile strengths were used as target datasets. Table 3.4 presents the ranges of input and target parameters.

Table 3.4 ANN Model Input and target attributes

Model Attributes	Range	
1. Input Parameters	Min.	Max.
Water, W [kg/m^3]	-	254
Cement, C [kg/m^3]	312	390
Rice husk ash, RHA [kg/m^3]	-	78
Fine virgin aggregate, FVA [kg/m^3]	356	712
Fine reclaimed asphalt pavement, $FRAP$ [kg/m^3]	-	356
Coarse virgin aggregates, CVA [kg/m^3]	796	1593
Coarse reclaimed asphalt pavement, $CRAP$ [kg/m^3]	-	796
Water to cement ratio, W/C	-	0.65
Composite fineness modulus, CFM	-	2.65
Fine aggregates composite water absorption, CWA_{fa} [%]	1.49	3.95
Coarse aggregates composite water absorption, CWA_{ca} [%]	2.02	2.41
Fine aggregates composite specific gravity CSG_{fa} [%]	2.37	2.43
Coarse aggregates composite specific gravity, CSG_{ca} [%]	2.51	2.62
Nominal aggregate size, NAs [mm]	-	19.5
Average curing temperature, CT_{av} [^{o}C]	24	25
2. Desired Output Parameters		
Compressive strength, f_c [MPa]	14.75	32.58
Tensile splitting strength, f_{ts} [MPa]	1.22	2.49

3.4.2   Network Training

The constructed 33 ANNs were trained by varying hidden neurons and activation functions. Log-sigmoid, tan-sigmoid and purelin linear activation functions were used to arrive at optimum activation functions by evaluating their performance against the model mean squared values. According to Shmueli et al (2017), the activation functions are defined in Equations (3.13), (3.14) and (3.15).

$$\text{Tan-sigmoid: g}(x) = \frac{2}{1+e^{-x}} - 1 \tag{3.13}$$

$$\text{Log-sigmoid: g}(x) = \frac{1}{1+e^{-x}} \tag{3.14}$$

$$\text{Purelin: g}(x) = \text{x} \tag{3.15}$$

Trainlm learning function was used to improve network training efficiency. Learndgm was used as an adaptation function to overcome local minima. Backpropagation algorithm was used for training the networks. The backpropagation algorithm trains the network layer by layer doing forward and backward computations (Koivo, 2008). Algorithm updating formulae are presented in Equations (3.16), (3.17), (3.18) and (3.19). The Backpropagation algorithm has two phases (Duan et al., 2013). First, input signals are multiplied by free parameters and added together with the bias term. The results are inputs to the activation function as presented in Equation (3.16). The network then propagates the input signals forward until the desired output is generated as shown in Figure 3.5. If the output is different from the target, an error is calculated by Equation (3.17) and backpropagated from the output layer to the hidden layer. The free parameters are updated when errors are propagated as presented in Equations (3.18) and (3.19). In particular, the errors for the output nodes are distributed across

all the hidden nodes so that each node is assigned "responsibility" for part of the error (Shmueli et al., 2017).

$$y_j = g(\sum_{i=0}^{n_l} w_{ji}^l x_i + \theta_j^l) \tag{3.16}$$

$$\delta_j^L = (d_j^L - y_j^L)(y_j^L)' \tag{3.17}$$

$$\Delta w_{ji}^l = \eta \, \delta_j^l \, y_j^{l-1} \tag{3.18}$$

$$w_{ji(new)}^l = w_{ji(old)}^l + \Delta w_{ji}^l \tag{3.19}$$

Where: y_j is the output of the jth neuron in hidden layer; δ_j^L is the error gradient for the output neuron; Δw_{ji}^l is the weight correction; $w^l_{ji(new)}$) is the updated weight; w is the connection weight between two neurons; d is the desired response (target); x is the input; y is the neuron's output; g is the activation function; η is the learning rate; l is the number of layer; L is the output layer and i or j is the number of neuron in each layer; w_{ji}^l is the weight between the jth neuron in the lth layer and the ith neuron in the $(l-1)^{th}$ layer; θ_j^l is the jth neuron's bias; d_j^L is the desired response of the output neuron; and n_l is the number of neurons in the lth layer.
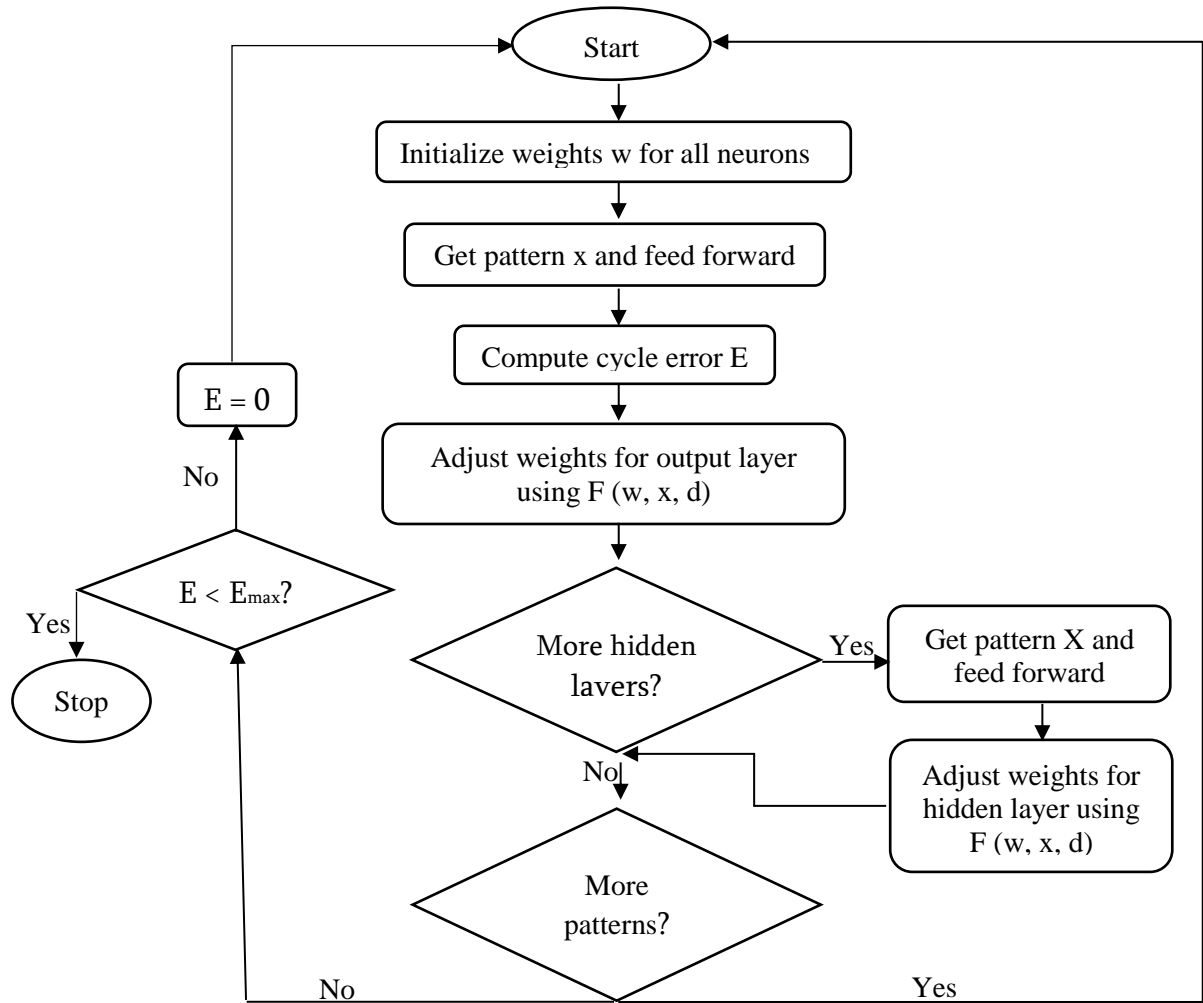
Figure 3.5 Backpropagation algorithm flow chart

3.4.3 Model Performance Evaluation

The ANN model was trained on the training data, applied to the validation data and measures of accuracy then use the prediction errors on that validation set. The model's predictive accuracy was measured through computing mean absolute error, average error, mean absolute percentage error and root mean square error using Equations (3.20), (3.21), (3.22) and (3.23) respectively.

$$MAE = \frac{1}{n}\sum_{i=1}^{n}\left|a_i - p_i\right| \tag{3.20}$$

53

$$AE = \frac{1}{n}\sum_{i=1}^{n}\left(a_i - p_i\right) \qquad (3.21)$$

$$MAPE = \frac{100}{n}\sum_{i=1}^{n}\frac{\left|a_i - p_i\right|}{\left|a_i\right|} \qquad (3.22)$$

$$RMSE = \sqrt{\frac{\sum_{i=1}^{n}(a_i - p_i)^2}{n}} \qquad (3.23)$$

Where: *MAE* is the mean absolute error; *AE* is the average error; *MAPE* is the mean absolute percentage error; *RMSE* is the root mean square error; *a* is the actual/experimental value; *p* is the predicted value/model's output and *n* is the number of concrete specimens.

3.4.4 Sensitivity Analysis

The main aim of the sensitivity analysis was to analyze the relative effect/importance of input variables/features on the outputs of the proposed ANN strength predictive model. Unlike classic statistical models, the task of determining the influence of independent variables/input parameters on the dependent variables/outputs does not seem easy in ANN due to its considerable complexity (Montan, 2003; Hosein et al., 2018). In this study, the relative influence of each input features on outputs was determined based on the magnitude of connection weights using the method proposed by (Milne, 1995), Equation (3.24).

$$IF = \dfrac{\displaystyle\sum_{j=1}^{n_{hid}} \dfrac{w_{ji}}{\displaystyle\sum_{l=1}^{n_{inp}} \left| w_{jl} \right|} \times w_{oj}}{\displaystyle\sum_{k=1}^{n_{inp}} \left(\displaystyle\sum_{j=1}^{n_{hid}} \left| \dfrac{w_{jk}}{\displaystyle\sum_{l=1}^{n_{inp}} \left| w_{jl} \right|} \times w_{oj} \right| \right)} \qquad (3.24)$$

Where: *IF* is the influence factor; *Ninp* is the number of inputs; *nhid* is the number of hidden units; *w* is the connection weight; *i* is the input unit, and *o* is the output unit.

3.4.5 Data Processing and Analysis

The required parameters were obtained from the experimental setup and the developed ANN model. The variables acquired from the model outputs were then analyzed using Excel 2016, ANOVA and MathLab version R2017a to get graphs, tables and figures for making contemplated comparisons and conclusion. Data interpretation was conducted by comparing the actual (experimental studies) and model outputs.

CHAPTER FOUR

RESULTS AND DISCUSSION

4.1   Introduction

This chapter focuses on results and discussion of results obtained from experimental investigation and ANN model. The results of material characterization are presented and discussed. The effects of RHA and RAP on wet and hardened properties of concrete are also discussed in detail. Finally, the outputs of the ANN model are presented and discussed.

4.2   Material Characterization

The materials were characterized in terms of gradation, fineness modulus, water absorption, specific gravity, bulk density, void content, chemical analysis, aggregate crushing and impact values.

4.2.1   Physical, Mechanical and Chemical Properties of Materials

Gradation results (derived from Tables A1 - A4, Appendix A) of coarse and fine aggregates are depicted in Figures 4.1 and 4.2 respectively. The results show that the particle size distributions of CVA and FVA met the grading requirements of BS 882.
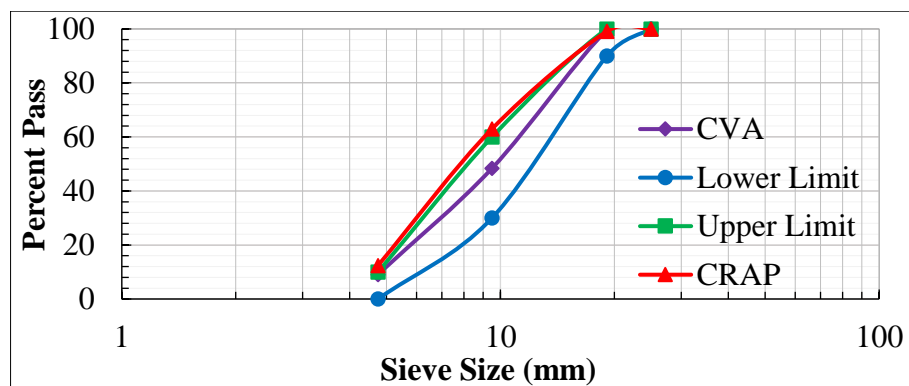
Figure 4.1 Coarse aggregate particle size distribution
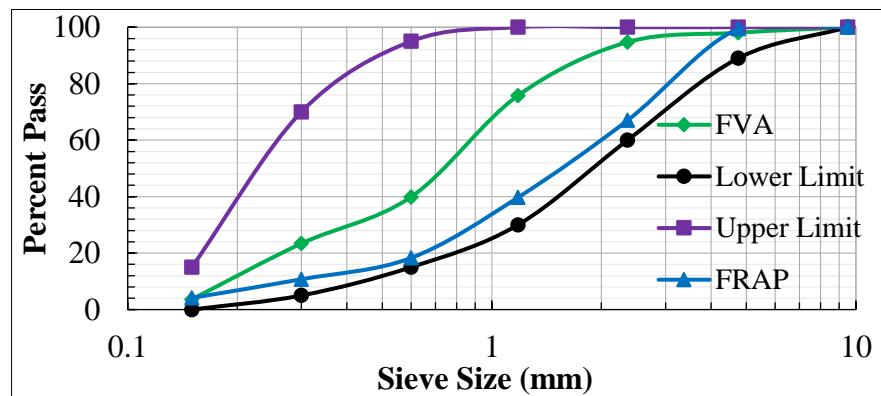
Figure 4.2 Fine aggregate particle size distribution

The grading of CRAP was slightly outside the limits while that of FRAP was within the limits specified in BS 882. It is apparent from Figure 4.1 that CRAP was finer than CVA, whereas FRAP was coarser than FVA. Similar findings were reported by Abraham et al (2018). The fineness of CRAP and coarseness of FRAP might be attributed to the fragmentation of CRAP materials during crushing and agglomeration of particles respectively and their sources as well. Hence, aggregates which meet the grading requirements result to the maximum possible density that is desired in many construction applications because of its high stability and low binder content requirement.

All coarse aggregates used in this study had 19.1 mm nominal maximum aggregate sizes. The fine aggregate particle sizes were between 0.15 and 5 mm. FVA and FRAP had fineness modulus of 2.65 and 3.61 respectively. According to ASTM C33-3 (2001), the fineness modulus for fine aggregates should be in the range of 2.3 to 3.1, with a higher number being a coarser aggregate.

Three types of specific gravities of coarse and fine aggregates, namely bulk dry, bulk saturated surface dry and apparent specific gravities which are widely accepted and

57

used in portland cement and asphalt concrete mix design were determined and the results are tabulated in Table 4.1.

Table 4.1 Physical and mechanical properties of materials

Property	OPC	RHA	FVA	FRAP	CVA	CRAP
Fineness modulus	-	-	2.65	3.61	-	-
Silt Content [%]	-	-	5.19	0.81	-	-
Bulk specific gravity	3.12	2.03	2.43	2.32	2.62	2.41
Bulk specific gravity, SSD basis	-	-	2.52	2.37	2.68	2.45
Apparent specific gravity	-	-	2.68	2.46	2.80	2.51
Water Absorption [%]	-	-	3.95	2.42	2.41	1.63
Loose bulk density [kg/m^3]	1398	359	1456	1318	1421	1300
Rodded bulk density [kg/m^3]	1435	470	1577	1407	1584	1326
Voids in loose aggregates [%]	-	-	39.33	43.09	45.75	43.97
Voids in Rodded aggregates [%]	-	-	34.31	39.25	39.52	42.83
Maximum particle size (mm)	0.09	0.10	5	5	20	20
Aggregate crushing values [%]	-	-	-	-	18.73	15.92
Aggregate Impact values [%]	-	-	-	-	15.51	9.83

RAP materials had lower specific gravity than that of virgin aggregates. The lower specific gravity of RAP may be attributed to the substantial amounts of low density asphalt-mortar (asphalt binder-sand-filler matrix) coatings on the RAP surfaces. The specific gravity of aggregate has a potential influence on the wet and hardened concrete properties. Higher specific gravity results in heavier concrete and vice versa.

Although aggregates are inert, they can capture water in the surface voids. The water absorption values (derived from Tables A5 and A6, Appendix A) of CVA, CRAP, FVA and FRAP were determined and the values are presented in Table 4.1. The water

ingestion of RAP aggregates was observed to be lower than that of virgin aggregates. The reason might be credited to the asphalt coating around RAP aggregates.

The quantity of water absorbed by aggregates is imperative in the design of portland cement concrete, as the moisture captured in the voids of aggregate is not available to react with the cement or to improve the workability of the plastic concrete. Therefore, aggregates with low-absorption characteristics are desirable for concrete (John, 2011).

The bulk density of aggregate both in compacted and loose condition as well as the calculated voids between particles in fine and coarse aggregates were determined. The bulk densities (derived from Tables A7 and A8, Appendix A) are depicted in Table 4.1. RAP materials had lower loose and rodded bulk density than that of virgin aggregates. RAP materials also showed higher void space than that of virgin aggregates. The higher the void space between aggregate particles, the higher the amount of cement paste required to fill the total surface area that must be covered (John, 2011). Hence, the RAP materials might need a higher amount of cement paste in order to produce quality concrete.

The ACV test done on the CRAP exhibited anomalous result. The test specimen compressed into a single solid mass under loading. This might be due to the presence of asphalt film around RAP that could bind the crushed aggregates into a single solid dense mass. The ACV and AIV values of CVA and CRAP were below the maximum limit (45%) stipulated in IS 383, (2002). CRAP had lower ACV and AIV values (15.92 and 9.83%) than that of CVA (18.73 and 15.51%) respectively. ACV and AIV give relative measures of the resistance of an aggregate to crushing under a gradually

applied compressive and sudden shock or impact load respectively. Therefore, the CRAP might be tougher than the CVA and might also perform better in preventing crushing, degradation and disintegration. The test result may also be a likely sign that RAP is a less brittle and can absorb more impact load than the CVA.

The specific gravity of RHA (2.03) was less than that of cement (3.12) by 35%. The bulk density of RHA was also about 33% of that of cement. The lower the specific gravity and bulk density of RHA may result in a reduction of concrete density. The maximum particle size of OPC and RHA were 90 and 100 µm respectively.

X-ray fluorescence (XRF) was used in order to analyze major chemical components of OPC, RHA, FRAP and FVA (Table 4.2). The sum of the silicon dioxide (SiO_2), aluminium oxide (Al_2O_3) and iron oxide (Fe_2O_3) contents of RHA was 94.8%. This is an indication that RHA fulfilled the 70% minimum requirement of BS EN 450-1 (2012) to be used as a good pozzolana. The free calcium oxide (CaO) content was less than the upper bound (1.5%) specified in BS EN 450-1 (2012). This indicates the ability of the RHA to convert the free lime (Calcium hydroxide) to a C-S-H gel (BS EN 450-1, 2012). The loss on ignition (LOI) of RHA was higher than that of cement, but still within the limits (12%) specified in BS EN 450-1 (2012). LOI denotes the amount of unburnt carbon residue in the RHA that is responsible for an increase in water demand (Chao et al., 2011) which could have an effect on the fresh concrete property that is low workability.

Table 4.2 Chemical composition of materials

Major Components (%)	Chemical Composition (% by mass)			
	Cement	RHA	FRAP	FVA
CaO	63.38	0.86	2.00	1.03
SiO_2	20.62	92.97	58.85	80.00
Al_2O_3	5.06	0.93	15.6	11.00
MgO	0.82	0.48	0.04	2.00
Na_2O	0.16	2.43	6.20	3.20
K_2O	0.53	2.54	4.30	2.50
TiO_2	-	-	0.85	0.16
MnO	-	-	0.29	0.02
Fe_2O_3	3.23	0.88	5.44	1.00
C_3A	7.90	-	-	-
SO_3	2.76	4.84	-	-
Loss on ignition (LOI)	2.91	7.40	10.00	0.90

The physical and chemical properties of superplasticizers used in this study are given in Table 4.3.

Table 4.3 Properties of superplasticizers

Property	Superplasticizer	
	Sikament NNG	Sika ViscoCrete 3088
Appearance/color	Dark brown liquid	Yellowish liquid
Density (kg/l)	1.2	1.06
pH value	8	5.5
Chemical base	Naphthalene formaldehyde sulphonate	Aqueous solution of modified polycarboxylate
Dosage	0.5–3.0% by weight of cement	0.2–2% by weight of cement

4.3   Fresh and Hardened Concrete Properties

4.3.1   Fresh Concrete Properties

Fresh concrete was assessed in terms of slump, compacting factor and fresh density. Tables 4.4, 4.5 and 4.6 show the slump, compaction factor (CF) and density of fresh concrete incorporating RHA, RAP and both RHA and RAP respectively.

i. Slump

From trial mixes, it was observed that the partial replacement of cement by RHA caused a dramatic decrease in slump as compared to the control mix. The Sikament NNG SP was added to the mix in order to attain the desired workability. Experimental test result depicted in Figure 4.3a. shows that the slump increased by 23.33% from 60 to 74 mm at 5% RHA and 0.5% SP contents (by weight of cementitious material). Surprisingly, it was also discovered that as the content of RHA increased, the slump decreased considerably despite increasing the dosage of SP.

(**a**) RHA inclusive concrete   (**b**) RAP inclusive concrete
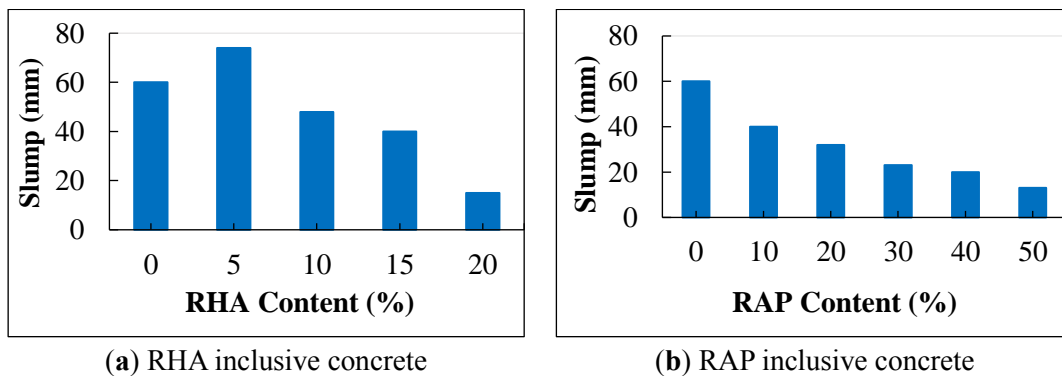
Figure 4.3 Slump of RHA and RAP inclusive concrete

The water demand of the mix increased dramatically when the RHA content increased that resulted in decrease in the slump by 20, 33.33, and 75% from 60mm to 48, 40, and 15mm at 10, 15, and 20% RHA with the addition of 0.85, 2, and 2.75% SP respectively.

The high-water demand might be attributed to the large specific surface area and high unburnt carbon content of RHA.

Like that of RHA inclusive concrete, the partial replacement of virgin aggregate by RAP resulted in a substantial decrease of slump as compared to the control mix as can be seen in Figure 4.3b. The slump decreased by 33, 47, 62, 67, and 78% from 60 mm to 40, 32, 23, 20, and 13 mm at 10, 20, 30, 40, and 50% RAP content respectively. The reduction in slump might be attributed to absorption of the mixing water by the fine dust layers around the RAP periphery. In addition, water might also be controlled by RAP particle and was not able to move freely.

The inclusion of both RHA and RAP in the mix was found to decrease the slump significantly as expected. However, there was a slight (3%) enhancement in the slump when 0.5% Sika ViscoCrete 3088 SP was added to the concrete mix containing 5% RHA and 10% RAP as shown in Figure 4.4. The slump decreased steadily as the RHA and RAP content increased regardless of the increases of SP dosages. This may be attributed to the combined effects of RHA and RAP as already discussed.
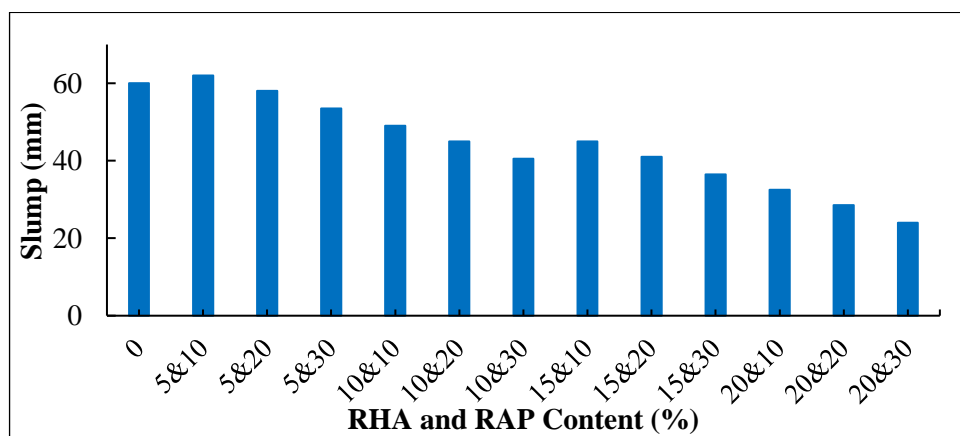

Figure 4.4 Slump of both RHA and RAP inclusive concrete

ii. Compaction Factor

The compacting factor (CF) test measures the inherent characteristics of fresh concrete and used to depict the workability of concrete. The CF values of the concrete ranged from 0.758 to 0.953 which are within the ranges specified in BS 1881-103 (1993) as shown in Tables 4.4, 4.5 and 4.6.

Table 4.4 Fresh properties of RHA inclusive concrete

Fresh Properties	Mix Designation (RHA)%				
	Control	(5)	(10)	(15)	(20)
Slump (mm)	60	74	48	40	15
Compaction Factor (CF)	0.935	0.944	0.912	0.908	0.758
Fresh Density (g/cm^3)	2.480	2.441	2.408	2.399	2.386

Table 4.5 Fresh properties of RAP inclusive concrete

Fresh Properties	Mix Designation (RAP)%					
	Control	(10)	(20)	(30)	(40)	(50)
Slump (mm)	60	40	32	23	20	13
Compaction Factor (CF)	0.935	0.931	0.922	0.921	0.902	0.892
Fresh Density (g/cm^3)	2.480	2.442	2.414	2.395	2.367	2.339

The CF of RHA inclusive concrete increased by 1% at 5% RHA content, whereas CF decreased by 19% as the RHA content increased to 20%. Figure 4.5a and Equation (4.1) (obtained by regression) show the relationship between slump and compaction factor. R^2 and standard error of estimate (SEE) of the model were 0.958 and 0.012 respectively. The CF values of concrete containing RHA ranged from 0.758 to 0.944 as shown in Table 4.4. This implies that the measurement of CF is suitable for determining the workability of concrete containing RHA since the values obtained were within the range 0.70 to 0.98 pursuant to BS 1881-103.

Similarly, the CF values of RAP inclusive concrete ranged from 0.892 to 0.930 which were within limits specified in BS 1881-103. The CF of RAP-inclusive concrete decreased by 5% from 0.935 to 0.892 at 50% RAP content relative to the control mix. Figure 4.5b and Equation (4.2) (obtained by regression) illustrate the relationship between slump and compaction factor. R^2 and SEE of the model were 0.965 and 0.002 respectively.

(**a**) RHA inclusive concrete   (**b**) RAP inclusive concrete
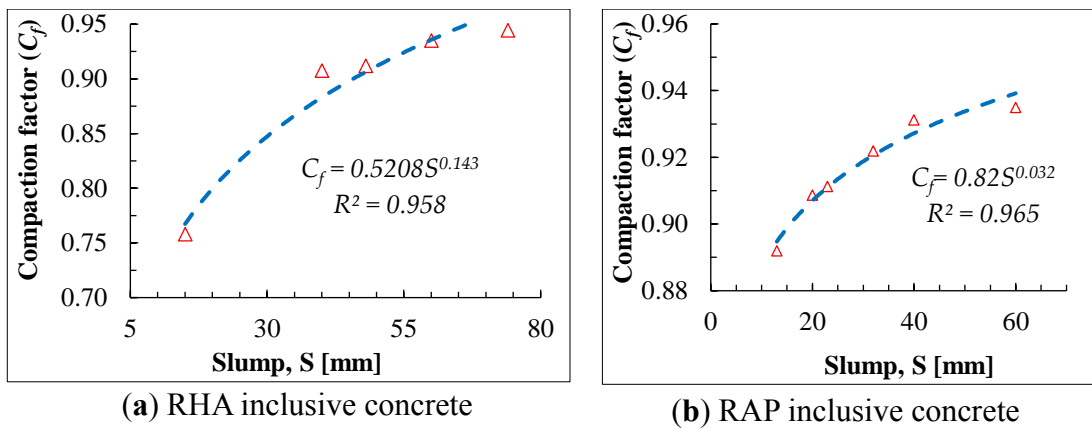
Figure 4.5 Relationship between slump and compaction factor

$$C_f = 0.52 \times S^{0.143} \tag{4.1}$$

where: C_f is compacting factor and S is the slump in mm for fresh RHA concrete

$$C_f = 0.82 \times S^{0.032} \tag{4.2}$$

where: C_f is the compacting factor and S is the slump in mm for fresh RAP concrete

The CF values of both RHA and RAP inclusive concrete also were within the BS 1881-103 limits as can be seen in Table 4.6.

Table 4.6 Fresh properties of both RHA and RAP inclusive concrete

Fresh Properties	Mix Designation (RHA + RAP) %					
	(5 + 10)	(5 + 20)	(5 + 30)	(10 + 20)	(10 + 30)	(10 + 30)
Slump (mm)	62.0	58.0	53.5	49.0	45.0	40.5
Compaction Factor (CF)	0.953	0.948	0.943	0.937	0.932	0.927
Fresh Density (g/cm^3)	2.441	2.427	2.418	2.421	2.411	2.401
Fresh Properties	(15 + 10)	(15 + 20)	(15 + 30)	(20 + 10)	(20 + 20)	(20 + 30)
Slump (mm)	45.0	41.0	36.5	32.5	28.5	24.0
Compaction Factor (CF)	0.934	0.930	0.924	0.860	0.855	0.850
Fresh Density (g/cm^3)	2.421	2.407	2.397	2.414	2.400	2.391

The CF values ranged from 0.850 to 0.953. A slight increase was observed in CF values at 5% RHA & [10–30] % RAP content, whereas CF decreased marginally for the remaining mixes. Figure 4.6 (obtained by regression) depicts the relationship between slump and compaction factor for both RHA and RAP inclusive concrete. R^2 and SEE of the model were 0.894 and 0.013 respectively.

$$C_f = -0.0001S^2 + 0.0117S + 0.617$$
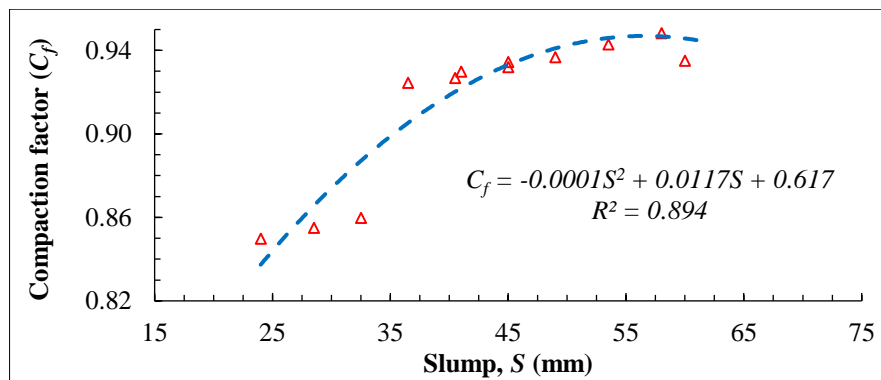$$R^2 = 0.894$$

Figure 4.6 Relationship between slump and compaction factor

The relationships between slump and compacting factor shown above can be used if one of the equipment is not available.

iii. Fresh Density

The fresh density of RHA inclusive concrete decreased by 3.8% from 2480 to 2386 kg/m^3 when the RHA content in the mix increased from 0 to 20% as can be seen from Table 4.4. The reduction in fresh density might be due to the fact that the particle density of RHA (2.03) was lower than that of cement (3.12). The relationship between fresh density and RHA content (obtained by regression) is depicted in Figure 4.7a. R^2 and SEE of the model were 0.990 and 0.008 respectively.

The mix incorporating RAP revealed relatively lower fresh density as compared to the mix containing virgin aggregates. The fresh density of RAP inclusive mix decreased by 5.7% from 2480 to 2339 kg/m^3 as the RAP content in the mix increased from 0 to 50% (see Table 4.5). The reduction in density might be attributed to the fact that specific gravities of both FRAP and CRAP were lower than those of both FVA and CVA respectively. Figure 4.7b (obtained by regression) gives the relationship between fresh density and RAP content. R^2 and SEE of the model were 0.993 and 0.005 respectively.

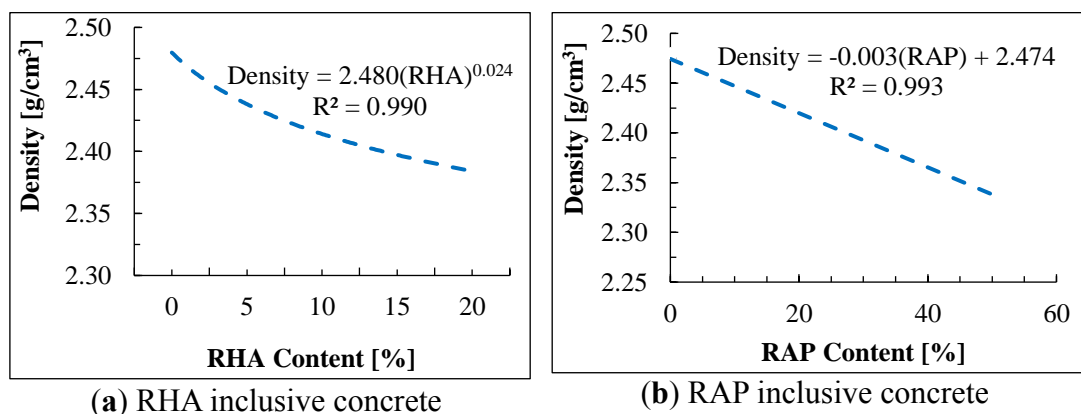(**a**) RHA inclusive concrete   (**b**) RAP inclusive concrete

Figure 4.7 Fresh density of concrete

The fresh density for mixes containing both RHA and RAP is graphically depicted in Figure 4.8. It was observed that the mixes containing both RHA and RAP had lower

fresh density compared to the control mix. The mix incorporating 20% RHA and 30% RAP showed 3.6% reduction in fresh density relative to that of the control mix. The reduction in fresh density might be attributed to the collective effects pertaining to RHA and RAP as has been explained.
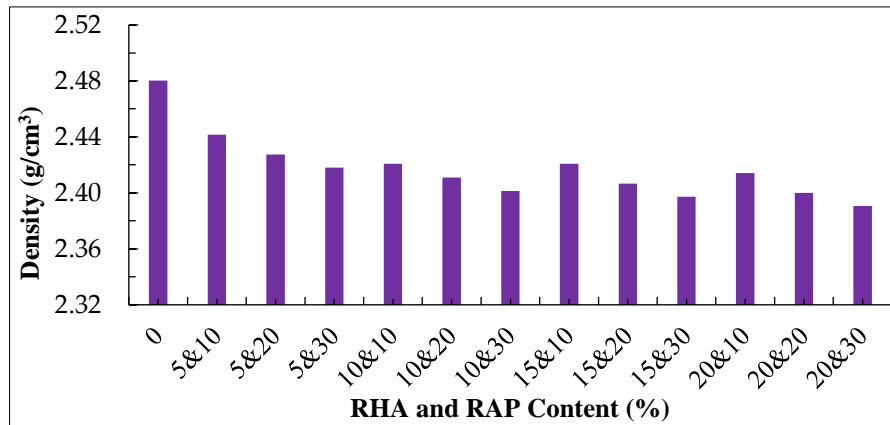
Figure 4.8 Fresh density for both RHA and RAPinclusive concrete.

4.3.2 Hardened Concrete Properties

The most important hardened properties of concrete used as major indicators of general quality control and important criteria to determine the durability of concrete are discussed under this section. Hardened concrete was assessed in terms of compressive, tensile splitting, and flexural strengths, water absorption, permeable void spaces, sorptivity and hardened densities. The Compressive strength (CS), tensile splitting strength (TSS), water absorption (w), permeable void spaces (v) and sorptivity (k) test results are presented in Table 4.7. Average value of three replicate specimens for each test are presented in the table. The values given in parentheses are the standard deviation of the three replicates.

Table 4.7 Hardened concrete properties

Mix Description	CS (MPa)		TSS (MPa)	w [%]	v [%]	K [mm/h$^{1/2}$]
	7 Days	28 Days	28 Days			
Control	17.34 (0.41)	26.72 (0.42)	2.13 (0.13)	7.24 (0.18)	17.33 (0.01)	1.96 (0.02)
RHA5%	19.42 (0.61)	27.90 (0.75)	2.19 (0.20)	7.19 (0.30)	17.09 (0.29)	1.92 (0.06)
RHA10%	20.13 (0.71)	29.60 (0.73)	2.26 (0.06)	7.16 (0.18)	17.02 (0.60)	1.90 (0.25)
RHA15%	21.23 (0.41)	30.05 (0.79)	2.29 (0.01)	7.15 (0.11)	16.90 (0.40)	1.80 (0.78)
RHA20%	20.90 (0.80)	29.13 (0.32)	2.25 (0.09)	7.15 (0.01)	16.77 (0.03)	1.75 (0.11)
RAP10%	16.75 (0.20)	20.87 (0.90)	1.87 (0.06)	6.86 (0.30)	16.86 (0.18)	1.82 (0.20)
RAP20%	16.14 (0.40)	19.56 (0.0.5)	1.69 (0.07)	6.74 (0.09)	16.61 (0.08)	1.30 (0.02)
RAP30%	14.51 (0.40)	17.86 (0.08)	1.50 (0.01)	6.65 (0.19)	16.28 (0.64)	1.16 (0.13)
RAP40%	12.73 (0.60)	16.36 (0.07)	1.39 (0.10)	6.54 (0.20)	15.98 (0.47)	0.91 (0.03)
RAP50%	11.08 (0.30)	14.87 (0.12)	1.26 (0.04)	6.45 (0.30)	15.68 (0.65)	0.69 (0.01)
[5RHA & 10RAP]%	18.37 (0.75)	23.00 (0.68)	2.05 (0.03)	6.69 (0.15)	16.94 (0.16)	1.88 (0.27)
[5RHA & 20RAP]%	16.90 (0.38)	21.42 (0.47)	1.85 (0.10)	6.65 (0.04)	16.79 (0.05)	1.81 (0.08)
[5RHA & 30RAP]%	15.00 (0.84)	19.42 (0.54)	1.77 (0.04)	6.62 (0.08)	16.53 (0.08)	1.69 (0.05)
[10RHA & 10RAP]%	19.66 (0.84)	25.12 (0.66)	2.12 (0.06)	6.68 (0.01)	16.92 (0.11)	1.80 (0.55)
[10RHA & 20RAP]%	17.00 (0.97)	23.62 (0.07)	2.09 (0.01)	6.49 (0.18)	16.72 (0.24)	1.65 (0.18)
[10RHA & 30RAP]%	16.65 (0.38)	20.4 4(0.61)	1.80 (0.03)	6.20 (0.10)	16.64 (0.06)	1.41 (0.17)
[15RHA & 10RAP]%	20.02 (0.55)	27.62 (0.54)	2.22 (0.25)	6.33 (0.06)	16.78 (0.02)	1.87 (0.35)
[15RHA & 20RAP]%	19.54 (0.24)	25.01 (0.56)	2.10(0.03)	6.32 (0.05)	16.76 (0.10)	1.61 (0.07)
[15RHA & 30RAP]%	17.14 (0.13)	21.69 (0.12)	1.89 (0.01)	6.30 (0.07)	16.60 (0.17)	1.47 (0.29)
[20RHA & 10RAP]%	18.95 (0.50)	25.48 (0.14)	2.15 (0.05)	6.30 (0.13)	16.81 (0.45)	1.92 (0.46)
[20RHA & 20RAP]%	17.30 (1.04)	22.19 (0.92)	1.99 (0.01)	6.25 (0.08)	16.88 (0.52)	1.89 (0.04)
[20RHA & 30RAP]%	16.38 (0.43)	20.20 (0.93)	1.79 (0.06)	6.25 (0.11)	16.48 (0.03)	1.65 (0.06)

i. Compressive Strength

The compressive strength (CS) of concrete mixtures containing RHA was studied at 7 and 28-days and the experimental test results are depicted in Figure 4.9a. As can be seen from the figure, RHA enhanced the 7-day CS by 12.0, 16.1, 22.4, and 20.5 % at 5, 10, 15, and 20% RHA content respectively relative to the control mix. Similarly, the 28-day compressive strength was also enhanced by 4.4, 10.8, 12.5, and 9.0% compared to the control mix. The highest strength gain was observed when 15% of cement was substituted by RHA.

It is apparent from the percentage increase in compressive strength that the 7-day strength showed a higher percentage increase than that of the 28-day. This might be due to the fact that calcium-silicate-hydrate (C-S-H) gel was developed more rapidly in RHA inclusive mixtures than that of the control mix at the early ages. This might be attributed to the very reactive nature of RHA due to its high surface area. In general, the enhancement in compressive strength is believed to be a benefit from RHA's siliceous property (SiO_2=92.97% by mass) which, in itself, possesses little cementitious value, but in the presence of water, it reacts chemically with calcium hydroxide to form compounds possessing cementitious properties (ASTM C595, 2003). Thus, RHA might have generated an opportunity to convert the free lime (Calcium hydroxide) to a C-S-H gel that makes the hydrated cement paste strong.

The 7- and 28-days compressive strength test results of RAP inclusive concrete are shown in Figure 4.9b. A dramatic reduction in compressive strength was observed with an increment of RAP content in the concrete mixtures. The 7- and 28-days compressive strength decreased by 36.1 and 44.3% respectively, relative to the control mix at 50% RAP content. The reduction in compressive strength might be attributed to the combined effects of higher porosity in the interfacial transition zone and preferential asphalt cohesion failure that occurs instead of the adhesive failure of the cement-asphalt interface or cohesive failure of the ITZ (Huang, et al, 2013; Ibrahim, et al, 2014).
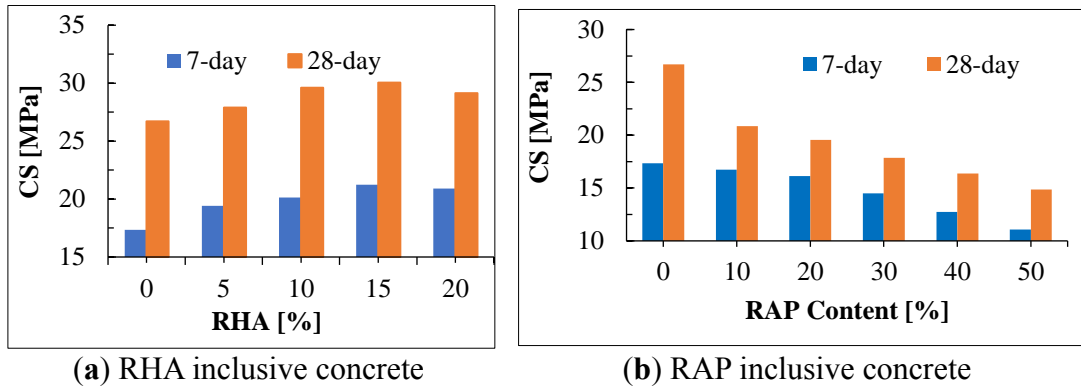
(**a**) RHA inclusive concrete   (**b**) RAP inclusive concrete

Figure 4.9 Compressive strength

The relationship between RHA content and the 28-day CS is given in Figure 4.10a (obtained by regression). The regression model had R^2 and SEE values of 0.950 and 0.444 respectively. The CS decreased linearly with RAP content as shown in Figure 4.10b. From the regression analysis, linear form relationship, Equation (4.3) was found. R^2 and SEE values of the model were 0.902 and 1.476 respectively.

$$f_c = f_{co} - 0.21 \times RAP \tag{4.3}$$

where: f_c is the 28-days CS of the RAP-inclusive concrete in MPa; f_{co} is the 28-days CS of the mix with no RAP content in MPa, and *RAP* is the reclaimed asphalt pavement content in %.

(**a**) RHA inclusive concrete   (**b**) RAP inclusive concrete
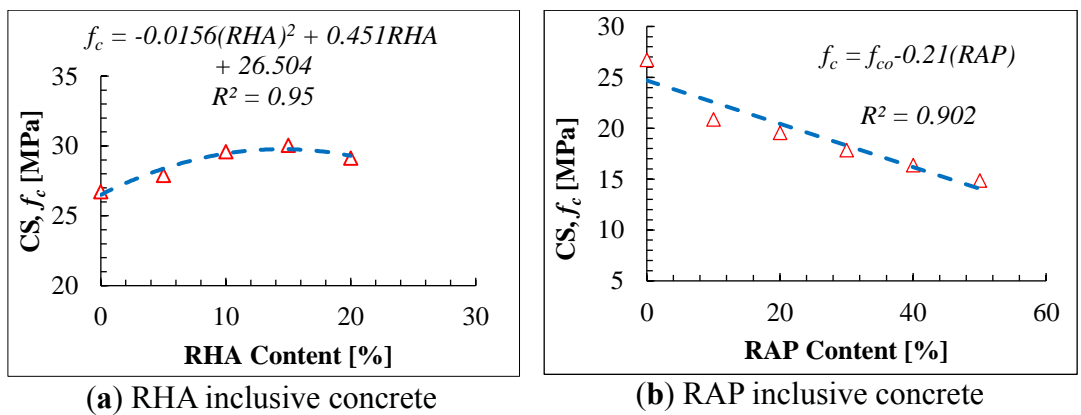
Figure 4.10 Relationship between RHA and RAP contents and CS

Figure 4.11 portrays the compressive strength of both RHA and RAP inclusive concrete at 7 and 28-day. The partial replacement of cement by RHA improved the CS of RAP inclusive concrete moderately. This might be credited to the development of additional C-S-H gel due to the high reactive silica content of RHA and/or filler effect.

Mixtures incorporating 10% RHA and 10% RAP, 15% RHA and 10% RAP, 15% RHA and 20% RAP, and 20% RHA and 10% RAP showed comparable strength. The maximum compressive strength (27.62 MPa) was obtained at 15% RHA and 10% RAP combination. Thus, it is evident that the treatment of RAP by RHA possibly will be an effective way to enhance the mechanical properties of RAP incorporating concrete.
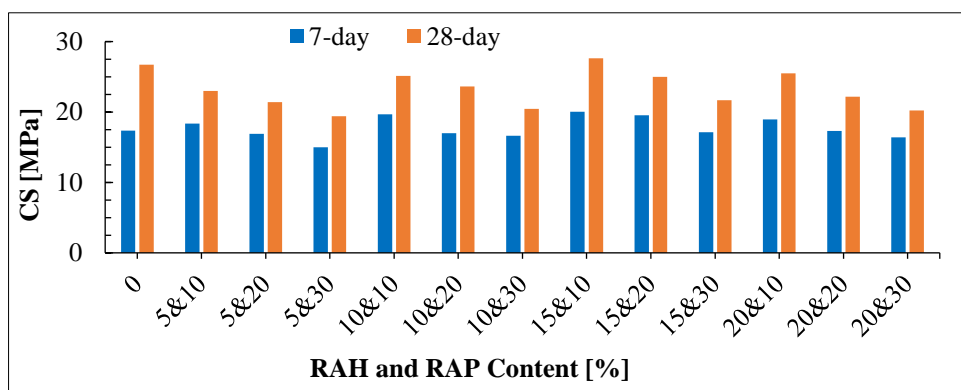
Figure 4.11 Compressive strength for both RHA and RAP inclusive concrete

ii. Tensile Splitting Strength

The 28-day tensile splitting strength (TSS) of the mixtures containing RHA is represented in Figure 4.10a. TSS increased at an increasing rate up to 15% RHA content. The TSS peaked at 15% RHA and then increased at a decreasing rate beyond 15% RHA content. However, still 20% RHA inclusive concrete showed better strength than the control mix. The increment in strength was 2.8, 6.1, 7.5, and 5.6% at 5, 10, 15, and 20% RHA content respectively, relative to the control mix. TSS increased in

a second-order polynomial with RHA content as depicted in Figure 4.12a ($R^2 = 0.96$

and SEE = 0.018). The trend for TSS was similar to that of CS. The increment in TSS

might be ascribed to the development of extra of C-S-H gel due to the active silica

content of RHA as already explained.

TSS decreased linearly with increasing RAP content as can be seen in Figure 4. 12b

($R^2 = 0.98$ and SEE = 0.052). TSS decreased by 12.2, 20.7, 29.6, 34.7, and 40.8% for

10, 20, 30, 40, and 50% RAP respectively. The decreasing pattern for TSS was similar

to that of the CS. However, the rate of strength reduction in the TSS mixtures was

lower compared to the CS's.

(**a**) RHA inclusive concrete   (**b**) RAP inclusive concrete

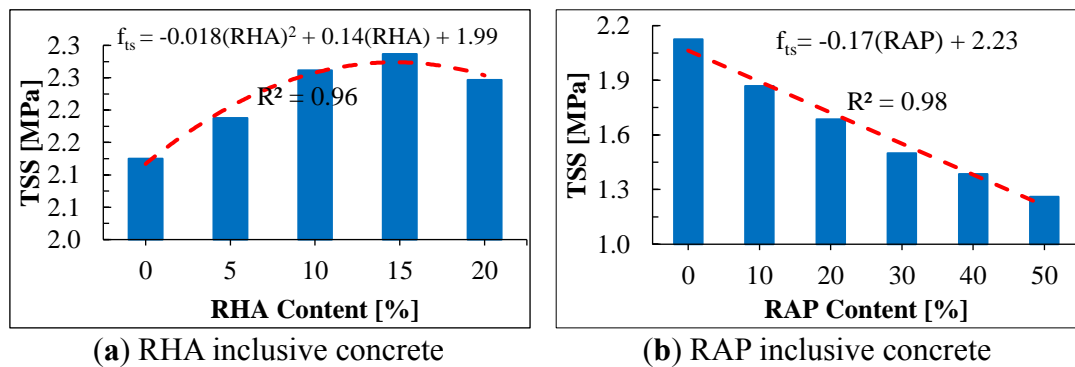**Figure 4.12** Tensile Splitting strength for RHA and RAP inclusive concrete

From the regression analysis, a power form relationship was found between the 28-

day TSS and CS of RHA inclusive concrete as shown in Equation (4.4) and Figure

4.13a ($R^2 = 0.99$ and SEE= 0.004).

$$f_{ts} = 0.28 \times f_c^{0.6} \tag{4.4}$$

where: f_c and f_{ts} are the 28-days CS and TSS of the RHA inclusive concrete

respectively, in MPa.

The exponential form relationship was found between the 28 days TSS and CS of RAP inclusive concrete as presented in Figure 4.13b (R^2 = 0.97 and SEE = 0.0526). Equations (4.5) and (4.6) were obtained by regression.

$$f_{ts} = -0.17 \times RAP + 2.23 \tag{4.5}$$

$$f_{ts} = 0.105 \times f_c^{0.93} \tag{4.6}$$

where: f_c and f_{ts} are the 28-days CS and TSS of the RAP inclusive concrete respectively, in MPa.

(**a**) RHA inclusive concrete   (**b**) RAP inclusive concrete
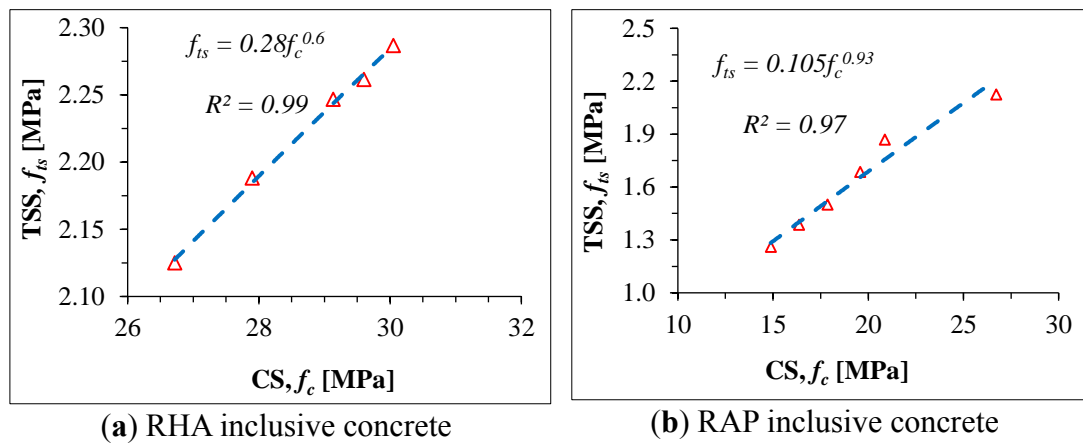
Figure 4.13 Relationship between CS and TSS for RHA and RAP concrete

The experimental results of TSS of both RHA and RAP inclusive concrete and its relationship with CS are depicted in Figures 4.14 and 4.15 respectively. TSS improved by 4.7% relative to the control at 15% RHA and 10% RAP content. The enhancement in tensile splitting strength might be accredited to the high reactive silica content of RHA. TSS and CS were positively correlated (R^2 = 0.928 and SEE = 0.065) with a power function as given in Equation (4.7).

$$f_{ts} = 0.235 \times f_c^{0.68} \tag{4.7}$$
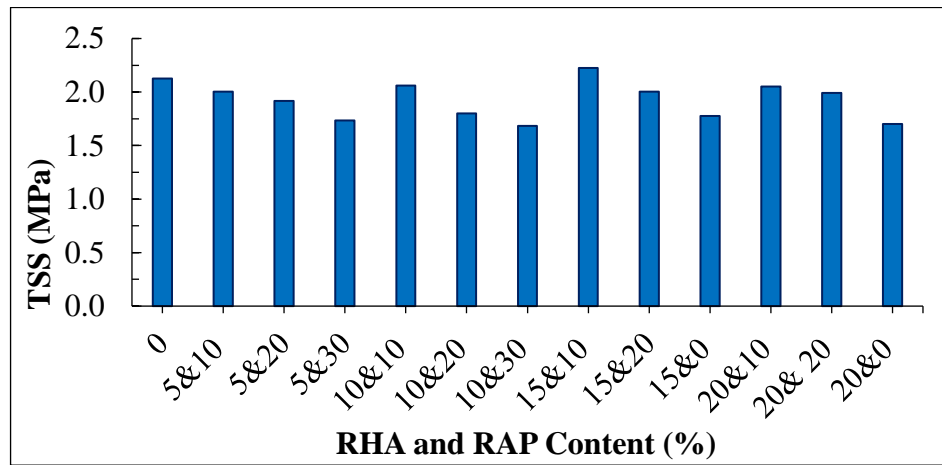
Figure 4.14 Tensile splitting strength for RHA and RAP inclusive concrete

$$f_{ts} = 0.235 f_c^{0.680}$$
$$R^2 = 0.928$$
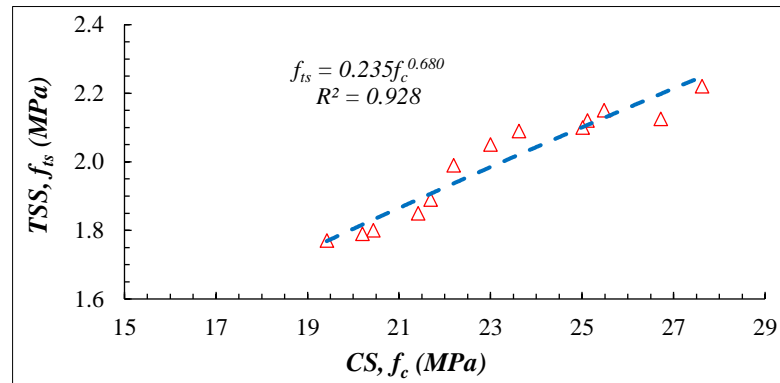
Figure 4.15 Relationship between TSS and CS for both RHA and RAP inclusive concrete

iii. Flexural Strength

Flexural strength test results are presented in Table 4.8. There was a slight improvement in flexural strength (0.81%) at 15 % RHA and 10 % RAP combination compared to the control mix. The flexural strength decreased by 9.18% at 20 % RHA and 20% RAP relative to the control specimens.

Table 4.8 Flexural strength

Mix Designation	Flexural Strength (MPa)				Standard Deviation (MPa)
	Sample 1	Sample 2	Sample 3	Average	
Control	3.278	3.305	3.281	3.288	0.012
15%RHA&10%RAP	3.315	3.302	3.327	3.315	0.010
20%RHA&20RAP%	2.998	2.895	2.986	2.960	0.046

iv. Hardened Density

The dry bulk density (DBD), bulk density after immersion (BDI), bulk density after immersion and boiling (BDIB) and apparent density (AD) of RHA inclusive concrete at 28 days were found to decrease slightly with increasing RHA content in the mixes. As can be seen from Figure 4.16, the least hardened densities (HDs) recorded were 2322, 2488, 2490 and 2790 kg/m^3 for DBD, BDI, BDIB and AD respectively at 20% RHA content. The maximum percentage reduction in HD was observed to be 1.2, 1.3, 1.4 and 1.9 % for the corresponding least HDs while the highest HDs obtained were 2347, 2516, 2518 and 2831 kg/m^3 for DBD, BDI, BDIB and AD respectively, at 5% RHA content. The minimum percentage of reduction in HD were 0.2, 0.2, 0.3 and 0.5% for the corresponding highest HDs.

The reduction in density could be due to the fact that the particle density of RHA was 34.9% lower than that of cement. The bulk dry density fell in the range between 2000 and 2600 kg/m^3. Thus, the RHA inclusive concrete is classified as normal weight concrete according to BS EN 206 (2014).
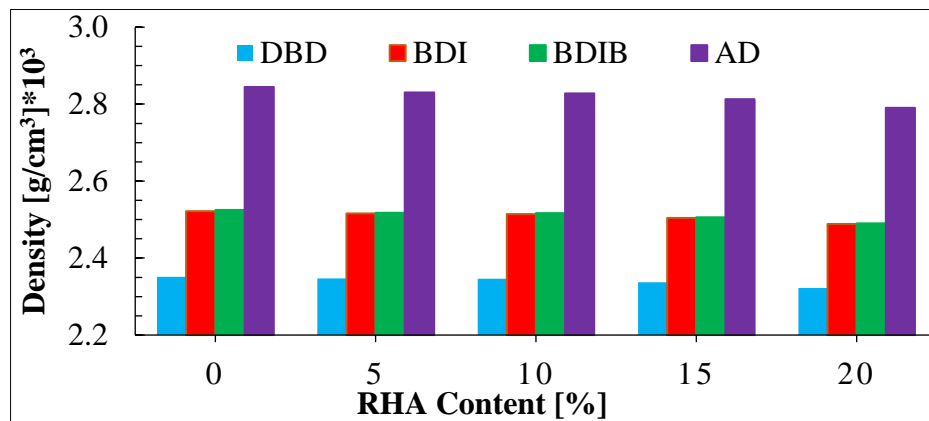

Figure 4.16 Hardened density of RHA inclusive concrete

The HDs of RAP inclusive concrete at 28 days are depicted in Figure 4.17. The replacement of natural aggregates by FRAP and CRAP resulted in a moderate reduction of HD. A linear percentage reduction of HD was observed with an increase of RAP content in the mixtures. It is apparent from Figure 4.17 that the least HDs obtained were 2269, 2416, 2426 and 2692kg/m^3 for DBD, BDI, BDIB and AD respectively at 50% RAP content.
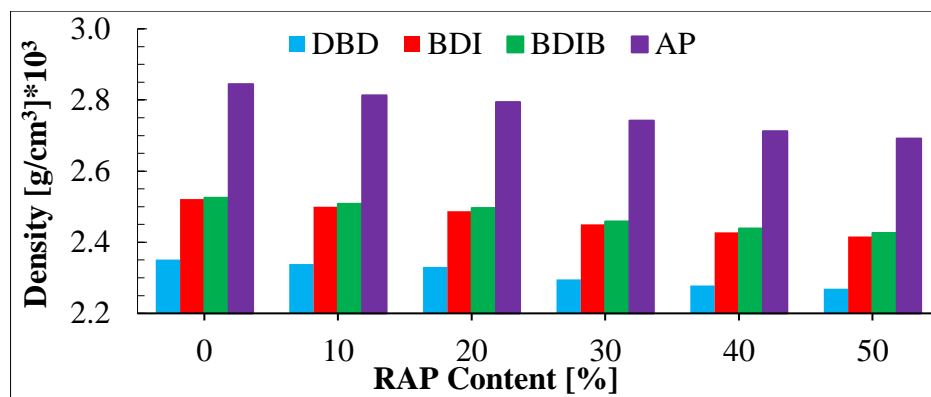
Figure 4.17 Hardened density of RAP inclusive concrete

The maximum percentage of reduction in HD were observed to be 3.5, 4.2, 3.9 and 5.3% for the corresponding least HDs relative to that of the control specimens. The highest HDs found were 2339, 2499, 2508 and 2813 kg/m^3 for DBD, BDI, BDIB and AD respectively at 10% RAP content. The corresponding percentage reduction in these highest HDs were 0.5, 0.9, 0.7 and 1.1% respectively. The reduction in density might be explained by the fact that the particle densities of FRAP and CRAP were 4.5 and 8.0% lower than that of FVA and CVA respectively. However, the DBD fell within the range of normal-weight concrete [2000 to 2600 kg/m^3] as per BS EN 206 (2014).

The results for the HDs of RHA and RAP inclusive concrete at 28 days are depicted in Figure 4.18. As can be seen from these results, the HD decreased as RHA and RAP content increased. Surprisingly, the percentage reduction of HD is lower than both

those of RHA inclusive concrete and RAP inclusive concrete. The least densities found were 2336, 2482, 2501 and 2797 kg/m^3 for DBD, BDI, BDIB and AD respectively at 20%RHA and 30% RAP combination.

The maximum percentage of reduction in HD were observed to be 0.6, 1.6, 1.0 and 1.7% for the corresponding least HDs relative to that of the control specimens. Whereas, the highest density of 2345, 2502, 2514 and 2823 kg/m^3 were recorded for DBD, BDI, BDIB and AD respectively at 5% RHA and 10% RAP combination. The minimum percentage of reduction in HD were 0.3, 0.8, 0.4 and 0.71% for the corresponding highest HDs.
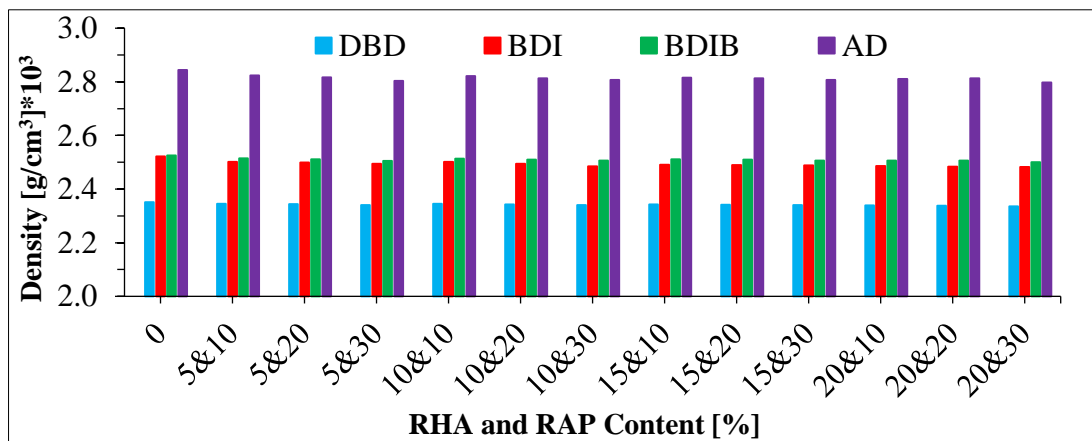
Figure 4.18 Hardened density for both RHA and RAP inclusive concrete

The DBDs of RHA and RAP inclusive concrete were also within the range of normal-weight concrete [2000 to 2600 kg/m^3] as per BS EN 206 (2014) requirements. Reduction in density can result in significant savings in construction cost as smaller sections for supporting concrete members could be selected. Nevertheless, the reduction in concrete density might also lead to a reduction in concrete strength.

v. Water Absorption

The water absorption (derived from Table B2, Appendix B) after immersion (w_i) and after immersion and boiling ($w_{i\&b}$) decreased with increasing RHA content as shown in Figure 4.19a. The minimum relative percentage of reduction in water absorptions were 0.7 and 1.2% for w_i and $w_{i\&b}$ respectively at 5% RHA content, whereas the maximum relative percentage of reduction in absorption were 1.3 and 2.0% for w_i and $w_{i\&b}$ respectively at 20% RHA content. This reduction could be due to the fact that the finer RHA particles might have filled the pore spaces of the concrete. The water absorption is correlated to RHA content in a power function as shown in Equations (4.8) and (4.9). The $w_{i\&b}$ values are slightly higher than those of w_i.

The water absorption of RAP inclusive concrete decreased with increasing RAP content, as can be seen from Figure 4.19b (derived from Table B2, Appendix B). The minimum w_i and $w_{i\&b}$ were 6.4 and 6.9% with relative percentage reduction of 10.94 and 6.20% respectively at 50% RAP content. The reductions in water absorption might be due to the low water absorption of RAP aggregates compared to that of virgin aggregate. The other possible reason could be due to the melted asphalt and dust layer engulfed around the aggregates that might fill void spaces in the hardened concrete. The water absorption is related to RAP content in a power function as shown in Equations (4.10) and (4.11). The $w_{i\&b}$ values were somewhat higher than those of w_i.

(**a**) RHA inclusive concrete　　　　　　(**b**) RAP inclusive concrete
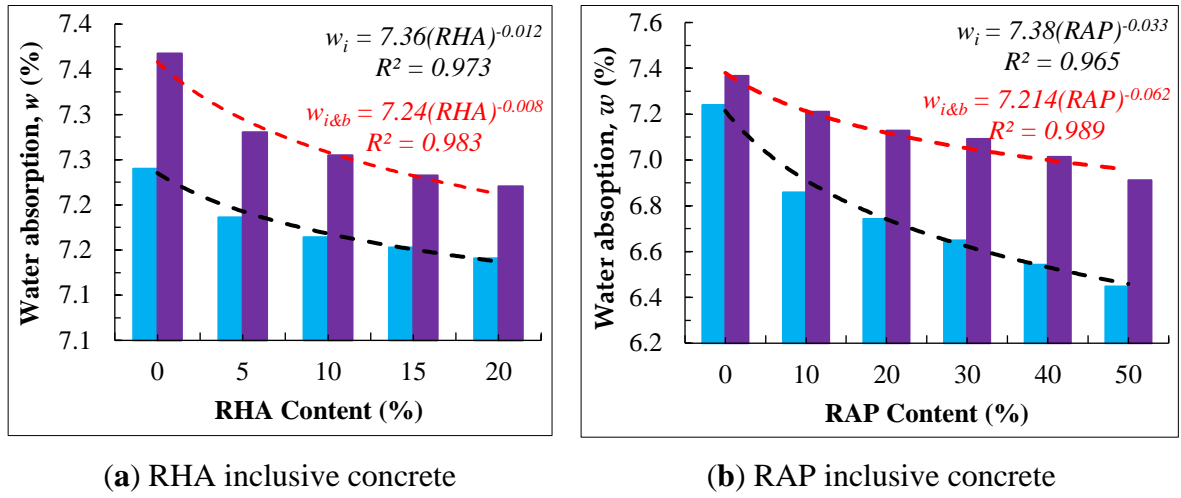
Figure 4.19 Water absorption by RHA and RAP inclusive concrete

$$w_i = 7.36 \times RHA^{-0.012} \tag{4.8}$$

$$w_{i\&b} = 7.24 \times RHA^{-0.008} \tag{4.9}$$

$$w_i = 7.38 \times RAP^{-0.033} \tag{4.10}$$

$$w_{i\&b} = 7.24 \times RAP^{-0.062} \tag{4.11}$$

where: w_i is the water absorption after immersion in %; $w_{i\&b}$ is the water absorption after immersion and boiling; RHA is the rice husk ash content in % and RAP is reclaimed asphalt pavement content in %.

The water absorption of RHA and RAP inclusive concrete at 28 days are depicted in Figure 4.20 (derived from Table B2). Both w_i and $w_{i\&b}$ decreased as RHA and RAP content increased. The relative percentage reduction of $w_{i\&b}$ (13.7%) was more than both that of RHA inclusive concrete (1.30%) and RAP inclusive concrete (10.94%). The least w_i and $w_{i\&b}$ found were 6.25 and 7.06% respectively at 20% RHA and 30% RAP combination. The maximum relative percentage of reduction in absorption were 13.7 and 4.2% for the respective least absorptions. The reduction of water absorption might be due to the collective effect of RHA and RAP discussed above.

80
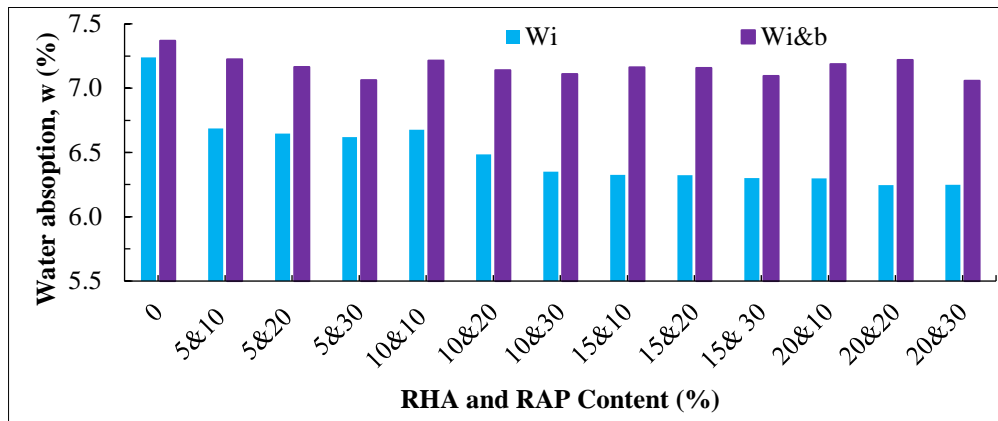
Figure 4.20 Water absorption by both RHA and RAP inclusive concrete

Water absorption measures the total amount of water that penetrates into concrete samples when submerged. The lower the absorption, the better the performance of concrete. High water absorption has an adverse effect on the durability of concrete, especially in aggressive environments. Therefore, based on the results of this study, the concrete incorporating RHA and RAP can be regarded as durable concrete holding other factors constant.

vi. Volume of Permeable Void Spaces

The volume of permeable void spaces in hardened RHA inclusive concrete decreased slightly with an increment of RHA content. The voids decreased by 3.22% from 17.32 to 16.77% as the RHA content increased from 0 to 20%. The reduction in void space might be attributed to the finer siliceous particles which could fill a portion of void spaces that exist in the concrete matrix. As can be seen from Figure 4.21a and Equation (4.12), a power function was found as a good fit ($R^2 = 0.970$ and SEE = 0.026) to correlate RHA content with the voids.

81

Figure 4.21b depicts the volume of permeable void spaces in RAP inclusive concrete. It is clear from the figure that voids decreased exponentially with the increment of RAP content. The voids decreased by 9.47% from 17.32 to 15.68% as the RAP content increased from 0 to 50%. The reduction in void space could be due to the oozed out asphalt film which could fill a portion of voids spaces in the concrete. As can be seen from Equation (4.13), an exponential function was obtained from the regression analysis to correlate RAP content with the voids ($R^2 = 0.995$ and SEE = 0.024).

(**a**) RHA inclusive concrete   (**b**) RAP inclusive concrete
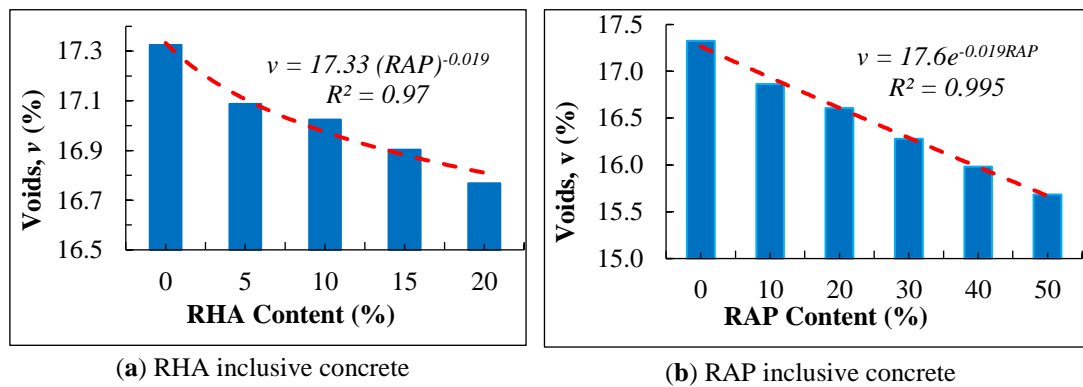
Figure 4.21 Voids in RHA and RAP inclusive concrete.

$$v = 17.33 \times RHA^{-0.019} \tag{4.12}$$

$$v = 17.36 \times e^{-0.019 \times RAP} \tag{4.13}$$

where: v is the volume of permeable void spaces in %; RHA is the rice husk ash content in % and RAP is the reclaimed asphalt pavement content in %.

A relationship between voids and water absorption for RHA concrete was determined as shown in Figure 4.22a and Equations (4.14) and (4.15). According to the correlation found, water absorption decreased exponentially as the void in concrete decreased. Water absorption by RAP concrete decreased exponentially with voids in concrete as shown in Figure 4.22b, and Equations (4.16) and (4.17).

(**a**) RHA inclusive concrete (**b**) RAP inclusive concrete
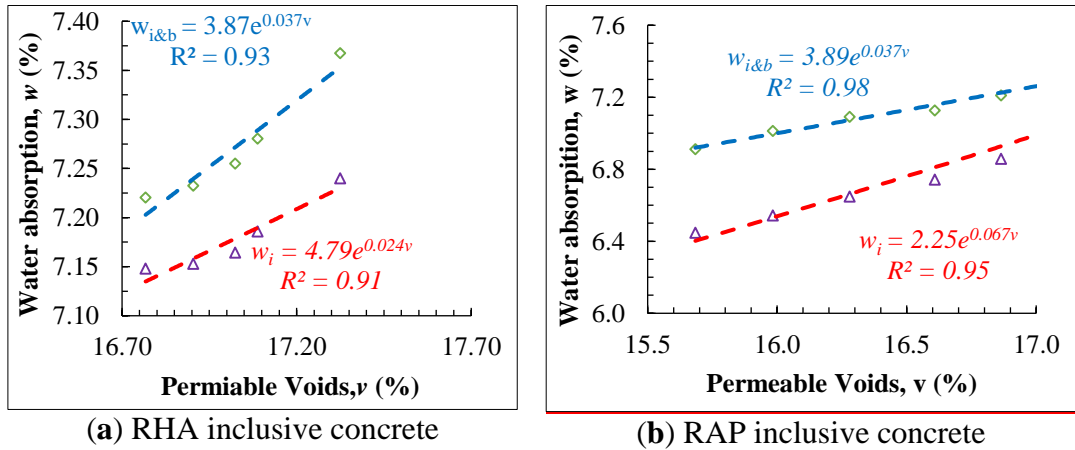
Figure 4.22 Relationship between water absorption and voids

$$w_i = 4.79 \times e^{0.024 \times v} \tag{4.14}$$

$$w_{i\&b} = 3.87 \times e^{0.027 \times v} \tag{4.15}$$

$$w_i = 2.25 \times e^{0.067 \times v} \tag{4.16}$$

$$w_{i\&b} = 3.89 \times e^{0.037 \times v} \tag{4.17}$$

where: w_i is absorption after immersion in %; $w_{i\&b}$ is absorption after immersion and boiling and v is the volume of permeable void spaces in %.

The volume of permeable void spaces in both RHA and RAP inclusive concrete is portrayed in Figure 4.23. As expected, the relative percentage of reduction of voids (4.86%) in both RHA and RAP inclusive concrete is higher than that of RHA inclusive concrete (3.22%) but lower than that of RAP inclusive concrete (9.47) by 1.64 and 4.61% respectively.
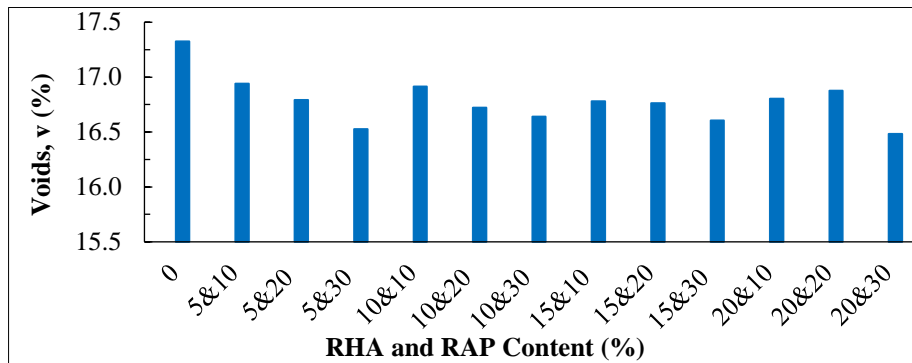
Figure 4.23 Void in both RHA and RAP inclusive concrete

The durability of concrete is mainly dependent on the capacity of a fluid to penetrate the concrete's microstructure that is called permeability. The permeability of concrete has a strong relationship with the characteristics of its pore structure in the cement paste and the intensity of microcracks at the aggregate-cement paste interface as well as within the paste itself. High permeability leads to the introduction of molecules that react and destroy its chemical stability. Whereas, low permeability of concrete can improve resistance to the penetration of water, sulphate ions, chloride ions, alkali ions, and other harmful substances that caused a chemical attack (Zhang & Zong, 2014). Concrete containing RHA and RAP showed desirable permeable void spaces in this regard.

vii. Sorptivity

The sorptivity by RHA concrete (derived from Figure B1, Appendix B), shown in Table 4.9, was obtained from the slope of the line that is the best fit to the cumulative amount of water absorption (I) plotted against the square root of time ($t^{1/2}$). The sorptivity by RAP inclusive concrete (derived from Figure B2, Appendix B) is tabulated in Table 4.10.

Table 4.9 Sorptivity by RHA inclusive concrete

RHA Content [%]	[0]	[5]	[10]	[15]	[20]
Sorptivity, K [mm/h$^{1/2}$]	1.964	1.922	1.899	1.799	1.746
Determination Coefficient [R^2]	0.969	0.976	0.974	0.982	0.977
Correlation Coefficient [R]	0.984	0.988	0.987	0.991	0.988

Table 4.10 Sorptivity by RAP inclusive concrete

RAP Content [%]	[0]	[10]	[20]	[30]	[40]	[50]
Sorptivity (mm/h$^{1/2}$)	1.964	1.816	1.301	1.164	0.908	0.694
Determination Coefficient [R^2]	0.969	0.971	0.989	0.983	0.985	0.993
Correlation Coefficient [R]	0.984	0.985	0.994	0.992	0.993	0.997

The effect of RHA content on the sorptivity of concrete is depicted in Figure 4.24a. As can be seen from Equation (4.18), the sorptivity decreased linearly as the RHA content increased. The sorptivity decreased by 11.1% from 1.964 to 1.746 mm/h$^{1/2}$ when RHA content increased from 0 to 20%. The reduction in sorptivity might be due to the fact that finer RHA particles filled up air voids exist in the concrete matrix, as a result of which the rate of ingress of water was inhibited.

The influence of RAP content on the sorptivity of concrete is also portrayed in Figure 4.24b. Sorptivity decreased significantly as the content of RAP increased. A linear relationship (see Equation (4.19)) was found between RAP content and sorptivity. Similar findings were reported in the previous studies (Ibrahim et al, 2014). The main reason being given for the reduction in sorptivity was the melted asphalt layer surrounding the RAP aggregates. In addition, the authors of this study believed that the reduction in sorptivity might also be ascribed to the lower water absorption by the RAP aggregates compared to that of the virgin aggregates.

(a) RHA inclusive concrete (b) RAP inclusive concrete
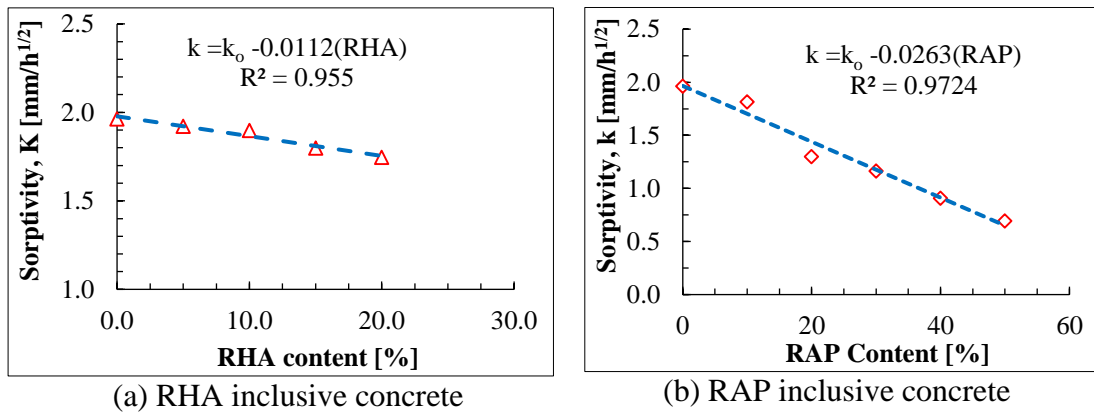
Figure 4.24 Relationship between sorptivity and RHA and RAP contents

$$k = k_O - 0.0112 \times RHA \qquad (4.18)$$

where: k and k_o are the sorptivity by RHA-inclusive concrete and concrete without RHA respectively in mm/h$^{1/2}$ and *RHA* is the rice husk ash content in %.

$$k = k_O - 0.0236 \times RAP \qquad (4.19)$$

where: k and k_o are the sorptivity by RAP inclusive concrete and concrete without RAP, respectively in mm/h$^{1/2}$ and *RAP* is reclaimed asphalt pavement content in %.

The sorptivity by both RHA and RAP inclusive concrete (derived from Figures B3–B6, Appendix B) is tabulated in Table 4.11.

Table 4.11 Sorptivity by both RHA and RAP inclusive concrete

RHA and RAP Content	Sorptivity [mm/h$^{1/2}$]	Determination Coefficient (R^2)	Correlation Coefficient (R)
Control	1.964	0.9688	0.984
5% RHA & 10% RAP	1.883	0.971	0.985
5% RHA & 20% RAP	1.808	0.975	0.987
5% RHA & 30% RAP	1.688	0.978	0.989
10% RHA & 10% RAP	1.801	0.972	0.986
10% RHA & 20% RAP	1.653	0.98	0.990
10% RHA & 30% RAP	1.411	0.986	0.993
15% RHA & 10% RAP	1.867	0.977	0.988
15% RHA & 20% RAP	1.610	0.983	0.991
15% RHA & 30% RAP	1.474	0.973	0.986
20% RHA & 10% RAP	1.919	0.983	0.991
20% RHA & 20% RAP	1.891	0.988	0.994
20% RHA & 30% RAP	1.646	0.982	0.991

It is evident from experimental results that the sorptivity by RHA and RAP inclusive concrete decreased as expected. The reduction in sorptivity ranged from 2.29 to 28.16% relative to the control specimens. The reduction in sorptivity could be due to the combined influences of RHA and RAP as already discussed.

Although sorptivity value alone does not suffice to envisage the service life of a structure (Martys and Ferraris, 1997), according to the research conducted by Hinczak, Conroy and Lewis, cited in the study (Menéndez and Irassar, 2007), a concrete is said to be durable if sorptivity is less than 6 mm/h$^{1/2}$. The experimental results of this study revealed that all concrete specimens had sorptivity values under the limit specified.

Thus, the concrete incorporating RHA and RAP can be considered as durable concrete holding other factors constant.

4.4 Strength Prediction by Artificial Neural Network Model

4.4.1 Artificial Neural Network Architecture

Determining ANN architecture is the first important step for developing the ANN model that best suits the problem at hand. However, there is no guideline for selecting the optimum ANN architecture; it is open to investigation (Ming & Zhou, 2003). Consequently, after many trials and errors, as tabulated in Table 4.12, the network architecture shown in Figure 4.25 was selected
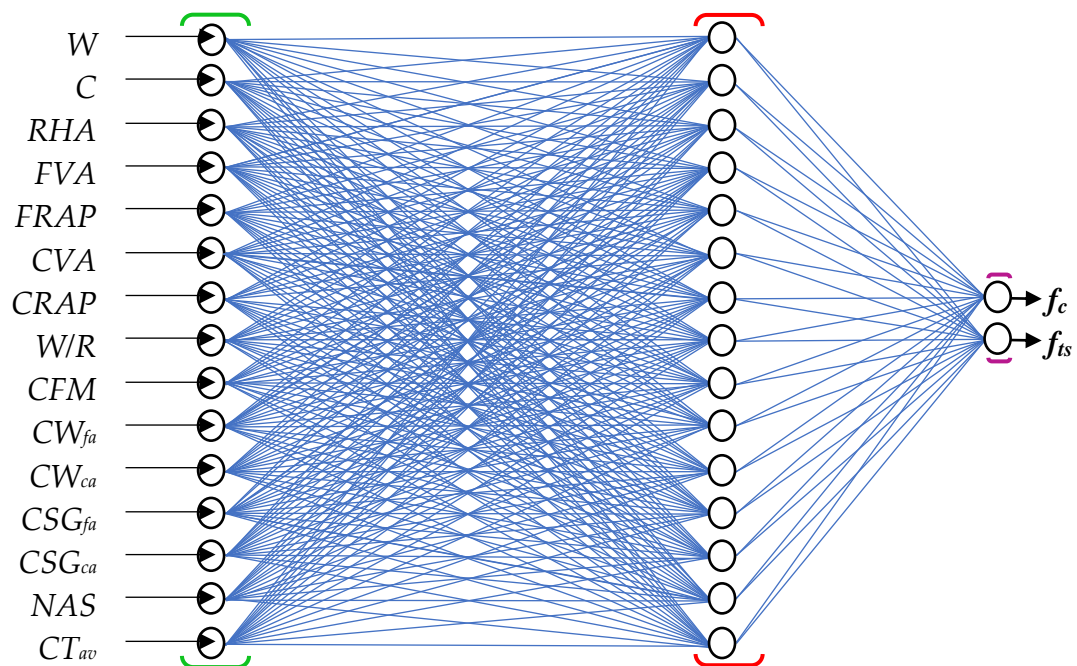
Figure 4.25 Proposed artificial neural network architecture

Figure 4.26 shows the effect number of neurons and transfer functions in the hidden layer on the performances of different ANN architectures. The regression values of the networks having a various number of hidden neurons and activation functions are also

presented in Figure 4.27. It is apparent from Figures 4.26 and 4.27 that the best possible ANN architecture found was L15-15-2 (fifteen input neurons, a single hidden layer having fifteen neurons and two output neurons) with Log-sigmoid activation function. It exhibited satisfactory results compared to all 33 ANN architectures investigated as can be seen from Table 4.12.

Figure 4.26 Variations of RMSE against number of hidden neurons

Figure 4.27 Variations of the coefficients of determination

Table 4.12 Network performance against activation function

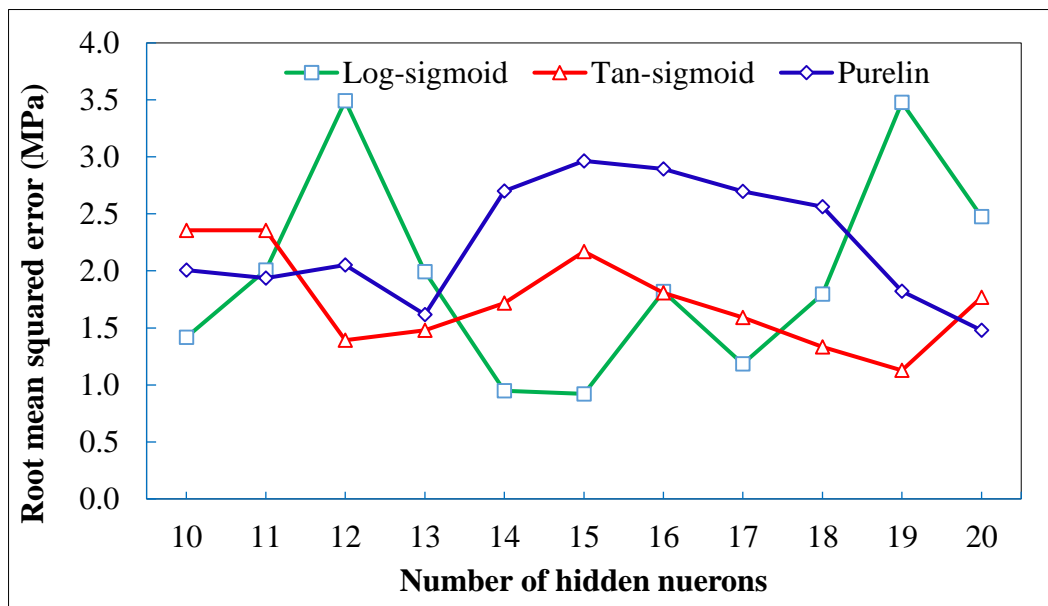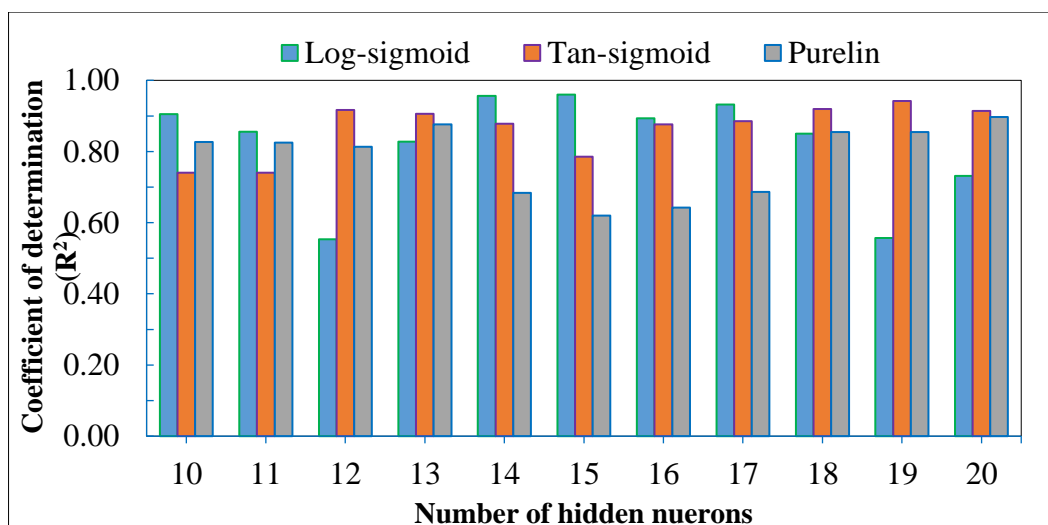| Activation Functions	Network Code	Network Performance					
		MAE	AE	MAPE	MSE	RMSE	R^2
Purelin	P15-10-2	1.272	-0.403	5.414	4.033	2.008	0.827
	P15-11-2	1.305	0.178	5.607	3.747	1.936	0.825
	P15-12-2	1.285	-0.319	5.427	4.207	2.051	0.814
	P15-13-2	1.176	-0.156	5.011	2.609	1.615	0.876
	P15-14-2	1.465	0.412	6.150	7.296	2.701	0.684
	P15-15-2	1.932	0.443	8.311	8.793	2.965	0.620
	P15-16-2	2.137	1.012	8.565	8.379	2.895	0.643
	P15-17-2	1.453	0.596	6.106	7.279	2.698	0.686
	P15-18-2	1.477	0.754	6.099	6.574	2.564	0.854
	P15-19-2	1.228	-0.303	5.254	3.317	1.821	0.854
	P15-20-2	1.146	-0.190	4.978	2.187	1.479	0.897
Tan-sigmoid	T15-10-2	1.463	0.282	5.878	5.552	2.356	0.741
	T15-11-2	1.463	0.282	5.878	5.552	2.356	0.741
	T15-12-2	0.848	-0.388	3.642	1.938	1.392	0.917
	T15-13-2	1.039	-0.529	4.680	2.185	1.478	0.906
	T15-14-2	0.993	-0.401	4.307	2.950	1.718	0.878
	T15-15-2	1.010	0.504	4.162	4.711	2.170	0.785
	T15-16-2	0.978	-0.262	4.067	3.272	1.809	0.876
	T15-17-2	0.881	0.337	3.723	2.529	1.590	0.885
	T15-18-2	0.793	-0.254	3.384	1.779	1.334	0.919
	T15-19-2	0.704	-0.246	3.011	1.271	1.127	0.942
	T15-20-2	1.283	-0.907	5.447	3.129	1.769	0.914
Log-sigmoid	L15-10-2	0.886	-0.173	3.719	2.006	1.416	0.905
	L15-11-2	1.433	-1.004	6.448	4.025	2.006	0.856
	L15-12-2	2.324	-0.792	10.312	12.189	3.491	0.554
	L15-13-2	1.048	-0.199	4.429	3.967	1.992	0.828
	L15-14-2	0.643	-0.147	2.758	0.897	0.947	0.956
	L15-15-2	0.587	0.138	2.484	0.848	0.921	0.960
	L15-16-2	1.109	-0.868	4.799	3.304	1.818	0.893
	L15-17-2	0.868	0.147	3.700	1.401	1.184	0.932
	L15-18-2	0.924	0.325	3.839	3.231	1.797	0.850
	L15-19-2	2.415	0.454	10.215	12.098	3.478	0.557
	L15-20-2	1.178	0.298	4.885	6.125	2.475	0.732

Figure 4.28 shows the performance of the proposed ANN that portrays how the error

drops when the network learns as expected for the well-trained ANN. This is a good

indication of the network's learning process. The figure comprises three lines since the input and desired output vectors are randomly assigned into three sets (70%:15%:15% for training, validation and test respectively). The blue line portrays the decreasing error on the training data. The green line displays the validation error. It measures the network generalization ability and stops training as soon as generalization halts improving.

Thus, training stops when the validation error stops decreasing that inherently avoids over-fitting. As can be seen from the figure, the training error was smaller than that of the validation as expected. This justifies that there was no problem of overfitting. Prediction errors (residuals) based on the training set tell us about the model fit, whereas errors based on the validation set measure the model's ability to predict new data (predictive performance). The red line shows the error on the test data indicating how well the model generalizes to the data and provides an independent measure of network performance during and after training. The training state is depicted in Figure 4.29.

Figure 4.28 Model performance plot

91
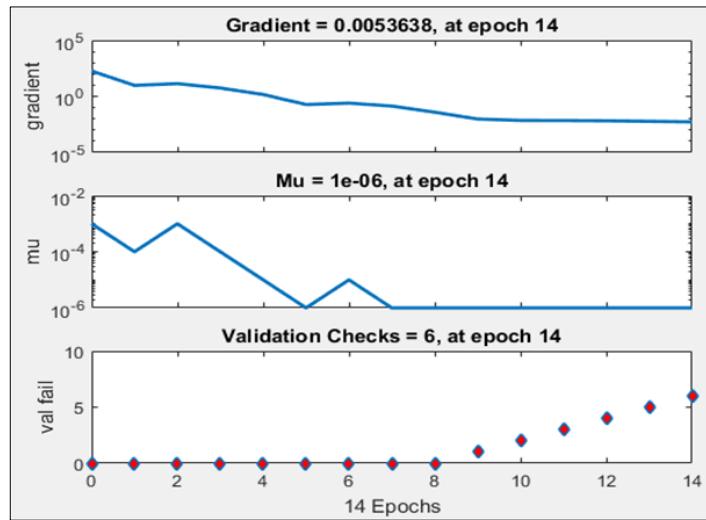
Figure 4.29 Training state

The regression values of the proposed ANN (L15-15-2) are 0.982, 0.990 and 0.985 for

training, validation and testing, respectively, as shown in Figure 4.30.
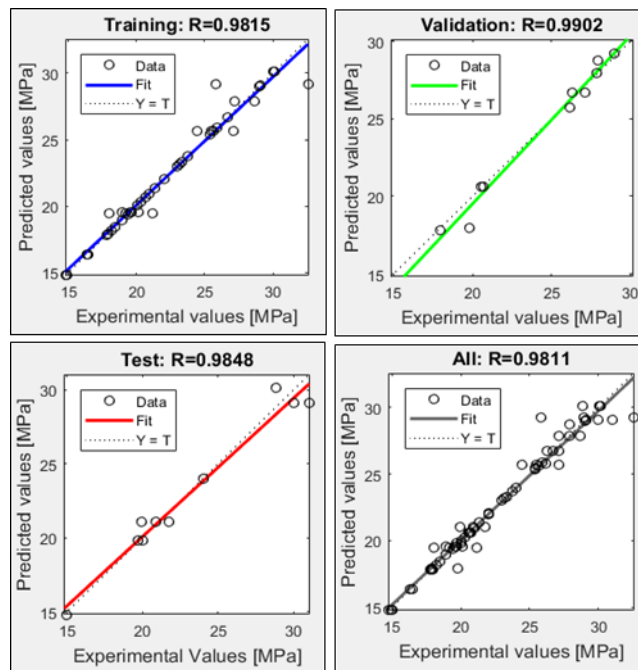
Figure 4.30 Regression for training, validation and test

4.4.2 Predicted Compressive and Tensile Splitting Strength

The compressive and tensile splitting strength values generated by the ANN model (see Table C1, Appendix C) were very close to those of experimental counterparts as shown in Figures 4.31 and 4.32 respectively. The performance of the ANN model was evaluated using the model accuracy measures as tabulated in Table 4.13.
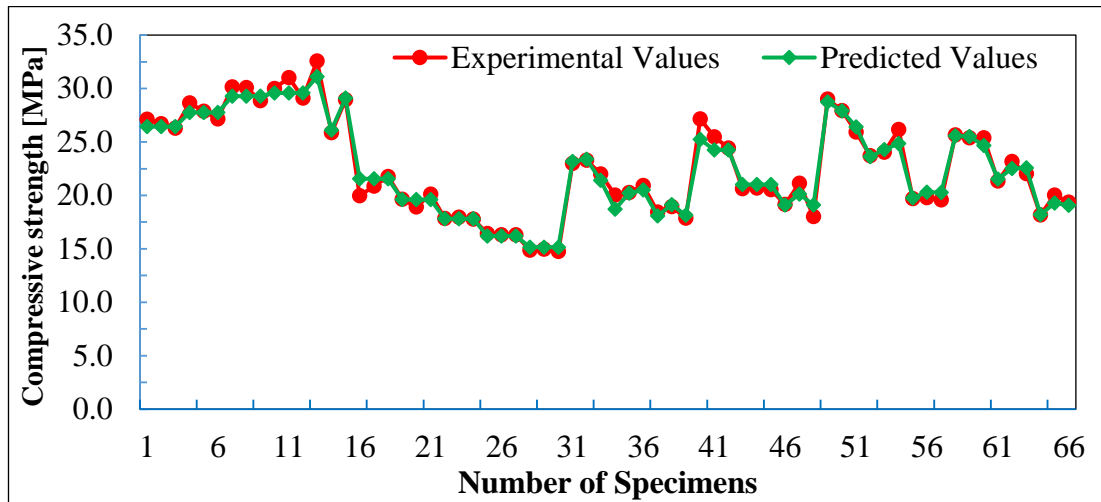
Figure 4.31 Comparison between predicted and experimental results
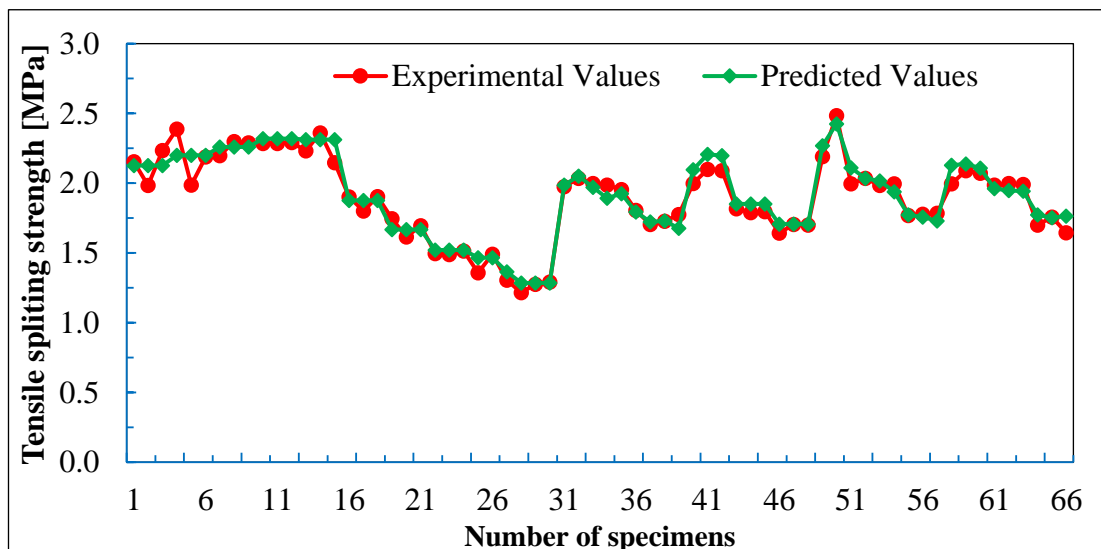
Figure 4.32 Comparison between predicted and experimental data

Table 4.13 ANN strength predictive model accuracy measures

Predicted	Model Performance			
Strength	MAE [MPa]	AE [MPa]	MAPE [%]	RMSE [MPa]
Compressive	0.481	0.123	2.088	0.648
Tensile	0.055	-0.019	2.905	0.072

The ANN model predicted the compressive strength with a RMSE value of 0.648 MPa. This indicates that the differences between predicted and experimental compressive strength values were small. The model overpredicted the compressive strength on average by 0.123 MPa. MAPE value indicates that the predicted compressive strength deviated on average by 2.088% from experimental data. Figures 4.31 clearly exhibits that the predicted compressive strength values were in strong coherence with those of experimentally determined values. This justifies that the model was able to reproduce the experimental compressive strength results with high accuracy.

The ANN predictive model estimated the tensile splitting strength with a RMSE value of 0.072 MPa. This shows that the differences between predicted and experimentally obtained results were negligible. In fact, when the predicted tensile splitting strength values were compared to experimental data, the prediction was on average 0.019 MPa less. The predicted tensile splitting strength swerved on average by 2.905% from the actual results. Figure 4.32 clearly exhibits that the predicted tensile splitting strength values were in strong coherence with experimental ones. This indicates that the model was able to generate the experimental tensile splitting strength results accurately.

4.4.3 Sensitivity Analysis

Input features contain information about the desired outputs. Usually, more features mean more information and better predictive power. However, some features might be irrelevant or redundant that can cause the curse of dimensionality. Irrelevant features introduce noise and fool the training algorism. Redundant features do not contribute additional information and may lead to degradation in the performance of learning algorism.

The relative influence of each input features on outputs was determined based on the magnitude of connection weights generated after training the proposed ANN strength predictive model with experimental data (see Table C2, Appendix C). Figure 4.33 (derived from Table C3, Appendix C) represents the average influence of each input parameters on the predicted compressive and tensile splitting strengths.
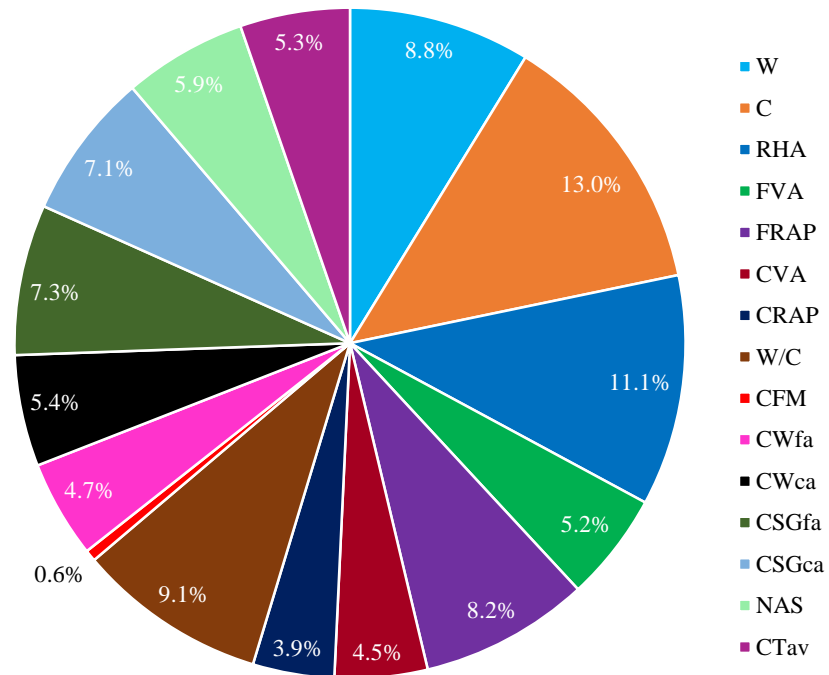
Figure 4.33 Average percentage influence of input features

The sensitivity analysis results seem to indicate that the contents of water, cement, RHA and water to cementitious ratio were strongly relevant for strength prediction with the average percentage influence factor values of 8.8, 13.0, 11.1 and 9.1 respectively. On the other hand, the fineness modulus of fine aggregates can be left out as its contribution in the prediction was close to zero (0.6%). It is worth to mention that the remaining input features had moderate influences on predicted strength as can be seen from Figure 4.33.

CHAPTER FIVE

CONCLUSIONS AND RECOMMENDATIONS

5.1   Conclusions

(i) Characterization of Materials

The materials used in the study were characterized in terms of gradation, specific gravity, density, water absorption, void content, chemical analysis, aggregate impact and crushing values. Based on experimental results obtained, both virgin aggregates and fine reclaimed asphalt pavement were well graded, but coarse reclaimed asphalt pavement was slightly outside of the grading limits to the finer side. RAP materials showed lower specific gravity, density, water absorption, aggregate impact and crashing values relative to virgin aggregates. In addition, RAP materials exhibited higher voids than those of virgin aggregates. From the chemical analysis result, it was observed that RHA satisfies the requirement to be used as a good natural pozzolana in concrete production.

(ii) Effects of RAP and RHA on Wet and Dry Concrete

The physical, mechanical and durability properties of concrete were assessed by partially replacing cement and virgin aggregates with RHA and RAP, up to 20% and 50% respectively. A total of 22 mixes were studied, twelve of which were devoted to studying the collective effects of RHA and RAP on engineering properties of concrete. Based on experimental results, RHA and RAP decreased slump, compacting factor, density, water absorption and sorptivity. RHA increased compressive and tensile splitting strength, whereas RAP decreased compressive and tensile splitting strength.

However, when 15% RHA was combined with up to 20% RAP, comparable strength, favourable absorption and sorptivity values were obtained.

(iii) Strength Prediction by ANN

An artificial neural network strength predictive model was developed to evaluate the compressive and tensile splitting strength of concrete incorporating RHA and RAP based on predetermined attributes of concrete constituent materials. The contents of water, cement, RHA and water to cement ratio played an important role on the predicted strength. The model accurately predicted the compressive strength and tensile splitting strength of concrete.

5.1.1   Recommendations

This investigation revealed that up to 20% RAP can be blended with 15% RHA in order to obtain strong and durable concrete. The study has shown that RAP and RHA inclusive concrete exhibited low absorption and sorptivity values. Therefore, RHA and RAP inclusive concrete can be used for general concreting works as well as for structures subjected to aggressive environment such as retaining walls, external walls, drainage structures, and road pavements.

The study results further indicate that the ANN is an efficient model to be used as a tool for predicting the compressive and tensile strengths of concrete incorporating RHA and RAP. However, care should be taken while selecting input features to avoid irrelevant or redundant variables that can cause the curse of dimensionality. Therefore, sensitivity analysis is recommended before deciding on input features, but contents of water, cement, RHA and water to cement ratio should not be left out in any case.

5.1.2 Recommendations for Further Research Work

1. It would be interesting to establish the relationship between reclaimed asphalt pavement properties such as binder content, percent agglomerated RAP and RAP inclusive concrete performance.

2. The absorption and sorptivity characteristics of RHA and RAP inclusive concrete indicate positive results. However, long-term detailed durability study is highly required to verify whether RHA and RAP inclusive concrete satisfies acceptable long-term durability requirements.

3. A lifecycle analysis is required to assess economic, social and environmental benefits of using RHA and RAP in structural concrete applications.

4. It is fascinating to understand whether properties of concrete, such as modulus of elasticity, creep, durability and shrinkage can also be modelled by ANN.

REFERENCES

Abraham, and Ransinchung. (2018). Strength and permeation characteristics of cement mortar with Reclaimed Asphalt Pavement Aggregates. *Construction and Building Materials*, *167*, 700–706. https://doi.org/10.1016/j.conbuildmat.2018.02.075

Adom-asamoah, M. (2013). Comparative study of the physical properties of palm kernel shell concrete and normal concrete in Ghana. *Journal of Science and Multidisciplinary Research*, (January).

African Union. (2012). *Financing of the programme for infrastructure development in Africa* (Vol. 17).

Alex, J., Dhanalakshmi, J., & Ambedkar, B. (2016). Experimental investigation on rice husk ash as cement replacement on concrete production. *Construction and Building Materials*, *127*, 353–362. https://doi.org/10.1016/j.conbuildmat.2016.09.150

Aprianti, E., Shafigh, P., Bahri, S., & Nodeh, J. (2015). Supplementary cementitious materials origin from agricultural wastes – A review. *Construction and Building Materials*, *74*, 176–187. https://doi.org/10.1016/j.conbuildmat.2014.10.010

Arthur Nilson; David Darwin; Charles Dolan. (2010). *Design of Concrete Structures* (14th ed.). New York: MCGRAW-Hill.

ASTM C1585. (2013). *Standard Test Method for Measurement of Rate of Absorption of Water by Hydraulic Cement Concretes* (Vol. 41). ASTM International. https://doi.org/10.1520/C1585-13.2

ASTM C188. (2016). Standard Test Method for Density of Hydraulic Cement, *i*, 1–3. https://doi.org/10.1520/C0188-16.2

ASTM C29 / C29M. (2003). *Standard Test Method for Bulk Density ("Unit Weight") and Voids in Aggregate*. West Conshohocken: ASTM International. https://doi.org/10.1520/C0029_C0029M-17A

ASTM C595. (2003). *Standard Specification for Blended Hydraulic Cement* (Vol. 14). ASTM International. https://doi.org/10.1520/C0595-03

ASTM C642. (2013). *Standard Test Method for Density, Absorption, and Voids in Hardened Concrete*. ASTM International. https://doi.org/10.1520/C0642-13.5.

Behfarnia, K., & Khademi, F. (2017). A comprehensive study on the concrete compressive strength estimation using the artificial neural network and adaptive neuro-fuzzy inference system. *International Journal of Optimization in Civil Engineering*, *7*(1), 71–80.

Benhelal, E., Zahedi, G., Shamsaei, E., & Bahadori, A. (2013). Global strategies and potentials to curb CO 2 emissions in the cement industry. *Journal of Cleaner Production*, *51*, 142–161. https://doi.org/10.1016/j.jclepro.2012.10.049

Berry, Stephens, Bermel, Hagel, and S. (2013). *Feasibility of reclaimed asphalt pavement as aggregate in Portland cement concrete*.

Bharathi, S. D., Manju, R., & Premalatha, J. (2017). Prediction of Compressive Strength for Self- Compacting Concrete (SCC) using Artificial Intelligence and Regression Analysis. *International Journal of ChemTech Research*, *10*(8), 263–275.

Bida, Danraka, and Ma'ali. (2016). Performance of Reclaimed Asphalt Pavement (RAP) as a Replacement of Fine Aggregate in Concrete. *International Journal of Science and Research (IJSR)*, *5*(4), 2015–2017.

Biswajit; Gauravuday. (2007). *Function approximation using backpropagation algorithm in artificial neural networks*. Rourkel National Institute of Technology.

Bolden, Lebdeh, and Fini. (2013). Utilization of recycled and waste materials in various construction applications. *American Journal of Environmental Science, 9*(1), 14–24. https://doi.org/10.3844/ajessp.2013.14.24

Brand, and Roesler. (2016). Bonding in cementitious materials with asphalt-coated particles : Part I – The interfacial transition zone. *Construction and Building Materials*. https://doi.org/10.1016/j.conbuildmat.2016.10.019

Brand, And Roesler. (2016). Bonding in cementitious materials with asphalt-coated particles : Part II – Cement-asphalt chemical interactions. *Construction and Building Materials*. https://doi.org/10.1016/j.conbuildmat.2016.10.013

Brand, A. S., Roesler, J. R., & Al-qadi, I. L. (2012). *Fractionated Reclaimed Asphalt Pavement (FRAP) as a Coarse Aggregate Replacement in a Ternary Blended Concrete Pavement*.

Brand, A. S., Roesler, J. R., & Al-qadi, I. L. (2014). Fractionated Reclaimed Asphalt Pavement (FRAP) as a Coarse Aggregate Replacement in a Ternary Blended

Concrete Pavement Prepared By, (12).

Brito, J. De, & Robles, R. (2010). Recycled aggregate concrete (RAC) methodology for estimating its long-term properties. *Indian Journal of Engineering & Materials Sciences Vol. 17, December 2010, Pp. 449-462*, *17*(December), 449–462.

BS 1881-103. (1993). *Testing concrete, Part 103: Method for determination of compacting factor*.

BS 1881-125. (2013). *BSI Standards Publication Testing concrete — Part 125 : Methods for mixing and sampling fresh concrete in the*. British Standards Institution 2014.

BS 8500-2. (2012). *Concrete Complementary British Standard to BS EN 206: constituent materials and concrete*. BSI Standards Limited 2013.

BS 882. (1992). Specification for aggregates from natural sources for concrete, (1).

BS EN 1097-6. (2013). *BSI Standards Publication Tests for mechanical and physical properties of aggregates Part 6 : Determination of particle density and water absorption*. Brussels: BSI Standards Limited 2013.

BS EN 12350-1. (2009). *Testing fresh concrete, Part 1: Sampling fresh concrete*.

BS EN 12350-2. (2009). *Testing fresh concrete, Part 2: Slump test*.

BS EN 12390-1. (2012). *Concrete – Complementary British Standard to BS EN 206-1 – guidance for the specifier*. BSI Standards Limited 2012.

BS EN 12390-2. (2009). *Testing hardened concrete, Part 2: Making and curing specimens for strength tests*. BSI Standards Limited 2009.

BS EN 12390-3. (2009). *Testing hardened concrete, Part3: Compressive strength of test specimens*. British Standards Institution.

BS EN 12390-4. (2000). *Testing hardened concrete, Part 4: Specification for Compressive strength testing machines*.

BS EN 12390-5. (2009). Testing hardened concrete.

BS EN 12390-6. (2009). *Testing hardened concrete, Part 6: Tensile splitting strength of test specimens*. BSI Standards Limited 2009.

BS EN 196-2. (2013). *Method of testing cement, Part 2 : Chemical analysis of cement. European Committee for Standardization*. BSI Standards Limited 2012.

BS EN 206. (2014). *Concrete Specification , performance , production and conformity*.

British Standards Institution 2014.

BS EN 450-1. (2012). *Fly ash for concrete, Part 1 : Definition, specifications and conformity criteria*. BSI Standards Limited 2012.

BS EN 932-1. (1997). *Tests for general properties of aggregates: Part 1. Methods for sampling*.

BS EN 933-1. (2012). *Tests for geometrical properties of aggregates Part 1 : Determination of particle size distribution — Sieving method. BSI Standards Publication*.

BS ISO 3310-2. (2013). *Test sieves — Technical requirements and testing Part 2 : Test sieves of perforated metal plate*.

Chao-lung, H., Anh-tuan, B. Le, & Chun-tsun, C. (2011). Effect of rice husk ash on the strength and durability characteristics of concrete. *Construction and Building Materials*, *25*(9), 3768–3772. https://doi.org/10.1016/j.conbuildmat.2011.04.009

Chinnaraj, Sivaranjani, Arthi, Dhamodharan, R. (2017). Experimental Study on Behavior of Concrete by Replacement of Cement using Rice Husk Ash. *South Asian Journal of Engineering and Technology*, *3*(7), 1–7.

Chopra, P. (2014). Regression Models for the Prediction of Compressive Strength of Concrete with & without Fly ash. *International Journal of Latest Trends in Engineering and Technology (IJLTET*, *3*(4), 400–406.

Chopra, P., Sharma, R. K., & Kumar, M. (2016). Prediction of Compressive Strength of Concrete Using Artificial Neural Network and Genetic Programming. *Hindawi Publishing Corporation Advances in Materials Science and Engineering*, *2016*.

Courard, L., Michel, F., & Delhez, P. (2010). Use of concrete road recycled aggregates for Roller Compacted Concrete. *Construction and Building Materials*, *24*(3), 390–395. https://doi.org/10.1016/j.conbuildmat.2009.08.040

David R. Wilburn and Thomas G. Goonan. (1998). *Aggregates from Natural and Recycled Sources Economic Assessments for Construction Applications — A Materials Flow Analysis. Central Region, Denver, Colorado*. Colorado. Retrieved from http://greenwood.cr.usgs.gov/pub/circulars/c1176/c1176.html

Duan, Z. H., Kou, S. C., & Poon, C. S. (2013). Prediction of compressive strength of recycled aggregate concrete using artificial neural networks. *Construction and BuildingbMaterials*, *40*, 1200–1206.

https://doi.org/10.1016/j.conbuildmat.2012.04.063

Duggal, K. (2008). *Building Materials*. New Age International (P) Ltd., Publishers. Retrieved from www.newagepublishers.com

El, S., Ben, E., El, S., Khay, E., Achour, T., & Loulizi, A. (2017). Modelling of the adhesion between reclaimed asphalt pavement aggregates and hydrated cement paste, *152*, 839–846. https://doi.org/10.1016/j.conbuildmat.2017.07.078

Engineering, S., Jayaranjini, A., & Engineering, S. (2016). Prediction of compressive strength of high-performance concrete containing industrial by-products using artificial neural networks. *International Journal of Civil Engineering and Technology (IJCIET)*, *7*(2), 302–314.

Ephraim, M., Akeke, G., & Ukpata, J. (2012). The compressive strength of concrete with rice husk ash as partial replacement of ordinary Portland cement. *Scholarly Journal of Engineering Research*, *1*(May), 32–36.

FAO. (2017). *FAO Rice Market Monitor, December 2017, Volume XX - Issue No. 4* (Vol. XX).

Faruqi, M. A., Agarwala, R., Sai, J., & Francisco, A. (2015). Application of Artificial Intelligence to Predict Compressive Strength of Concrete from Mix Design Parameters : A Structural Engineering Application. *Journal of Civil Engineering Research*, *5*(6), 158–161. https://doi.org/10.5923/j.jce.20150506.05

Fried, A. N. (2016). Non-destructive evaluation of reclaimed asphalt cement concrete. *European Journal of Environmental and Civil Engineering*, *8189*(October 2017), 0. https://doi.org/10.1080/19648189.2016.1219877

Graupe, D. (2007). *Principles of Artificial Neural Networks*. (W.-K. Chen, Ed.) (2nd ed.). World Scientific Publishing Co. Pte. Ltd.

Gupta, A. I., & Wayal, A. S. (2015). Use of Rice Husk Ash in Concrete : A Review. *IOSR Journal of Mechanical and Civil Engineering (IOSR-JMCE)*, *12*(4), 29–31. https://doi.org/10.9790/1684-12412931

Gupta, N., Kumar, P., Mishra, A., & Prakashsrivastava, R. (2015). Characterization and Application of Rice Husk Ash As Pozzolanic Material In Concrete. *IOSR Journal of Mechanical and Civil Engineering*, *12*(3), 28–32. https://doi.org/10.9790/1684-12332832

Heidari, A., Hashempour, M., & Tavakoli, D. (2017). Using of Backpropagation

Neural Network in Estimating of Compressive Strength of Waste Concrete. *Journal of Soft Computing in Civil Engineering*, *1*, 54–64.

Hossain, Z., & Ph, D. (2017). Performance of Rice Husk Ash (RHA) as Sustainable Construction Material in Concrete Pavement.

Hossiney, N., Tia, M., & Bergin, M. J. (2010). Concrete Containing RAP for Use in Concrete Pavement, *3*(5), 251–258.

Huang, Shu, and Burdette. (2006). Mechanical properties of concrete containing recycled asphalt pavements. *Magazine of Concrete Research*, (5), 313–320.

Huang, Shu, and Li. (2013). Laboratory investigation of portland cement concrete containing recycled asphalt pavements. *Cement and Concrete Research 35 (2005) 2008 – 2013.* https://doi.org/10.1016/j.cemconres.2005.05.002

Huang, H., Gao, X., Wang, H., & Ye, H. (2017). Influence of rice husk ash on strength and permeability of ultra-high performance concrete. *Construction and Building Materials*, *149*, 621–628. https://doi.org/10.1016/j.conbuildmat.2017.05.155

Ibrahim, Mahmoud, Khodair and Patibandla. (2014). Fresh, Mechanical, and Durability Characteristics of Self-Consolidating Concrete Incorporating Recycled Asphalt Pavements. *Journal Of Materials In Civil Engineering*, (April), 668–676. https://doi.org/10.1061/(ASCE)MT.1943-5533.0000832.

IS 2386: Part IV. (2002). *Methods of Test for Aggregates for Concrete: Part IV Mechanical Properties*.

IS 383. (2002). *Specification for coarse and fine aggregates from natural sources for concrete*.

Ismail, S., Wai, K., & Ramli, M. (2013). Sustainable aggregates : The potential and challenge for natural resources conservation. *Procedia - Social and Behavioral Sciences*, *101*, 100–109. https://doi.org/10.1016/j.sbspro.2013.07.183

Jain, N., Garg, M., & Minocha, A. K. (2015). Green Concrete from Sustainable Recycled Coarse Aggregates : Mechanical and Durability Properties. *Hindawi Publishing Corporation Journal of Waste Management Volume 2015, Article ID 281043, 8 Pages http://dx.doi.org/10.1155/2015/281043*, *2015*.

Jamalaldin, S., Hakim, S., Noorzaei, J., Jaafar, M. S., & Jameel, M. (2011a). Application of artificial neural networks to predict compressive strength of high strength concrete, *6*(5), 975–981.

Jamalaldin, S., Hakim, S., Noorzaei, J., Jaafar, M. S., & Jameel, M. (2011b). Application of artificial neural networks to predict compressive strength of high strength concrete. *International Journal of the Physical Sciences*, *6*(5), 975–981.

Jamil, M., Kaish, A. B. M. A., Raman, S. N., & Zain, M. F. M. (2013). Pozzolanic contribution of rice husk ash in cementitious system. *Construction & Building Materials*, *47*, 588–593. https://doi.org/10.1016/j.conbuildmat.2013.05.088

Jamil, M., & Karimc, M. R. (2014). Strength and Durability of Mortar and Concrete Containing Rice Husk Ash : A Review Sustainable Construction Materials and Building Systems (SUCOMBS) Research Group , Dhaka University of Engineering and Technology (DUET), Gazipur , Bangladesh. *World Applied Sciences Journal*, *32*(5), 752–765.
https://doi.org/10.5829/idosi.wasj.2014.32.05.984

Jaya, R. P., Bakar, B. H. A., Azmi, M., & Johari, M. (2011). Effect of rice husk ash to the performance of concrete block. *International Journal of Applied Science and Technology*, (September 2015). Retrieved from www.ijastnet .com%0Ac)

Jin, R., & Chen, Q. (2013). An Investigation of Current Status of " Green " Concrete in the Construction Industry. In *American society of Civil Engineers Annual International Conference Proceedings*.

John, M. (2011). *Materials for Civil and Construction Engineers*. (H. Stark, Ed.) (3rd ed.). New Jersey: Pearson Education Limited.

Juenger, M. C. G., & Siddique, R. (2015). Cement and Concrete Research Recent advances in understanding the role of supplementary cementitious materials in concrete. *Cement and Concrete Research*.
https://doi.org/10.1016/j.cemconres.2015.03.018

Kalra, G., & Joseph, E. (2016). Research Review and Modeling of Concrete Compressive Strength Using Artificial Neural Networks. *IJISET - International Journal of Innovative Science, Engineering & Technology*, *3*(2), 672–677.

Kene, S., Domke, P., & Deshmukh, S. (2015). Assessment of concrete strength using fly ash and rice husk ash. *International Journal of Engineering Research and Applications (IJERA)*, *1*(3), 524–533.

Kett, I. (2010). *Engineered Concrete Mix Design and Test Methods* (2nd ed.). United States of America: CRC Press, Taylor & Francis Group. Retrieved from

http://www.taylorandfrancis.com

Khan, R., Jabbar, A., Ahmad, I., Khan, W., Naeem, A., & Mirza, J. (2012). Reduction in environmental problems using rice-husk ash in concrete. *Construction and Building Materials*, *30*, 360–365. https://doi.org/10.1016/j.conbuildmat.2011.11.028

Khassaf, S. I., Jasim, A. T., & Mahdi, F. K. (2014). Investigation the Properties of Concrete Containing Rice Husk Ash to Reduction the Seepage in Canals . *International Journal of Scientific & Technology*, *3*(4), 348–354.

Koivo, H. N. (2008). Neural Networks Basics using MATLAB Neural Network Toolbox, 1–59.

Kosmatka, A. W. (2011). *Design and Control of Concrete Mixtures* (Fifteenth). Portland Cement Association.

Kulkarni, M. S., Mirgal, P. G., Bodhale, P. P., & Tande. (2014). Effect of Rice Husk Ash on Properties of Concrete. *Journal of Civil Engineering and Environmental Technology*, *1*(1), 26–29.

Kumar, Tomar, Gupta, A. kumar. (2016). Replacement of Cement in Concrete with Rice Husk Ash. *International Journal of Civil Engineering*, *3*(7), 127–129.

Lakra, K., & Gupta, V. (2016). Effect of Partial Replacement of Cement by Fly Ash , Rice Husk Ash with Using Steel Fiber in Concrete. *International Journal of Engineering Science and Computing*, *6*(8), 2092–2100.

Lam, T. Van, Bulgakov, B., Aleksandrova, O., Larsen, O., & Ngoc, P. (2018). Effect of rice husk ash and fly ash on the compressive strength of high performance concrete. In *doi.org/10.1051/e3sconf/20183302029* (Vol. 2030, pp. 1–13). EDP Sciences. https://doi.org/doi.org/10.1051/e3sconf/20183302030

Li, Z. (2011). *Advanced Concrete Technology*. Canada: Zongjin Li. Retrieved from www.wiley.com/go/permissions.%0ALimit

Ling, T. (2011). Prediction of density and compressive strength for rubberized concrete blocks w. *Construction and Building Materials*, *25*(11), 4303–4306. https://doi.org/10.1016/j.conbuildmat.2011.04.074

Lun, L. T. (2015). *Effects of rice husk ash produced from different temperatures on the performance of concrete*. Faculty of Engineering and Green Technology Universiti Tunku Abdul Rahman.

Madurwar, M. V, Ralegaonkar, R. V, & Mandavgane, S. A. (2013). Application of agro-waste for sustainable construction materials : A review. *Construction and Building Materials*, *38*, 872–878. https://doi.org/10.1016/j.conbuildmat.2012.09.011

Mahmoud, E., Ibrahim, A., El-chabib, H., & Patibandla, V. C. (2013). Self-Consolidating Concrete Incorporating High Volume of Fly Ash , Slag , and Recycled Asphalt Pavement. *International Journal of Concrete Structures and Materials*, *7*(2), 155–163. https://doi.org/10.1007/s40069-013-0044-1

Martys, N. S., & Ferraris, C. E. (1997). Pii sooos-8846(97)00052-5 capillary transport in mortars and concrete, *27*(5), 747–760.

McCormac, R. H. B. (2013). *Design of Reinforced Concrete* (9th ed.). John Wiley & Sons, Inc. Retrieved from www.wiley.com/go/permissions

Menéndez, G., & Irassar, V. L. B. E. F. (2007). Hormigones con cementos compuestos ternarios . Parte II : Mecanismos de transporte Ternary blend cements concrete . Part II : Transport mechanism, *57*, 31–43.

Meyer, C. (2009). The greening of the concrete industry. *Cement and Concrete Composites*, *31*(8), 601–605. https://doi.org/10.1016/j.cemconcomp.2008.12.010

Michael S. Mamlouk, J. P. (2011). *Materials for civil and construction engineers* (3rd ed.). Pearson Education.

Milne, L. (1995). Feature Selection Using Neural Networks with Contribution Measures. In *Australian Conference on Artificial Intelligence* (pp. 1–8).

Ming, Z. (2003). *Intelligent Systems: Technology and Applications*. (C. T. Leondes, Ed.) (Vol. I). Washington, D.C.: CRC Press LLC.

Modarres, A., & Hosseini, Z. (2014). Mechanical properties of roller compacted concrete containing rice husk ash with original and recycled asphalt pavement material. *JOURNAL OF MATERIALS&DESIGN*, *64*, 227–236. https://doi.org/10.1016/j.matdes.2014.07.072

Mohammadinia, A., Arulrajah, A., Haghighi, H., & Horpibulsuk, S. (2017). Effect of lime stabilization on the mechanical and micro-scale properties of recycled demolition materials. *Sustainable Cities and Society*. https://doi.org/10.1016/j.scs.2017.01.004

Montan, J. J. (2003). Numeric sensitivity analysis applied to feedforward neural

networks. *Neural Comput & Applications*, *12*, 119–125. https://doi.org/10.1007/s00521-003-0377-9

Naderpour, H., Hossein, A., & Fakharian, P. (2018). Compressive strength prediction of environmentally friendly concrete using artificial neural networks. *Journal of building engineering*, *16*(October 2017), 213–219. https://doi.org/10.1016/j.jobe.2018.01.007

Naderpour, H., Kheyroddin, A., & Amiri, G. G. (2010). Prediction of FRP-confined compressive strength of concrete using artificial neural networks. *Composite Structures*, *92*(12), 2817–2829. https://doi.org/10.1016/j.compstruct.2010.04.008

Nair, D. G., Sivaraman, K., & Thomas, J. (2013). Mechanical Properties of Rice Husk Ash on High strength Concrete. *American Journal of Engineering Research (AJER)*, 14–19.

Naji, A., Abdul, S., Nora, F., Aziz, A., Amran, M., & Salleh, M. (2010). Assessment of the effects of rice husk ash particle size on strength, water permeability and workability of binary blended concrete. *Construction and Building Materials*, *24*(11), 2145–2150. https://doi.org/10.1016/j.conbuildmat.2010.04.045

Nathen, A. N. S., & Ravi, S. R. (2017). Indian Rice Husk Ash – Improving the Mechanical Properties of Concrete : A Review. *International Journal of Engineering Research and Application*, *7*(1), 76–79.

Noorzaei, J., Hakim, S. J. S., Jaafar, M. S., & Thanoon, W. A. M. (2007). Development of artificial neural networks for predicting concrete compressive strength. *International Journal of Engineering and Technology*, *4*(2), 141–153.

Okafor, F. O. (2010). Performance of Recycled Asphalt Pavement as Coarse Aggregate in Concrete. *Leonardo Electronic Journal of Practices and Technologies*, (17), 47–58.

Omran, B. A., & Chen, Q. (2014). Prediction of Compressive Strength of " Green " Concrete Using Artificial Neural Networks. In *50th ASC Annual International Conference Proceedings*.

Pacheco, F., & Labrincha, J. A. (2013). The future of construction materials research and the seventh UN Millennium Development Goal : A few insights. *Construction and BuildingbMaterials*, *40*, 729–737.

https://doi.org/10.1016/j.conbuildmat.2012.11.007

Paiva, C. E. L. De, Cesar, P., Oliveira, A. De, & Peixoto, C. D. F. (2017). The influence of milling asphalt rates from wearing surface to the flexural strength applied to a recycled layer with Portland cement. *Construction and Building Materials*. https://doi.org/10.1016/j.conbuildmat.2017.07.014

Philips, E. S., Mutuku, R. N., & Mwero, J. N. (2018). Effects of Palm Kernel Shell and Rice Husk Ash as Partial Replacements of Normal Weight Aggregate and Ordinary Portland Cement in Concrete. *European International Journal of Science and Technology*, *6*(8), 42–54. Retrieved from www.eijst.org.uk

Rao, P. P., Kumar, A. P., & Singh, B. B. (2014). A Study on Use of Rice Husk Ash in Concrete. *International Journal of Education and Applied Research*, *33*, 75–81.

Ryu, J., & Monteiro, P. J. M. (2002). E V ect of specific c gravity of coarse aggregate on interfacial transition zone, permeability, and strength of concrete. *British Ceramic Transactions*, *101*. https://doi.org/10.1179/096797801225000806

Sahoo, K., Sarkar, P., & P, R. D. (2016). Artificial Neural Networks for Prediction of Compressive Strength of Recycled Aggregate Concrete. *Int'l Journal of Research in Chemical, Metallurgical and Civil Engg. (IJRCMCE) Vol.*, *3*(1), 1–5.

Saif, A., & Alquzweeni, S. (2015). Artificial Neural Network Model for Predicting Compressive Strength of High Strength Concrete after Burning Against spalling Material. *International Journal of Civil & Environmental Engineering IJCEE-IJENS Vol:*, (December).

Saravanan, & Sivaraja. (2016). Mechanical Behavior of Concrete Modified by Replacement of Cement by Rice Husk Ash. *An International Journal of Engineering, Technology and Techniques*, *59*(December), 1–11.

Saride, Avirneni, And Challapalli. (2016). Micro-mechanical interaction of activated fly ash mortar and reclaimed asphalt pavement materials. *Construction and Building Materials*, *123*, 424–435. https://doi.org/10.1016/j.conbuildmat.2016.07.016

Settari, C., Debieb, F., Hadj, E., & Boukendakdji, O. (2015). Assessing the effects of recycled asphalt pavement materials on the performance of roller compacted concrete. *Construction and Building Materials*, *101*, 617–621. https://doi.org/10.1016/j.conbuildmat.2015.10.039

Shi, Mukhopadhyay and, Liu. (2017). Mix design formulation and evaluation of portland cement concrete paving mixtures containing reclaimed asphalt pavement. *Construction and Building Materials 152 (2017) 756–768 Contents*, *152*, 756–768. https://doi.org/10.1016/j.conbuildmat.2017.06.174

Shmueli, G., Bruce, P. C., Stephens, M. L., & Patel, N. R. (2017). *Data mining for business analytics* (Third). Canada: John Wliley & Sons, Inc. https://doi.org/9781118877432

Silva, F. O. K. and C. de. (2004). *Soft Computing and Intelligent Systems Design*. Pearson Education Limited.

Singh, Ransinchung, and Kumar. (2017). An economical processing technique to improve RAP inclusive concrete properties. *Construction and Building Materials*, *148*, 734–747. https://doi.org/10.1016/j.conbuildmat.2017.05.030

Singh, V., & Pareek, R. K. (2015). Effect of rice husk ash and plastic fibres on concrete strength. *International Journal of Civil and Structural Engineering*, *6*(1), 25–33. https://doi.org/10.6088/ijcser.6003

Siraj, N. (2015). *Prediction of Compressive Strength of Concrete using Artificial Neural Network, Fuzzy System Model and Thermodynamic Methods*. Addis Ababa University Institute of Technology.

Smith, T., & Maillard, P.-L. (2007). The Sustainable Benefits of Concrete Pavement.

Solanki, and Dash. (2015). Mechanical Properties of Concrete Containing Recycled Asphalt Pavement and Class C Fly Ash. In *2015 World of Coal Ash (WOCA) Conference in Nasvhille, TN - May 5-7, 2015*.

Su, Y., & Chen, Y. (2012). Use of reclaimed asphalt, (October).

Suba, S. (2009). Prediction of mechanical properties of cement containing class C fly ash by using artificial neural network and regression technique. *Academic Journals*, *4*(4), 289–297. Retrieved from http://www.academicjournals.org/SRE

Suhendro, B. (2014). Toward green concrete for the better sustainable environment. *Procedia Engineering*, *95*(Scescm), 305–320. https://doi.org/10.1016/j.proeng.2014.12.190

Surender, Ransinchung, G. D. R. N., Debbarma, S., & Kumar, P. (2017). Utilization of reclaimed asphalt pavement aggregates containing waste from Sugarcane Mill for production of concrete mixes. *Journal of Cleaner Production*.

https://doi.org/10.1016/j.jclepro.2017.10.179

Tam, V. W. Y. (2010). Rate of Reusable and Recyclable Waste in Construction. In *Second International Conference on Sustainable Construction Materials and Technology*.

Tayfur, G., Erdem, T. K., Önder, K., & Ph, D. (2014). Strength Prediction of High-Strength Concrete by Fuzzy Logic and Artificial Neural Networks. *Journal of Materials in Civil Engineering, 26*(11), 1–7. https://doi.org/10.1061/(ASCE)MT.1943-5533.0000985.

Version, D. (2013). *Construction and demolition waste recycling into innovative building materials for sustainable construction in Tanzania Construction and demolition waste recycling into innovative building materials for sustainable construction in Tanzania i*. Eindhoven University of Technology, The Netherlands. All. https://doi.org/10.6100/IR757934

Wankhade, K. and. (2013). Prediction of Compressive Strength of Concrete using Artificial Neural. *International Journal of Scientific Research and Reviews Prediction*, *2*(June), 11–26.

Wilson, M. L. (2011). *Design and Control of Concrete Mixtures* (15th ed.). Portland CementAssociation.

World Economic Forum. (2016). Shaping the Future of Construction: A Breakthrough in Mindset and Technology, (May).

Zhang, S. P., & Zong, L. (2014). Evaluation of Relationship between Water Absorption and Durability of Concrete Materials. *Advances in Materials Science and Engineering*, *2014*. Retrieved from http://dx.doi.org/10.1155/2014/650373%0AResearch

Zhen-Hua Duan, Shi-Cong Kou, and C.-S. P. (2013). Prediction of compressive strength of recycled aggregate concrete using artificial neural networks. *Construction and Building Materials*, (March). https://doi.org/10.1016/j.conbuildmat.2012.04.063

APPENDICES

A. Material Characterizations

Table A1 Sieve analyses for fine virgin aggregate

Sieve Size (mm)	Weight of FVA Retained (g)				Commutative Retained (%)	Total Pass (%)	BS 882 Specification	
Sample	I	II	III	Average			Lower limit	Upper limit
9.50	0.00	0.00	0.00	0.00	0.00	100.00	100.00	100.00
4.75	21.00	12.50	25.00	19.50	1.96	98.04	89.00	100.00
2.36	39.00	36.00	24.50	33.17	5.28	94.72	60.00	100.00
1.18	174.40	198.00	194.00	188.80	24.22	75.78	30.00	100.00
0.60	352.00	357.50	364.50	358.00	60.12	39.88	15.00	100.00
0.30	152.00	180.50	160.50	164.33	76.60	23.40	5.00	70.00
0.15	221.60	178.50	191.50	197.20	96.37	3.63	0.00	15.00
Pan	38.50	34.50	35.50	36.17	100.00			
Total	998.50	997.50	995.50	997.17				

Table A2 Sieve analyses for FRAP

Sieve Size (mm)	Weight. of FRAP Retained (g)				Commutative Retained (%)	Total Pass (%)	BS 882 Specification	
Sample	I	II	III	Average	-	-	Lower limit	Upper limit
9.50	-	-	-	-	-	100.00	100.00	100.00
4.75	4.00	7.00	6.00	5.67	0.57	99.43	89.00	100.00
2.36	316.00	328.00	326.00	323.33	32.98	67.02	60.00	100.00
1.18	265.00	281.00	272.00	272.67	60.31	39.69	30.00	100.00
0.60	216.50	209.00	215.00	213.50	81.71	18.29	15.00	100.00
0.30	81.50	69.00	76.00	75.50	89.27	10.73	5.00	70.00
0.15	70.00	62.00	65.00	65.67	95.86	4.14	-	15.00
Pan	44.00	42.00	38.00	41.33	100.00	-	-	-
Total	997.00	998.00	998.00	997.67	-	-	-	-

Table A3 Sieve analyses for CVA

Sieve Size (mm)	Weight of CVA Retained (g)				Commutative Retained (%)	Total Pass (%)	BS 882 Specification	
Sample	I	II	III	Average	-	-	Lower limit	Upper limit
25	0.00	0.00	0.00	0.00	0.00	100.00	100.00	
19.1	11.50	12.00	28.50	17.33	0.58	99.40	90.00	100.00
12.5	103.00	95.00	105.50	101.17	3.95	96.00	-	-
9.5	1401.50	1416.50	1467.00	1428.33	51.58	48.40	30.00	60.00
4.75	1209.50	1207.50	1123.40	1180.13	90.94	9.10	0.00	10.00
Pan	273.50	267.50	274.50	271.83	100.00	-	-	-
Total	2999.00	2998.50	2998.90	2998.80	-	-	-	-

Table A4 Sieve analyses for CRAP

Sieve Size (mm)	Weight of CRAP Retained (g)				Commutative Retained (%)	Total Pass (%)	BS 882 Specification	
Sample	I	II	III	Average	-	-	Lower limit	Upper limit
25.00	0.00	0.00	0.00	0.00	0.00	100.00	100.00	
19.10	8.00	9.00	11.00	9.33	0.93	99.10	90.00	100.00
12.5	103.00	95.00	105.50	101.17	3.95	96.00	-	-
9.50	297.50	447.00	364.00	369.50	37.02	63.00	30.00	60.00
4.75	557.00	454.50	503.00	504.83	87.59	12.40	0.00	10.00
Pan	135.50	88.00	120.00	114.50	99.06	-	-	-
Total	998.00	998.50	998.00	998.17	-	-	-	-

Table A5 Specific gravity and water absorption of fine aggregates

Description		FVA			FRAP		
Sample No		I	II	Average	I	II	Average
Wt. of pycnometer + water	A	1415.00	1415.00	1415.00	1418.00	1419.25	1418.83
Wt. of pycnometer + aggregate (SSD) + water	B	1713.50	1718.25	1716.67	1717.00	1717.00	1717.00
Wt of oven-dry aggregate, gm	C	481.00	481.00	481.00	479.00	480.25	479.83
Weight of SSD aggregate, gm.	D	500.00	500.00	500.00	500.00	500.00	500.00
Bulk specific gravity, SSD basis	D/(A+D-B)	2.48	2.54	2.52	2.49	2.47	2.48
Bulk specific gravity, dry basis	C/(A+D-B)	2.39	2.45	2.43	2.38	2.37	2.38
Apparent specific gravity	C/(A+C-B)	2.64	2.71	2.68	2.66	2.63	2.64
Water Absorption, %	(D - C)/C*100	3.95	3.95	3.95	4.38	4.11	4.20

Description		CVA			CRAP		
Sample No		I	II	Average	I	II	Average
Wt in air. of SSD, gm	A	2121.00	2132.00	2126.50	1465.00	1460.00	1462.50
Wt. of water + sample + container, gm	B	5067.00	5079.00	5073.00	4690.50	4687.50	4689.00
Wt. In air of oven-dry sample, gm	C	2071.50	2081.50	2076.50	1446.00	1432.00	1439.00
Container + water	D	3739.00	3739.50	3739.25	3823.50	3823.50	3823.50
Bulk specific gravity, dry basis	C/(A+D - B)	2.61	2.63	2.62	2.42	2.40	2.41
Bulk specific gravity, SSD basis	A/(A+D - B)	2.67	2.69	2.68	2.45	2.45	2.45
Apparent specific gravity,	C/(C+D - B)	2.79	2.81	2.80	2.50	2.52	2.51
Water absorption, %	(A - C)*100/C	2.39	2.43	2.41	1.31	1.96	1.63

Table A6 Specific gravity and water absorption of coarse aggregates

Table A7 Density and voids in coarse aggregates

Description		CVA			CRAP		
Sample No		I	II	Average	I	II	Average
A. Capacity o measure (m³)		0.01	0.01	0.01	0.01	0.01	0.01
B. Wt. of measure (kg)		4.65	4.65	4.65	4.65	4.65	4.65
C. Wt. of measure + loose aggregates (kg)		18.10	18.20	18.15	16.50	17.50	17.00
D.Wt. of measure + rodded aggregates (kg)		19.65	19.75	19.70	17.00	17.50	17.25
E. Loose bulk density (kg/m³)	(C-B)/A	1415.79	1426.32	1421.05	1247.37	1352.63	1300.00
F. Compacted bulk density (kg/m³)	(D-B)/A	1578.95	1589.47	1584.21	1300.00	1352.63	1326.32
G. Bulk specific gravity, dry basis		2.61	2.63	2.62	2.32	2.32	2.41
H. % voids in loose aggregates	(G-E)/G*100	45.80	45.70	45.75	46.23	41.70	43.97
I. % voids in compacted aggregates	(G-F)/G*100	39.56	39.48	39.52	43.97	41.70	42.83

Table A8 Density and voids in fine aggregates

Description		FVA			FRAP		
Sample No		I	II	Average	I	II	Average
A. Capacity o measure (m³)		0.00	0.00	0.00	0.00	0.00	0.00
B. Wt. of measure(kg)		1.54	1.54	1.54	1.54	1.54	1.54
C. Wt. of measure + loose aggregates(kg)		4.49	4.47	4.48	4.25	4.15	4.20
D.Wt. of measure + rodded aggregates(kg)		4.72	4.73	4.72	4.31	4.45	4.38
E. Loose bulk density(kg/m³)	(C-B)/A	1459.67	1452.50	1456.09	1342.40	1292.92	1317.66
F. Compacted bulk density(kg/m³)	(D-B)/A	1573.23	1579.91	1576.57	1372.09	1441.37	1406.73
G. Bulk specific gravity, dry basis		2.39	2.41	2.43	2.31	2.32	2.32
H. % voids in loose aggregates	(G-E)/G*100	38.85	39.81	39.33	41.98	44.21	43.09
I. % voids in compacted aggregates	(G-F)/G*100	34.09	34.53	34.31	40.69	37.81	39.25

Description		Cement			RHA		
Sample No		I	II	Average	I	II	Average
Wt. of cement/RHA	A	90.00	90.00	90.00	64.00	64.00	64.00
Volume of Kerosene (1st reading)	B	251.00	251.00	251.00	251.00	251.00	251.00
Volume of Kerosene + displaced volume (2nd reading)	C	280.00	279.75	279.88	282.70	282.50	282.60
Net displaced volume	C-B	29.00	28.75	28.88	31.70	31.50	31.60
Specific gravity	A/(C-B)	3103.45	3130.43	3.12	2018.93	2031.75	2.03

Table A9 Specific gravity of cement and RHA

MINISTRY OF PETROLEUM AND MINING

e-mail:cg@mining.go.ke
When replying please quote ref No & date
Ref. No. ORIGINAL CERT NO....1108/18

MINISTRY OF PETROLEUM AND MINING
MACHAKOS ROAD
P.O. Box 30009-00100 GPO
NAIROBI
Date...29th March, 2018

ASSAY CERTIFICATE

SENDER'S NAME   :   GETAHUN MULUSEW
DATE   :   15.03.2018
SAMPLE TYPE   :   SAND
SAMPLE NO   :   1108/18

RESULT

Lab No.	Sender's Ref.	SiO_2	Al_2O_3	CaO	MgO	Na_2O	K_2O	TiO_2	MnO	Fe_2O_3	LOI
1108/18	SAND	80.0	11.0	1.03	2.0	3.20	2.50	0.16	0.023	1.00	0.90

The results are expressed in percentage (%) unless otherwise indicated.

RECTOR OF
GEOLOGICAL SURVEYS
0 4 APR 2018
P. O. Box 30009-C0100
NAIROBI

JORAM W. KATWEO
FOR: DIRECTOR OF GEOLOGICAL SURVEYS.
The results are based on the test sample only.

Plate A1 Chemical composition of FVA

MINISTRY OF PETROLEUM AND MINING

e-mail:cg@mining.go.ke
When replying please quote ref No & date
Ref. No. ORIGINAL CERT NO....1106/18

MINISTRY OF PETROLEUM AND MINING
MACHAKOS ROAD
P.O. Box 30009-00100 GPO
NAIROBI
Date...29th March, 2018

ASSAY CERTIFICATE

SENDER'S NAME	:	GETAHUN MULUSEW
DATE	:	15.03.2018
SAMPLE TYPE	:	SAND
SAMPLE NO	:	1106/18

RESULT

Lab No.	Sender's Ref.	SiO_2	Al_2O_3	CaO	MgO	Na_2O	K_2O	TiO_2	MnO	Fe_2O_3	LOI
1106/18	FRAP	58.85	15.6	2.0	0.04	6.20	4.30	0.85	0.29	5.44	10.00

The results are expressed in percentage (%) unless otherwise indicated.

JORAM W. KATWEO
FOR: DIRECTOR OF GEOLOGICAL SURVEYS.

DIRECTOR OF GEOLOGICAL SURVEYS
04 APR 2018
P. O. Box 30009-00100
NAIROBI
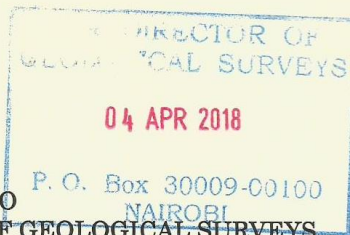
The results are based on the test sample only.

Plate A2 Chemical composition of FRAP

CEMENT ANALYSIS CERTIFICATE   Cert No. 06

Bamburi cement Ltd

CUSTOMER : General
CEMENT TYPE : PORTLAND CEMENT : **CEM I 42.5N (Powerplus)**
STANDARD SPECIFICATION : EN 197-1
VESSEL'S NAME : .... **DESTINATION: GENERAL** ....

CHEMICAL ANALYSIS

PARAMETER	SPECIFICATION	UNIT	RESULT
LOI (Loss on Ignition)	Not more than 5.0		2.90
SiO2	-		20.61
I.R.	Not more than 5.0		1.00
Al2O3	Not more than 8.0		5.05
Fe2O3	-		3.24
CaO	-	%	63.37
MgO	Not more than 3.0		0.81
SO3	Not more than 3.5		2.75
Na2O	-		0.15
K2O	-		0.52
Free CaO	-		0.63
Na.Eq	Not more than 0.6		0.49
C3A	-		7.91
Cl-	Not more than 0.1		<0.01

PHYSICAL TESTS

TEST		SPECIFICATION	UNIT	
SPECIFIC SURFACE		-	cm²/g	3197
H20 Demand		-	%	25.65
SETTING	INITIAL	Not less than 60	Minutes	160
TIME	FINAL			252
SOUNDNESS		Not more than 10	mm	0.3
MORTAR PRISM	At 2 days	Not less than 10	N/mm²	19.30
COMPRESSIVE STRENGTH	At 28 days	Not less than 42.5		48.94

REMARKS : The certificate represents dispatch for June 2017

FRANCIS KITSOVI
QUALITY MANAGER

A member of
LafargeHolcim

Plate A3 Chemical composition of cement

MINISTRY OF TRASPORT, INFRUSTRUCTURE, HOUSING & URBAN DEVELOPMENT
STATE DEPARTMENT OF INFRASTRUCTURE

MATERIALS TESTING AND RESEARCH DIVISION

INTERNAL MEMO

From: OiC Chemistry Laboratory	To: Chief Engineer(Materials)
Date. 19th March, 2018	

SUBJECT

CHEMICAL ANALYSIS OF RICE HUSK ASH

Reference is made to your memo Ref. M.35/R5/30 dated 12th January, 2018.

The sample you submitted on 12 January, 2018 gave the results shown below.

Constituent	Composition, % m/m
Silicon (IV) Oxide as SiO_2	92.97
Aluminum (III) Oxide as Al_2O_3	0.93
Iron (III) Oxide as Fe_2O_3	0.88
Calcium Oxide as CaO	0.86
Potassium Oxide as K_2O	2.54
Magnesium (II) Oxide as MgO	0.481
Sodium Oxide as Na_2O	2.43
Sulphur (IV) Oxide as SO_3	4.84
Loss on Ignition	7.40

Yours Faithfully,

J. N. Ngurungu
OiC- Chemistry Laboratory
C.C.

1. SPSE (RSPM)
2. SPSE (PDC)
3. Mulusew Aderaw Getahun CE 300-0004/17

Plate A4 Chemical composition of RHA

B. Hardened Concrete Properties

Table B1. Mix design procedures

Step 1 — Determining the target strength	
A. Characteristic compressive strength in MPa	20.000
B. Assumed standard deviation in MPa	3.000
C. Target average compressive strength in MPa at 28-day: A+1.65*B	24.950
Step 2 — Selection of water-cement ratio	
D. Maximum water-cement ratio	0.650
Step 3 — Selection of water content	
E. Maximum water content (kg/m^3) for 20 mm aggregate & 50 to 90 slump	240.000
F. Adjusted water content (kg/m^3): E+6%E	254.000
Step 4 – Calculation of cement content	
G. Specific gravity of cement	3.120
H. Cement Content (kg/m^3): F/D	390.770
Step 5: Proportion of volume of aggregates	
I. Volume of coarse aggregate corresponding to 20 mm size.	0.630
J. Specific gravity of coarse	2.680
k. Specific gravity of fine aggregate	2.520
Step 6: Estimation of concrete mix calculations per unit volume of concrete	

1. Volume of concrete (m^3)		1.000
2. Volume of cement (m^3)	H/G*1/1000	0.125
3. Volume of water (m^3)	F/1*1/1000	0.254
4. Total volume of aggregates (m^3)	1-(2+3)	0.630
5. Mass of coarse aggregates (kg/m^3)	I*4*J*1000	1592.700
6. Mass of fine aggregates (kg/m^3)	(1-I)*4*k*1000	712.150

Table B2. Water absorption and density of hardened concrete

| Mix Description	Water Absorption (%)	Density (kg/m³)		
	By Immersion & Boiling	After immersion	After immersion & Boiling	Apparent
Control	7.368(0.18)	2.522(0.01)	2.525(0.01)	2.844(0.60)
RHA5%	7.281(0.29)	2.5160.01()	2.518(0.01)	2.831(0.40)
RHA10%	7.255(0.18)	2.515(0.00)	2.517(0.00)	2.828(0.31)
RHA15%	7.233(0.11)	2.504(0.01)	2.506(0.01)	2.813(0.07)
RHA20%	7.220(0.01)	2.488(0.01)	2.490(0.01)	2.790(0.03)
RAP10%	7.210(0.09)	2.499(0.01)	2.508(0.00)	2.813(0.00)
RAP20%	7.128(0.05)	2.487(0.01)	2.496(0.01)	2.794(0.01)
RAP30%	7.091(0.10)	2.450(0.08)	2.459(0.08)	2.742(0.10)
RAP40%	7.014(0.02)	2.428(0.07)	2.439(0.07)	2.712(0.10)
RAP50%	6.911(0.19)	2.416(0.03)	2.426(0.04)	2.692(0.06)
[5RHA & 10RAP]%	7.224(0.11)	2.502(0.00)	2.514(0.01)	2.823(0.19)
[5RHA & 20RAP]%	7.166(0.14)	2.499(0.01)	2.511(0.02)	2.816(0.06)
[5RHA & 30RAP]%	7.063(0.28)	2.495(0.01)	2.505(0.01)	2.803(0.10)
[10RHA & 10RAP]%	7.215(0.25)	2.501(0.01)	2.514(0.02)	2.822(0.14)
[10RHA & 20RAP]%	7.140(0.06)	2.494(0.01)	2.509(0.01)	2.812(0.29)
[10RHA & 30RAP]%	7.111(0.21)	2.485(0.00)	2.506(0.01)	2.807(0.07)
[15RHA & 10RAP]%	7.162(0.12)	2.491(0.00)	2.511(0.00)	2.815(0.03)
[15RHA & 20RAP]%	7.157(0.20)	2.490(0.00)	2.510(0.01)	2.814(0.12)
[15RHA & 30RAP]%	7.0940.09()	2.488(0.01)	2.507(0.01)	2.807(0.21)
[20RHA & 10RAP]%	7.186(0.13)	2.486(0.02)	2.507(0.07)	2.811(0.52)
[20RHA & 20RAP]%	7.220(0.08)	2.484(0.03)	2.507(0.05)	2.812(0.64)
[20RHA & 30RAP]%	7.056(0.19)	2.482(0.00)	2.501(0.00)	2.797(0.03)
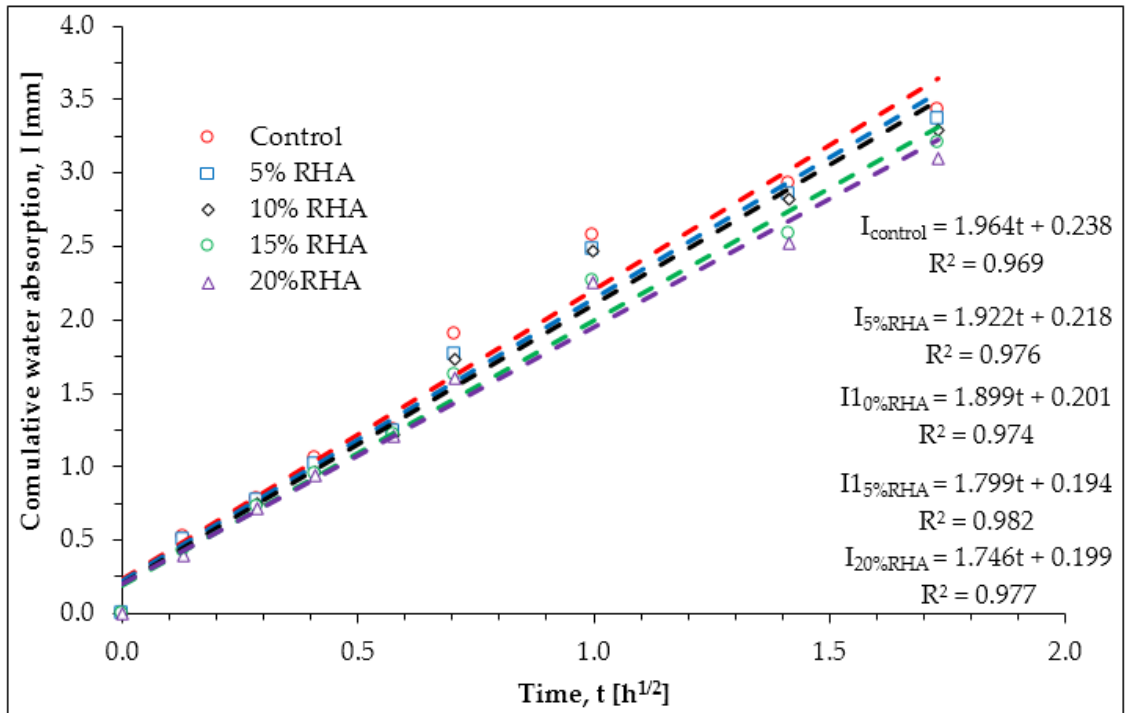
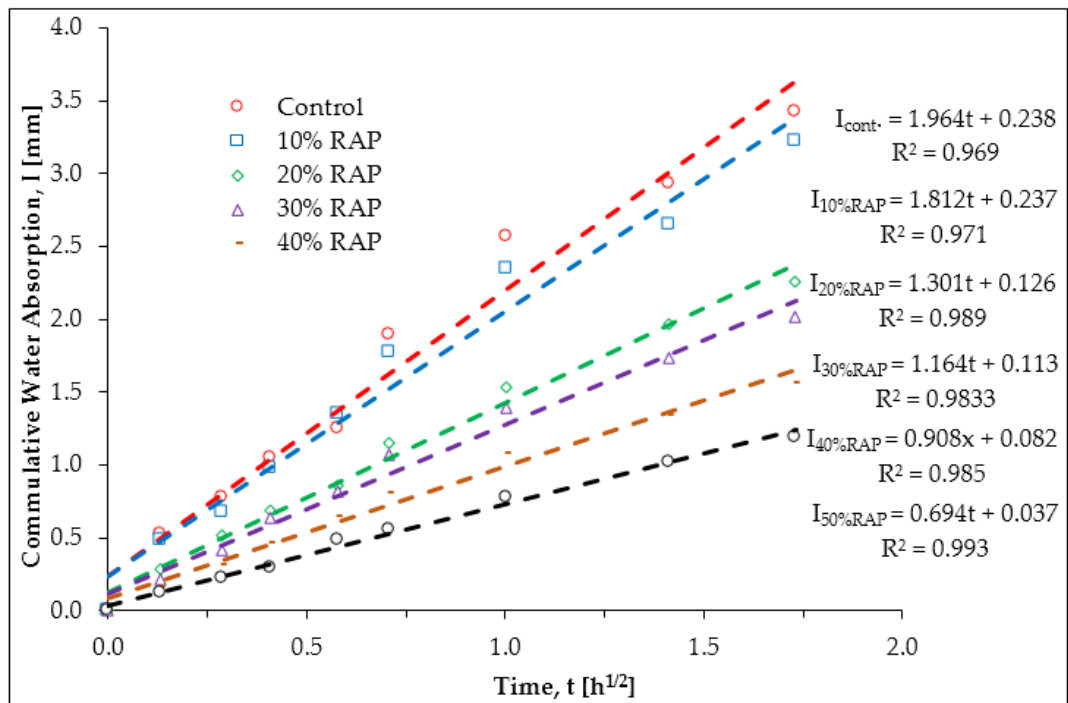**Figure B1**. Cumulative water absorption by RHA Concrete.

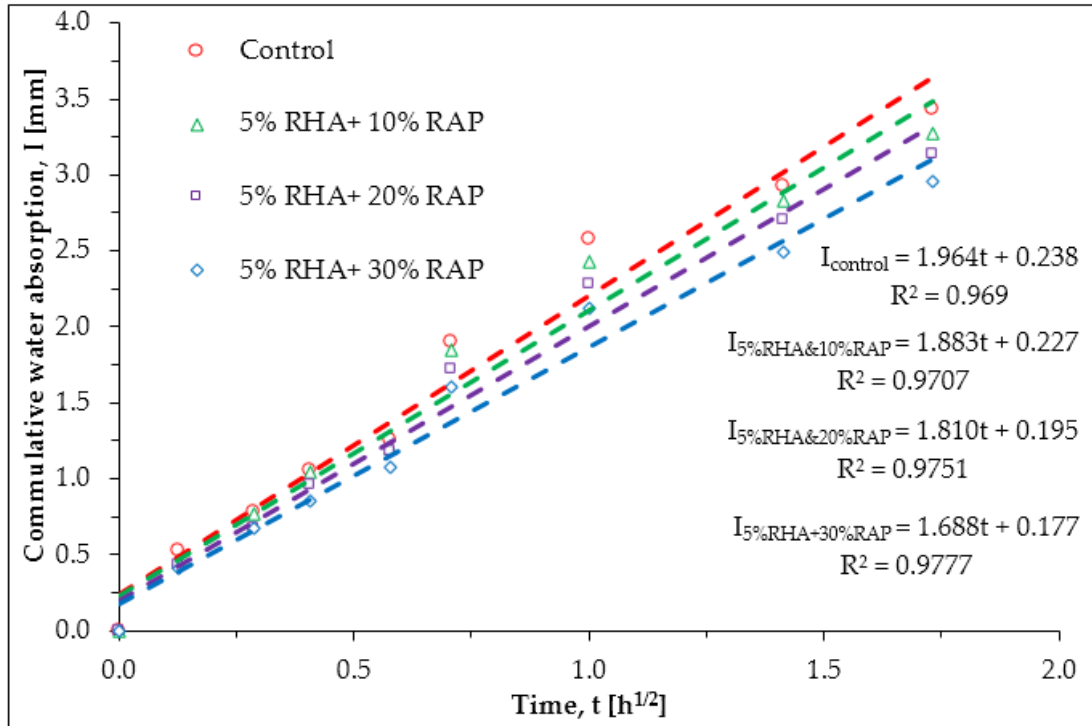**Figure. B2.** Cumulative water absorption by RAP Concrete.

Figure B3. Cumulative water absorption by 5% RHA and (10–30) % RAP inclusive concrete
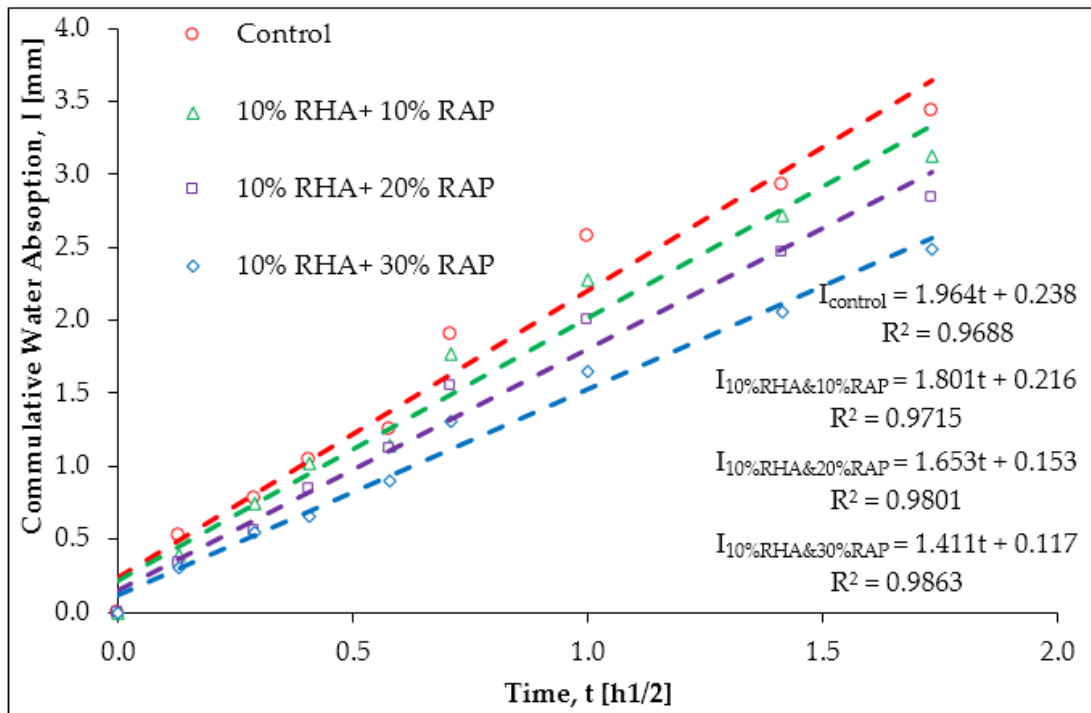

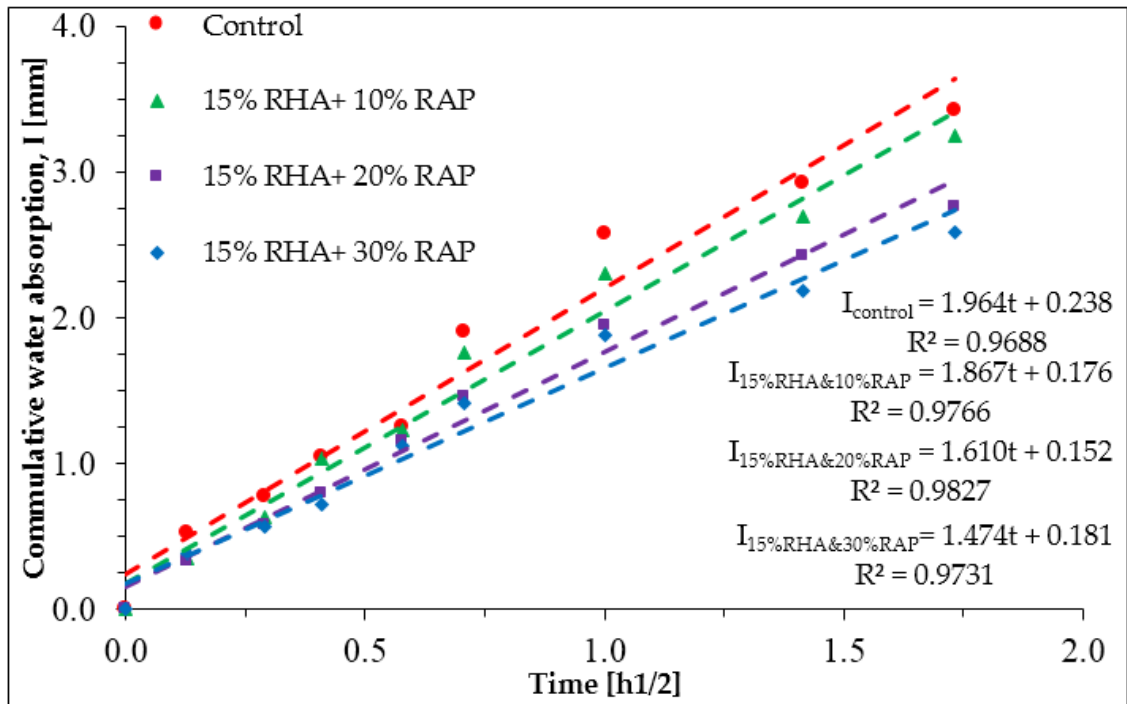**Figure B4** Cumulative water absorption by 10% RHA and (10–30) % RAP-inclusive concrete.

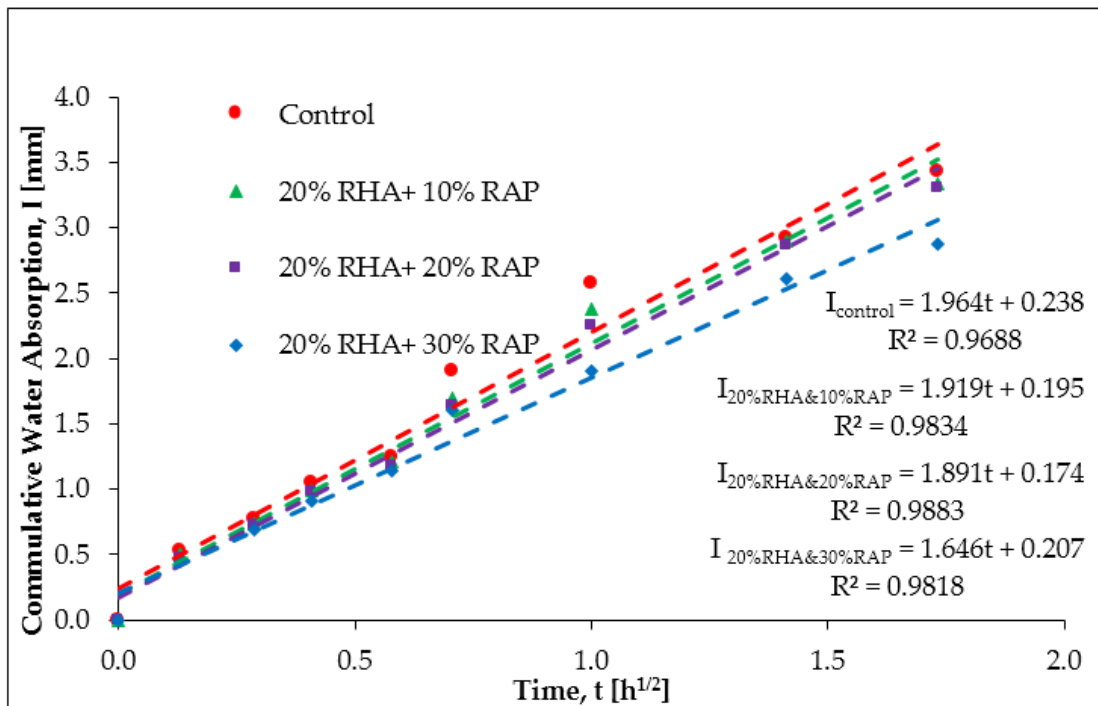**Figure B5** Cumulative water absorption by 15% RHA and (10–30) % RAP-inclusive concrete.

Figure B6 Cumulative water absorption by 20% RHA and (10–30) % RAP-inclusive concrete

C. Concrete Strength Prediction

Table C1 Comparison between experimental and model predicted data

| Sample No.	Experimental Values f_c	Experimental Values f_{ts}	Predicted Values f_c	Predicted Values f_{ts}	Sample No.	Experimental Values f_c	Experimental Values f_{ts}	Predicted Values f_c	Predicted Values f_{ts}
1	27.14	2.16	26.43	2.13	34	20.03	1.99	18.71	1.89
2	26.72	1.99	26.43	2.13	35	20.28	1.95	20.20	1.93
3	26.29	2.24	26.43	2.13	36	20.94	1.81	20.50	1.79
4	28.66	2.39	27.77	2.20	37	18.45	1.71	18.07	1.72
5	27.88	1.99	27.77	2.20	38	18.94	1.73	19.13	1.73
6	27.16	2.19	27.77	2.20	39	17.87	1.78	18.15	1.68
7	30.16	2.20	29.27	2.26	40	27.15	2.00	25.24	2.30
8	30.08	2.30	29.27	2.26	41	25.49	2.10	24.24	2.30
9	28.86	2.29	29.27	2.26	42	24.43	2.09	24.24	2.30
10	30.02	2.28	29.58	2.32	43	20.62	1.82	21.01	1.85
11	31.03	2.29	29.58	2.32	44	20.69	1.79	21.01	1.85
12	29.10	2.29	29.58	2.32	45	20.55	1.80	21.01	1.85
13	32.58	2.23	31.11	2.31	46	19.17	1.64	19.11	1.71
14	25.86	2.36	26.11	2.31	47	21.14	1.71	20.11	1.71
15	28.95	2.15	29.11	2.31	48	18.02	1.70	19.11	1.71
16	19.97	1.90	21.56	1.88	49	29.00	2.19	28.76	2.27
17	20.87	1.80	21.56	1.88	50	27.94	2.49	27.90	2.23
18	21.77	1.90	21.56	1.88	51	25.92	2.00	26.42	2.11
19	19.65	1.75	19.62	1.67	52	23.72	2.03	23.61	2.03
20	18.93	1.62	19.62	1.67	53	24.04	1.99	24.29	2.02
21	20.12	1.70	19.62	1.67	54	26.16	2.00	24.84	1.94
22	17.85	1.50	17.83	1.52	55	19.69	1.77	19.76	1.77
23	17.95	1.49	17.83	1.52	56	19.81	1.78	20.29	1.76
24	17.78	1.51	17.83	1.52	57	19.57	1.79	20.28	1.73
25	16.45	1.36	16.18	1.37	58	25.65	2.00	25.57	2.13
26	16.32	1.49	16.18	1.37	59	25.40	2.09	25.52	2.14
27	16.32	1.31	16.18	1.37	60	25.39	2.07	24.66	2.11
28	14.89	1.22	15.16	1.28	61	21.35	1.99	21.54	1.96
29	14.98	1.28	15.16	1.28	62	23.18	2.00	22.51	1.95
30	14.75	1.29	15.16	1.28	63	22.05	1.99	22.57	1.94
31	22.98	1.98	23.16	1.99	64	18.18	1.70	18.21	1.77
32	23.29	2.04	23.40	2.05	65	20.02	1.76	19.27	1.75
33	21.99	2.00	21.40	1.97	66	19.38	1.65	19.08	1.76

Table C2 Connection weights generated from the proposed artificial neural network

W (kg/m³)	C (kg/m³)	RHA (kg/m³)	FVA (kg/m³)	FRAP (kg/m³)	CVA (kg/m³)	CRAP (kg/m³)	W/C (-)	CFM (-)	CW$_{fa}$ (%)	CW$_{ca}$ (%)	CSG$_{fa}$ (-)	CSG$_{ca}$ (-)	NAS (mm)	CT$_{av}$ (°C)	F$_{cs}$ (MPa)	F$_{ts}$ (MPa)
-0.650	-0.322	-0.740	-0.057	-0.897	0.542	-0.614	-0.449	0.039	-0.537	-0.686	0.826	-0.457	0.158	-0.726	0.206	-0.135
-0.394	-0.835	0.007	0.413	0.271	0.395	-0.526	0.239	-0.056	0.912	-0.454	0.704	-0.137	0.448	0.350	0.452	0.558
-0.665	-0.790	0.486	0.370	0.069	0.010	0.342	0.350	0.362	-0.244	0.223	-0.257	-0.634	0.187	-0.261	0.364	0.468
0.032	0.448	-0.864	-0.842	0.065	-0.360	0.601	0.594	-0.776	0.284	-0.759	-0.702	0.382	0.886	0.303	0.254	-0.358
-0.463	0.307	-0.441	-0.484	0.270	0.228	0.258	0.298	0.439	0.277	-0.242	0.373	1.003	0.316	-0.753	-0.035	-0.227
-0.360	-0.121	0.136	0.020	0.499	-0.012	-0.393	-0.672	-0.503	0.371	-0.257	0.258	-0.553	0.219	-0.252	-0.557	-0.512
-0.381	0.448	-0.507	-0.269	-0.440	0.857	-0.475	-0.292	-0.672	-0.606	0.457	-0.296	0.219	0.582	-0.216	-0.001	-0.415
0.471	0.469	-0.005	0.369	-0.676	0.476	-0.471	-0.487	0.092	0.555	0.377	-0.248	-0.176	0.781	0.297	-0.269	0.037
0.030	-0.134	0.390	-0.586	-0.302	-0.717	0.325	-0.717	-0.608	-0.523	-0.570	-0.208	0.436	0.102	0.118	-0.177	-0.130
-0.503	0.159	-0.414	-0.456	-0.685	-0.717	-0.508	-0.597	-0.241	-0.192	-0.268	-0.529	0.869	0.080	0.170	0.493	-0.474
-0.378	-0.524	-0.496	0.912	0.386	0.044	-0.280	-0.642	0.849	0.346	-0.337	-0.516	-0.020	0.849	-0.425	0.148	-0.197
0.032	0.746	-0.017	0.320	-0.584	-0.161	-0.464	0.242	-0.428	0.784	0.308	-0.439	-0.004	0.296	0.114	0.281	-0.660
-0.079	-0.366	0.067	-0.028	-0.223	0.172	0.453	-0.301	-0.793	0.004	-0.648	-0.446	-0.388	0.031	0.021	0.402	0.350
-0.254	-0.040	-0.184	-0.024	-0.173	0.058	-0.135	-0.187	-0.177	0.110	-0.220	-0.114	0.042	0.036	-0.031	-0.470	-0.181
-0.254	-0.040	-0.184	-0.024	-0.173	0.058	-0.135	-0.187	-0.177	0.110	-0.220	-0.114	0.042	0.036	-0.031	-0.338	-0.167

Table C3. Relative percentage influence of input features on outputs

	W	C	RHA	FVA	FRAP	CVA	CRAP	W/C	CFM	CW$_{fa}$	CW$_{ca}$	CSG$_{fa}$	CSG$_{ca}$	NAS	CT$_{av}$
IF for F$_{cs}$	14.0%	11.8%	10.3%	2.6%	9.8%	4.2%	1.2%	11.9%	0.5%	2.1%	9.6%	7.6%	4.2%	2.3%	7.9%
IF for F$_{ts}$	3.5%	14.2%	12.0%	7.8%	6.6%	4.7%	6.6%	6.4%	0.6%	7.3%	1.1%	6.9%	9.9%	9.6%	2.7%
Average	8.8%	13.0%	11.1%	5.2%	8.2%	4.5%	3.9%	9.1%	0.6%	4.7%	5.4%	7.3%	7.1%	5.9%	5.3%

D. Publications
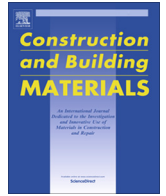
Artificial neural network based modelling approach for strength prediction of concrete incorporating agricultural and construction wastes

Mulusew Aderaw Getahun [a,b,*], Stanley Muse Shitote [c], Zachary C. Abiero Gariy [d]

[a] Civil Engineering Department, Pan African University Institute for Basic Sciences, Technology and Innovation (PAUSTI), 62000 00200 Nairobi, Kenya
[b] Ethiopian Roads Authority, 1770 Addis Ababa, Ethiopia
[c] Civil Engineering Department, Rongo University, 103-40404 Rongo, Kenya
[d] Civil Engineering Department, Jomo Kenyatta University of Agriculture and Technology (JKUAT), 5505 00100 Nairobi, Kenya

HIGHLIGHTS

- The concrete uses supplementary materials from construction and agricultural wastes.
- The 28-days compressive and tensile strengths were predicted accurately by ANN model.
- The cement, water, rice husk ash and w/c ratio had high influence on the predicted strength.

GRAPHICAL ABSTRACT
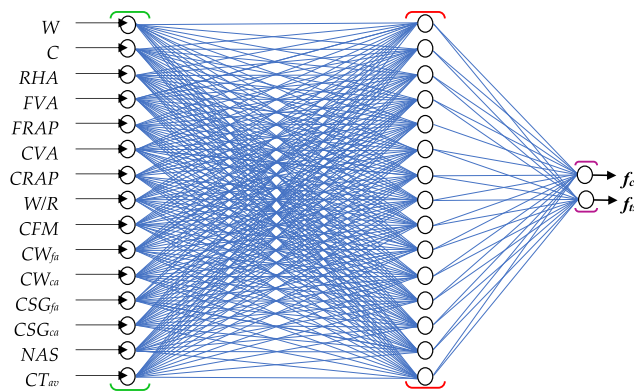
ABSTRACT

Construction debris and agricultural wastes are among the major environmental concerns in the world. Construction debris consumes about 28% of the nation's landfill facilities. Over 254.5 million tons of rice husk is available for disposal every year. A large amount of these materials can be recycled and reused as aggregate and cement substitutes for general construction and pavements among other works. In this study, effort was made to develop artificial neural network (ANN) model for predicting the 28-day strength of concrete incorporating rice husk ash (RHA) and reclaimed asphalt pavement (RAP) as partial replacements of Portland cement and virgin aggregates respectively. The ANN model predicted the compressive and tensile splitting strengths with prediction error values of 0.648 and 0.072 MPa respectively. The model overpredicted the compressive strength (f_c) on average by 0.123 MPa, whereas it underpredicted the tensile strength (f_{ts}) by 0.019 MPa. The predicted compressive and tensile strengths deviated on average by 2.088 and 2.905% respectively from experimental results. The results indicate that the ANN is an efficient model to be used as a tool for predicting the compressive and tensile strengths of concrete incorporating RHA and RAP.

© 2018 Elsevier Ltd. All rights reserved.

* Corresponding author at: Civil Engineering Department, Pan African University Institute for Basic Sciences, Technology and Innovation (PAUSTI), 62000 00200 Nairobi, Kenya.

E-mail addresses: mulusew06@gmail.com (M.A. Getahun), sshitote@rongovarsity.ac.ke (S.M. Shitote), zagariy@eng.jkuat.ac.ke (Z.C. Abiero Gariy).

1. Introduction

Concrete is a mixture of cement paste and aggregates that can be moulded into any practical shape and dimensions of the desired structures [1]. The global annual production of Portland cement concrete is estimated to be more than 10 billion tons [2,3]. Concrete production consumes a substantial amount of raw materials. For instance, cement production alone is both energy and resource intensive. Every ton of cement production consumes about 4 GJ of energy, 1.7 tons of raw materials and releases about 0.73–0.99 ton of CO_2 [2,4–6]. Portland cement concrete production also consumes about 8–12 billion tons of aggregate each year [6,7]. The high demand for construction materials will continue reducing natural stone deposits significantly thereby posing a negative impact on the environment [7–9]. Subsequently, the concrete industry is exploring ways to utilize alternative materials for use in concrete production so as to minimize environmental impact and achieve sustainable development [10]. Construction and Argo-industrial wastes have been utilized to substitute cement and aggregates aiming at producing cheaper concrete that contributes to natural resources preservation and solid waste management [11–18]. Recycled asphalt pavement (RAP) and rice husk ash (RHA) are among the construction and agro-industrial wastes which can be used as potential aggregate and cement substitutes respectively.

Conventional concrete is an assortment of cement, water, coarse and fine aggregates [10]. The concrete properties are influenced by several parameters such as quality and quantity of aggregates, cement type, water content and water to cement ratio [19]. The traditional approach used in modelling the effects of these parameters on mechanical properties of concrete starts with an assumed form of analytical equation [20]. This approach fails to grasp the actual scenario when some of the concrete constituents are not the conventional materials and when the assumption is wrong.

The compressive and tensile splitting strengths are vital mechanical properties of concrete and significant indexes in the design of concrete structures [21]. Concrete attains the majority of its final strength after 28 days of curing, which is a benchmark to compute the strength at any other given age [22,23].

Recently, many studies have been using various methods such as analytical modelling, mechanical modelling, statistical methods and artificial intelligence [10,22] for predicting the strength of concrete incorporating various ingredients. One of the areas in artificial intelligence that has grown fast and gained popular engineering applications is the artificial neural network (ANN) [24,25]. ANN has been employed in many civil engineering applications like detection of structural damage, structural system identification, material behaviour modeling, groundwater monitoring, foundation settlement prediction, concrete mix proportioning and concrete strength prediction [7,22,26–28].

Several studies [7,10,19,27–31] used ANN for predicting the strengths of different types of concrete. Jamalaldin et al. [32] made an effort to predict the compressive strength of high strength concrete using ANN. A total of 30 ANN architectures were studied of which the 8-10-6-1 was found to be the best possible architecture and their ANN model was able to mimic experimental results accurately. Duan et al. [10] also constructed an ANN model with one hidden layer. The model accurately predicted the compressive strength of recycled aggregate concrete. Chopra et al. [19] applied ANNs as strength predictive model. Based on the study results, it was reported that the ANN model with the Levenberg-Marquardt training function and sigmoid activation function was the best prediction tool. Kalra and Joseph [33] constructed 5-10-1 multi-layer feed-forward ANN architecture for predicting the compressive

strength of concrete. According to the study, the best validation performance was found at epoch 40 with mean squared error value of 10.99 MPa. Bharathi et al. [34] developed ANN model for predicting the fresh and hardened properties of self-compacting concrete containing fly ash as partial replacement of cement. Heidari et al. [35] also applied the ANN model for predicting the compressive strength of concrete. The study noted that the predicted results of neural network were accurate and closer to actual values. Hossein et al. [7] predicted the recycled aggregate concrete compressive strength accurately using ANN predictive model. The best validation performance of their model was 0.0044 MPa at epoch 5.

The primary reason for the wide recognition and application of ANN is due to its ability and effectiveness in solving difficult and complex engineering problems [25]. ANN can reveal astonishing capabilities in modeling the human brain [36]. The neural network processing elements are similar to the neurons in the human brain that comprise of computational units arranged in layers [20]. The multilayer perceptron (feed-forward network) has been a commonly used ANN architecture [37]. Multilayer perceptron (MLP) composed of a set of massively parallel computational neurons. Each node is fully connected to the other through connection weights and receives an input signal from neurons linked to it. The successive layers of nodes receive input from the previous layers; the outputs of nodes in each layer are inputs to nodes in the next layer.

ANN should be designed and trained properly with data regarding the problem to achieve the required task. The backpropagation algorithm has been extensively used for training MLPs [37]. Apart from the input, hidden and output neurons, activation function is an important factor that affects the ANN performance [38]. The most popular activation functions are tan-sigmoid, log-sigmoid and purelin [39].

The main objective of this study was to develop an ANN model for predicting the 28-days compressive and tensile splitting strengths of concrete incorporating RHA and RAP. Primary data was collected through laboratory experiments for use in ANN strength predictive model development. The concrete incorporating RAP and RHA is a new material itself; as a result, no research has not been done so far in this regard. The compositions and properties of concrete incorporating RAP and RHA is noticeably different from the conventional concrete, thus making it hard to predict its strength using analytical and statistical modeling approaches. The analytical approach is usually limited by problem complexity; is either too difficult to be constructed or useless due to unrealistic assumptions. Statistical model also uses a predetermined form and parameterization. On the other hand, the ANN model can capture non-linear complex relationships among variables by investigating important characteristics embedded in the data [37]. ANN can generate results to problems even when input variables contain mistakes and are incomplete due to its capability to learn and generalize from instances and experiences [39].

2. Material and methods

2.1. Materials

Materials used for this study were fine reclaimed asphalt pavement (FRAP), coarse reclaimed asphalt pavement (CRAP), fine virgin aggregate (FVA), coarse virgin aggregate (CVA), ordinary Portland cement (OPC) type I (42.5 N), rice husk ash (RHA) and water. All materials were obtained from different parts of Kenya. FVA (river sand) and CVA were purchased from Masinga and Molongo districts of Kenya respectively. RAP was obtained from an old distressed flexible pavement, Ruaka-Banana-Limuru Road (D407), sampled at the section near Tigoni, Kiambu County of Kenya. The road was constructed about 21 years ago and has served without major rehabilitation. RHA was collected from the dump site of Mwea Rice Milling Factory, Kenya. Fig. 1 shows the materials used for the current study.
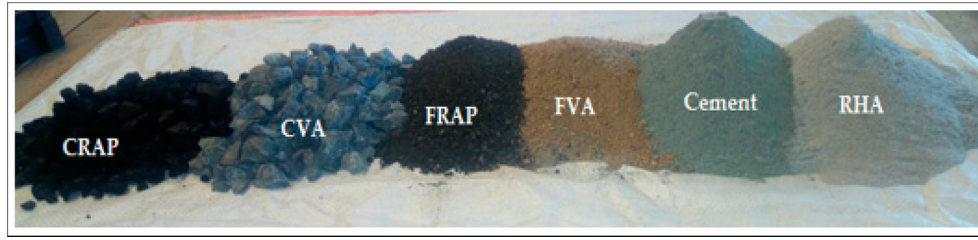
Fig. 1. Materials.

2.2. Material testing and result

Grading of the aggregates was determined in line with BS EN 933-1 [40] procedures using test sieve of the sizes complying with BS ISO 3310-2 [41]. The RAP material was obtained through ripping and milling of old existing pavement, and then crushed manually and finally sieved using 5 mm sieve in order to separate into FRAP and CRAP. RHA was sieved using a 0.10 mm sieve. The gradation results of fine and coarse aggregates are depicted in Figs. 2 and 3 respectively. As can be seen from the Figs., the particle size distributions of CVA and FVA met the grading requirements of BS 882.

The specific gravity and water absorption of coarse and fine aggregates were determined as per BS EN 1097-6 [42] test methods. Table 1 shows the materials' physical properties.

The composite properties of aggregates were calculated from the properties of individual components using Eqs. (1)–(3).

$$CFM_{FA} = \frac{FM_{fva} x P_{fva} + FM_{frap} x P_{frap}}{P_{fva} + P_{frap}} \tag{1}$$

$$CSG_a = \frac{1}{\frac{P_{va}}{SG_{va}} + \frac{P_{rap}}{SG_{rap}}} \tag{2}$$

Fig. 2. Fine aggregate particle size distribution.

Fig. 3. Coarse aggregate particle size distribution.

$$CWA_a = \frac{1}{\frac{P_{va}}{WA_{va}} + \frac{P_{rap}}{WA_{rap}}} \tag{3}$$

where: CFM_{fa} is composite fineness modulus of fine aggregates; FM_{fva} and FM_{frap} are the fineness modulus of fine virgin and reclaimed asphalt pavement aggregates respectively; P_{fva} and P_{frap} are the percentages of fine virgin and reclaimed asphalt pavement aggregates respectively; $CSGa$ and $CWAa$ are the composite specific gravity and water absorption of aggregates respectively; SG_{va} and SG_{rap} are the specific gravities of virgin and reclaimed asphalt pavements respectively; and WA_{va} and WA_{rap} are the water absorption of virgin and reclaimed asphalt pavements respectively.

The mix design for 25 MPa concrete was done in accordance with [43] and [44]. A total of 22 mixtures were prepared and each mix was assessed in three replicates. Table 2 portrays the particulars of studied mixture proportions. In all the mixtures, 254 kg/m³ of water and water to cementitious material ratio of 0.65 were kept constant.

Cubes of dimension 100 mm × 100 mm × 100 mm and cylinders with a diameter of 100 mm and 200 mm long conforming to BS EN 12390-1 [45] requirements were used to make concrete specimens for compressive and tensile splitting strength tests respectively. A total of 132 cube and cylinder specimens were made and cured in accordance with the methods specified in BS EN 12390-2 [46] for compressive and tensile splitting strength tests respectively. Specimens were loaded to failure in automatic computerized testing machine conforming to BS EN 12390-4 [47] requirements.

2.3. Artificial neural network

2.3.1. Ann's architecture design

A three-layer perceptron was created using MATLAB version R2017a. A total of 33 Artificial networks were constructed using 66 experimental datasets obtained from 22 laboratory concrete mixtures. The networks were composed of input neurons (input layer), computational neurons (hidden layer) and an output layer. Fifteen input signals/variables used are mass of water (W), cement (C), RHA, FVA, FRAP, CVA, CRAP, water to cement ratio (W/C), composite fineness modulus of fine aggregates (CFM_{fa}), composite water absorption of fine aggregates (CWA_{fa}), composite water absorption of coarse aggregates (CWA_{ca}), composite specific gravity of fine aggregates (CSG_{fa}), composite specific gravity of coarse aggregates (CSG_{ca}), nominal maximum size of aggregate (NAs) and average curing temperature (CT_{av}). The compressive and tensile strengths were used as target datasets/desired outputs. Table 3 presents the ranges of input and output parameters.

2.3.2. Network training

The constructed 33 ANNs were trained by varying hidden neurons and activation functions. Log-sigmoid, tan-sigmoid and purelin linear activation functions were used to arrive at optimum activation functions by evaluating their performance against the model mean squared values. According to Shmueli et al. [39], the activation functions are defined in Eqs. (4)–(6).

$$Tan - sigmoid : g(x) = \frac{2}{1 + e^{-x}} - 1 \tag{4}$$
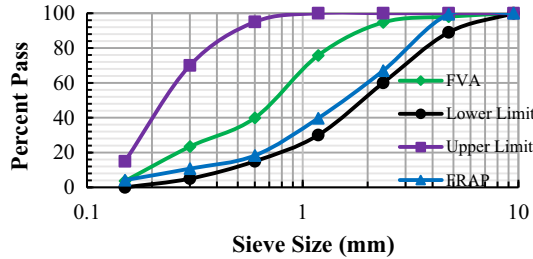
$$Log - sigmoid : g(x) = \frac{1}{1 + e^{-x}} \tag{5}$$
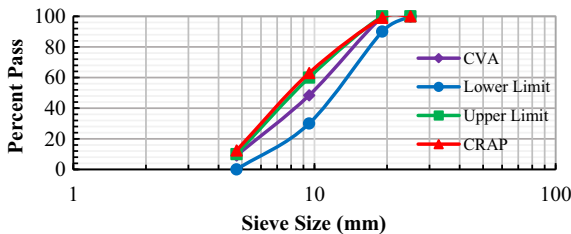
Table 1
Physical properties of materials.

Physical Property	Materials					
	OPC	RHA	FVA	FRAP	CVA	CRAP
Fineness modulus	–	–	2.65	3.61	–	–
Bulk specific gravity	–	–	2.43	2.32	2.62	2.41
Water Absorption [%]	–	–	3.95	2.42	2.41	1.63
Maximum particle size (mm)	0.09	0.10	5	5	20	20

Table 2
Mix proportions for 25 MPa concrete.

Mix description	Cement (kg/m³)	RHA (kg/m³)	FVA (kg/m³)	FRAP (kg/m³)	CVA (kg/m³)	CRAP (kg/m³)
Control	390	0	712	0	1593	0
[5–20]% RHA	[312–371]	[20–78]	712	0	1593	0
[10–50]% RAP	390	0	[356–641]	[71–356]	[796–1434]	[159–796]
5%RHA + [10–30]% RAP	371	20	[499–641]	[71–214]	[1115–1434]	[159–478]
10%RHA + [10–30]%RAP	351	39	[499–641]	[71–214]	[1115–1434]	[159–478]
15%RHA + [10–30]% RAP	332	59	[499–641]	[71–214]	[1115–1434]	[159–478]
20%RHA + [10–30]%RAP	312	78	[499–641]	[71–214]	[1115–1434]	[159–478]

Table 3
Model's input and output attributes.

Model Attributes	Range	
	Min.	Max.
1. *Input parameters*		
Water, W [kg/m³]	–	254
Cement, C [kg/m³]	312	390
Rice husk ash, RHA [kg/m³]	–	78
Fine virgin aggregate, FVA [kg/m³]	356	712
Fine reclaimed asphalt pavement, $FRAP$ [kg/m³]	–	356
Coarse virgin aggregates, CVA [kg/m³]	796	1593
Coarse reclaimed asphalt pavement, $CRAP$ [kg/m³]	–	796
Water to cement ratio, W/C	–	0.65
Composite fineness modulus, CFM	–	2.65
Fine aggregates composite water absorption, CWA_{fa} [%]	1.49	3.95
Coarse aggregates composite water absorption, CWA_{ca} [%]	2.02	2.41
Fine aggregates composite specific gravity CSG_{fa} [%]	2.37	2.43
Coarse aggregates composite specific gravity, CSG_{ca} [%]	2.51	2.62
Nominal aggregate size, NAs [mm]	–	19.5
Average curing temperature, CT_{av} [ºC]	24	25
2. *Desired output parameters*		
Compressive strength, f_c [MPa]	14.75	32.58
Tensile splitting strength, f_{ts} [MPa]	1.22	2.49

$$\text{Purelin} : g(x) = x \tag{6}$$

Trainlm and learndgm (gradient descent with momentum weight and bias) were used for training and adaptation learning function respectively. Backpropagation algorithm was used for training the networks. It trains the network layer by layer doing forward and backward computations [45,46]. Algorithm updating formulae are presented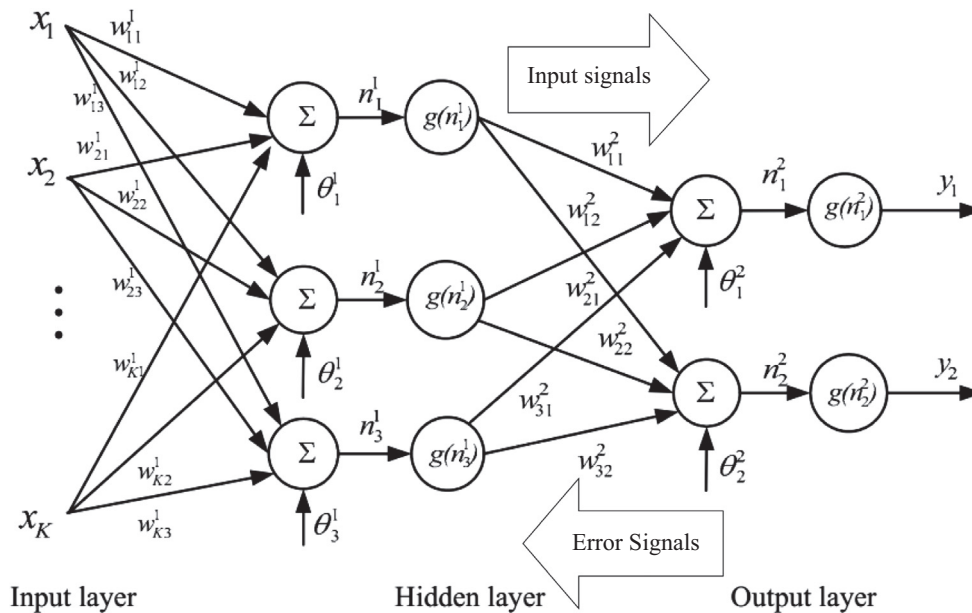 in Eqs. (7)–(10). The Backpropagation algorithm has two phases [10]. Input signals are multiplied by free parameters and added together with the bias term. The results are inputs to the activation function as presented in Eq. (7). The network then propagates the input signals forward until the desired output is generated by the output layer as shown in Fig. 4. If the output is different from the target, the error is calculated by Eq. (8) and backpropagated from the output layer to the source/input layer. The free parameters/connection weights are updated when errors are propagated as presented in Eqs. (9) and (10). In particular, the errors of the output nodes are distributed across all the hidden nodes so that each node is assigned "responsibility" for part of the error [39].

$$y_j = g\left(\sum_{i=0}^{n_l} w_{ji}^l x_i + \theta_j^l\right) \tag{7}$$

$$\delta_j^L = (d_j^L - y_j^L)(y_j^L)' \tag{8}$$

$$\Delta w_{ji}^l = \eta \delta_j^l y_j^{l-1} \tag{9}$$

$$w_{ji(new)}^l = w_{ji(old)}^l + \Delta w_{ji}^l \tag{10}$$

where: y_j is the output of the jth neuron in hidden layer; δ_j^l is the error gradient for the output neuron; Δw_{ji}^l is the weight correction; $w_{ji(new)}^l$ is the updated weight; w is the connection weight between two neurons; d is the desired response (target); x is the input; y is the neuron's output; g is the activation function; *PleaseCheck* π is the learning rate; *PleaseCheck* l is the number of layer; L is the output layer and i or j is the number of neuron in each layer; w_{ji}^l is the weight between the jth neuron in the lth layer and the ith neuron in the $(l-1)^{th}$ layer; θ_j^l is the jth neuron's bias; d_j^L is the desired response of the output neuron; and n_l is the number of neurons in the lth layer.

Fig. 4. Multilayer perceptron with one hidden layer [49].

2.3.3. Model performance evaluation

The ANN model was trained on the training data, applied to the validation data, and measures of accuracy then use the prediction errors on that validation set. The model's predictive accuracy was measured through computing mean absolute error, average error, mean absolute percentage error and root mean square error using Eqs. (11)–(14) respectively.

$$MAE = \frac{1}{n} \sum_{i=1}^{n} |a_i - p_i| \tag{11}$$

$$AE = \frac{1}{n} \sum_{i=1}^{n} (a_i - p_i) \tag{12}$$

$$MAPE = \frac{100}{n} \sum_{i=1}^{n} \frac{|a_i - p_i|}{|a_i|} \tag{13}$$

$$RMSE = \sqrt{\frac{\sum_{i=1}^{n} (a_i - p_i)^2}{n}} \tag{14}$$

where: MAE is the mean absolute error; AE is the average error; MAPE is the mean absolute percentage error; RMSE is the root mean square error; a is the actual/experimental value; p is the predicted value/model's output and n is the number of concrete specimens.

2.3.4. Sensitivity analysis

The main aim of the sensitivity analysis was to analyze the relative effect/importance of input variables/features on the outputs of the proposed ANN strength predictive model. Unlike classic statistical models, the task of determining the influence of independent variables/input parameters on the dependent variables/outputs does not seem easy in ANN due to its considerable complexity [7,47,50]. In this study, the relative influence of each input features on outputs was determined based on the magnitude of connection weights using the method proposed by L. Milne [51], Eq. (15).

$$IF = \frac{\sum_{j=1}^{n_{hid}} \frac{w_{ji}}{\sum_{l=1}^{n_{inp}} |w_{jl}|} \times w_{oj}}{\sum_{k=1}^{n_{inp}} \left(\sum_{j=1}^{n_{hid}} \left| \frac{w_{jk}}{\sum_{l=1}^{n_{inp}} |w_{jl}|} \times w_{oj} \right| \right)} \tag{15}$$

where: IF is the influence factor; N_{inp} is the number of inputs; n_{hid} is the number of hidden units; w is the connection weight; i is the input unit, and o is the output unit.

3. Results and discussion

3.1. ANN architecture

Determining ANN architecture is the first important step in developing an ANN model that best suits the problem at hand. However, there is no guideline for selecting the optimum ANN architecture, thus it is open to investigation [25,48]. Consequently, after many trials and errors, the network architecture shown in Fig. 5 was selected.

Fig. 6 shows the effect of neuron numbers and transfer functions in the hidden layer on the performances of different ANN
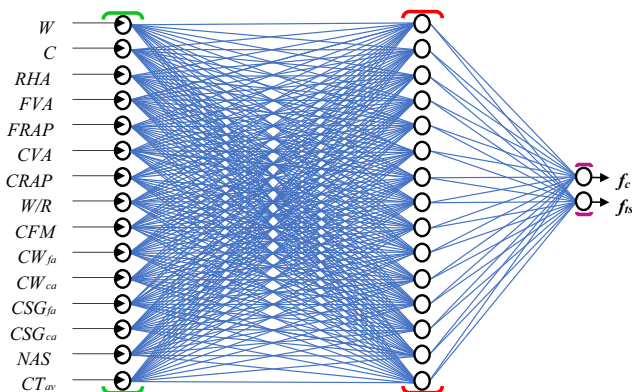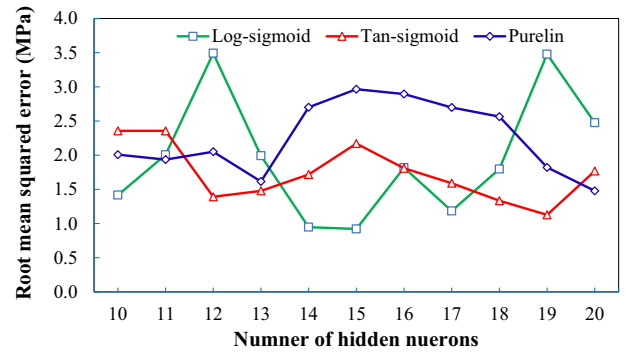
Fig. 6. Variations of RMSE against number of hidden neurones.

architectures. The regression values of the networks having various number of hidden neurons and activation functions are also presented in Fig. 7. It is apparent from Figs. 6 and 7 that the best possible ANN architecture found was L15-15-2 (fifteen input neurons, a single hidden layer having fifteen neurons and two output neurons) with Log-sigmoid activation function. It exhibited satisfactory results compared to all 33 ANN architectures investigated.

Fig. 8 shows the performance of the proposed ANN that portrays how the error drops when the network learns as expected for a well-trained ANN. This is a good indication of the network's
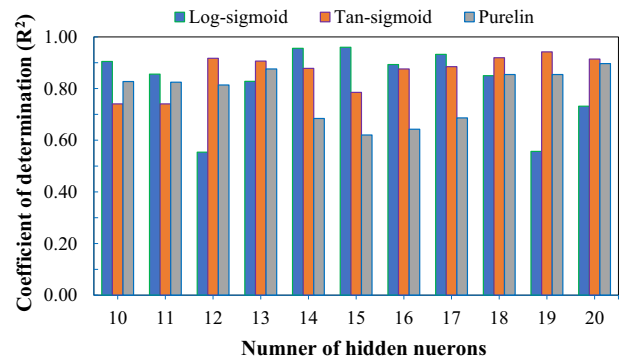
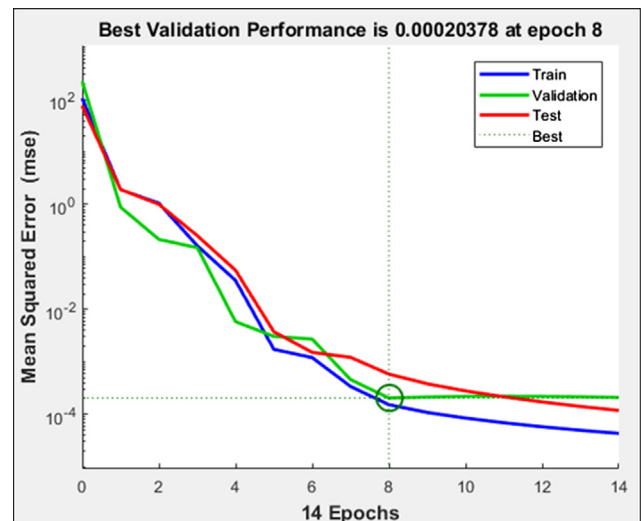**Fig. 7.** Variations of the coefficients of determination against number of hidden neurones.

Fig. 5. Proposed artificial neural network architecture (L15-15-2).
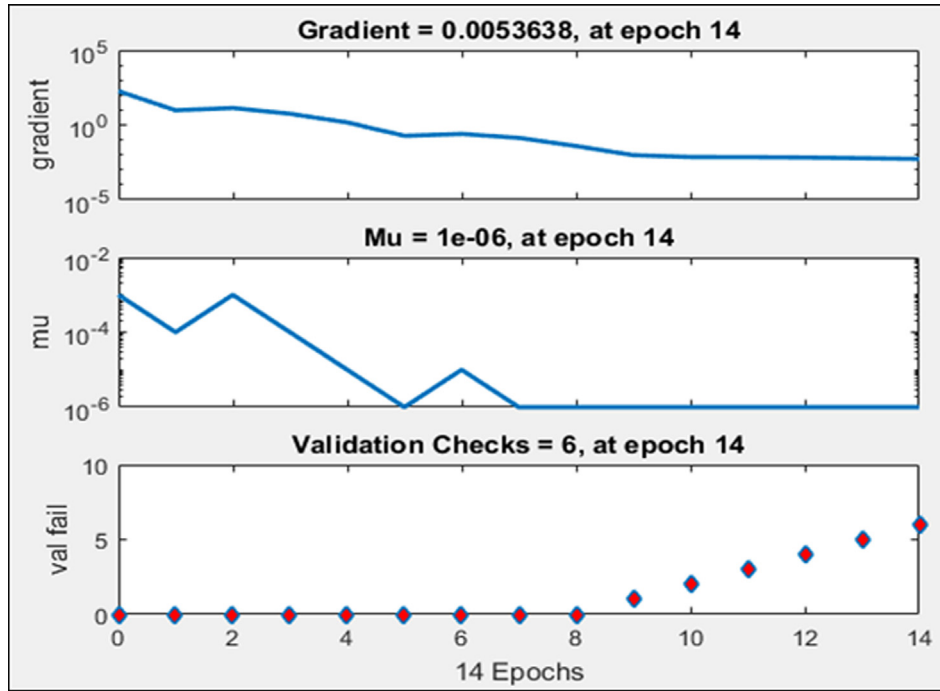
Fig. 8. Model performance plot.
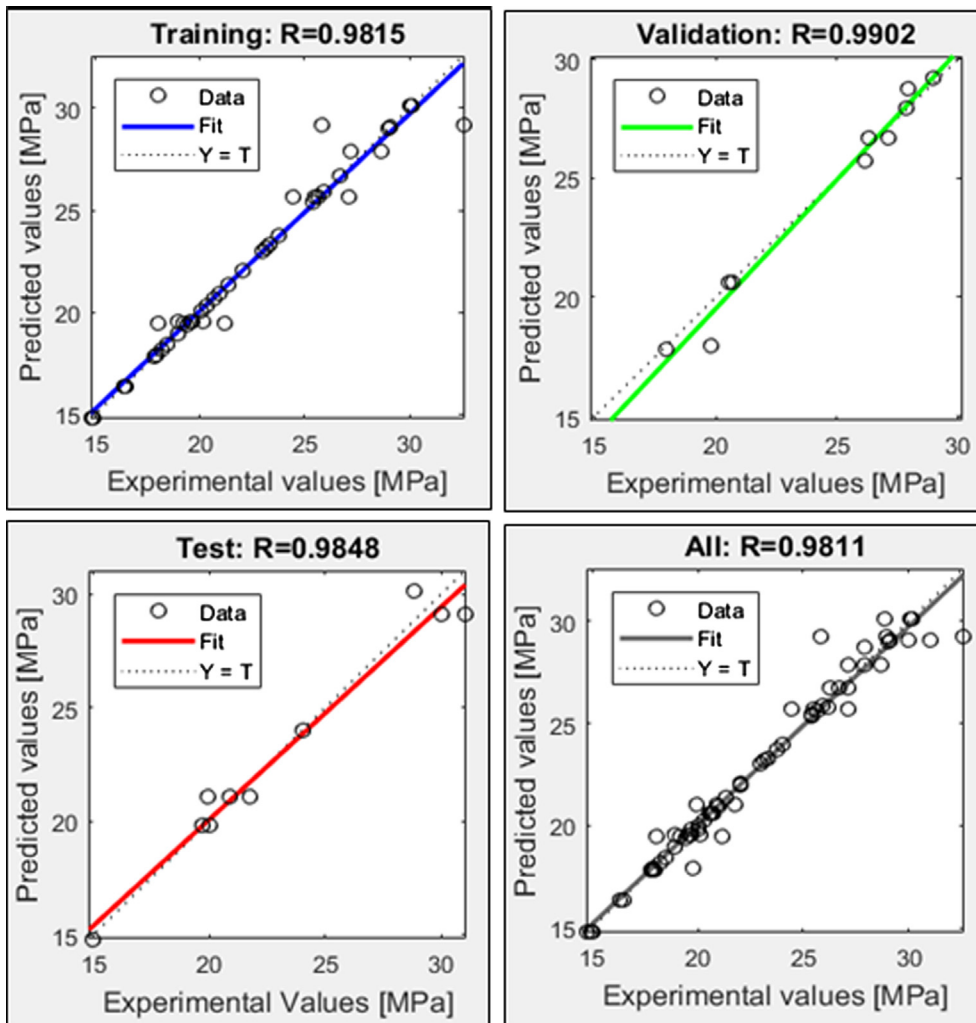
Fig. 9. Training state.

Fig. 10. Regression for training, validation and test.

learning process. The figure comprises three lines since the input and desired output vectors are randomly assigned into three sets (70%:15%:15% for training, validation and test respectively). The blue line portrays the decreasing error on the training data. The green line displays the validation error. It measures the network generalization ability and stops training as soon as generalization halts improving. Thus, training stops when the validation error stops decreasing that inherently avoids over-fitting. As can be seen from the figure, the training error was smaller than that of the validation as expected. This justifies that there was no problem of overfitting. Prediction errors (residuals) based on the training set tell us about the model fit, whereas errors based on the validation set measure the model's ability to predict new data (predictive performance). The red line shows the error on the test data indicating how well the model generalizes to the data and provides an independent measure of network performance during and after training. The training state is depicted in Fig. 9.

The regression values of the chosen ANN (L15-15-2) were 0.982, 0.990 and 0.985 for training, validation and testing, respectively, as shown in Fig. 10.

3.2. Predicted compressive and tensile strengths

The compressive and tensile splitting strength values generated by the model were very close to those of experimental counterparts as shown in Figs. 11 and 12 respectively. The performance of the model was evaluated using the model accuracy measures tabulated in Table 4.
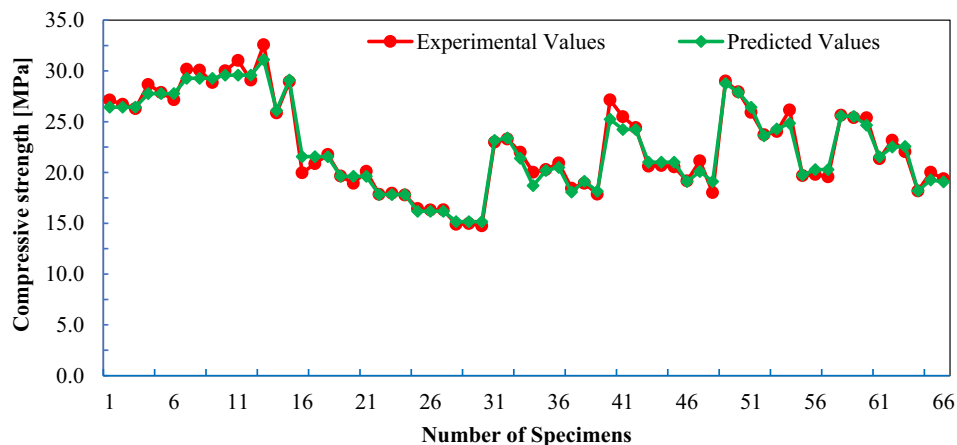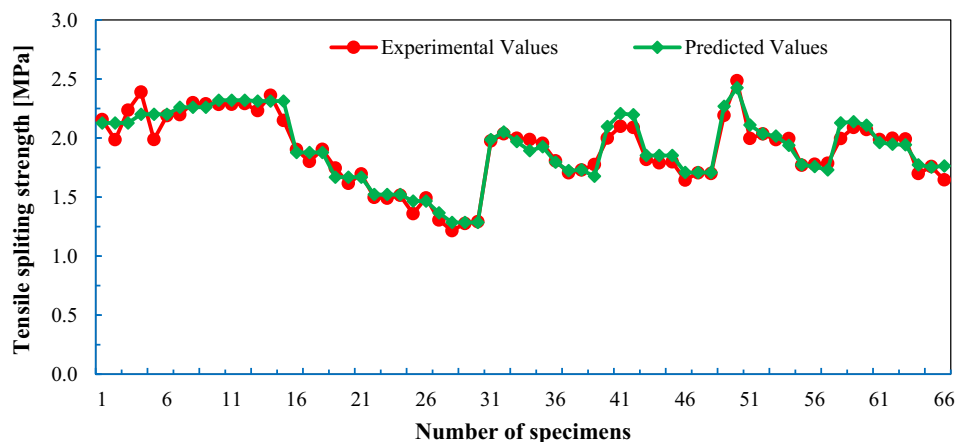
The ANN model (L15-15-2) predicted the compressive strength with a RMSE value of 0.648 MPa i.e., the differences between predicted and experimental compressive strength values were small. The model overpredicted the compressive strength on average by 0.123 MPa. MAPE shows that the predicted compressive strength deviated on average by 2.088% from experimental data. Fig. 11 clearly exhibits that the predicted compressive strength values were in strong coherence with those of experimentally determined values. This justifies that the model was able to reproduce the experimental compressive strength results with high accuracy.

The ANN strength predictive model (L15-15-2) estimated the tensile splitting strength with a RMSE value of 0.072 MPa. This indicates that the differences between predicted and experimentally obtained results were negligible. In fact, when the predicted tensile splitting strength values were compared to experimental values, the prediction was on average 0.019 MPa less. The predicted tensile splitting strength swerved on average by 2.905% from the actual results. Fig. 12 clearly exhibits that the predicted tensile splitting strength values were in strong coherence with experimental ones. This justifies that the model was able to generate the experimental tensile splitting strength results accurately.

3.3. Sensitivity analysis

Input features contain information about the desired outputs. Usually, more features mean more information and better predictive power. However, some features might be irrelevant or redundant that can cause curse of dimensionality. Irrelevant features

Fig. 11. Comparison between predicted and experimental results.

Fig. 12. Comparison between predicted and experimental data.

Table 4
Model performance measures.

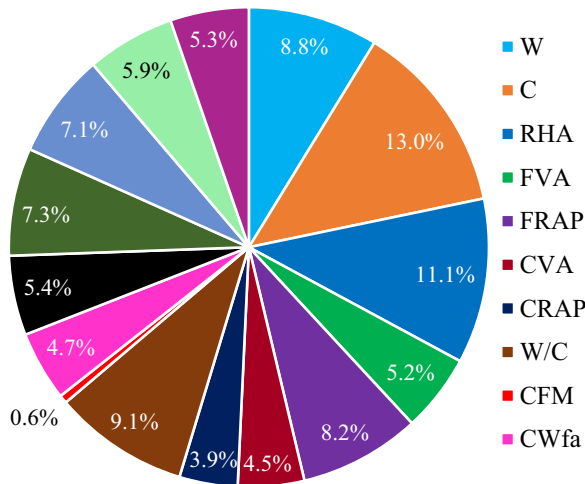| Predicted strength	Model Performance			
	MAE [MPa]	AE [MPa]	MAPE [%]	RMSE [MPa]
Compressive	0.481	0.123	2.088	0.648
Tensile	0.055	−0.019	2.905	0.072

Fig. 13. Average percentage influence of input features on the predicted strength.

introduce noise and they fool the training algorism. Redundant features do not contribute additional information and they may lead to degradation in the performance of learning algorism. The relative influence of each input features on outputs was determined based on the magnitude of connection weights. Fig. 13 represents the average influence of each input parameters on the predicted strength.

The sensitivity analysis results seem to indicate that the contents of water, cement, RHA and water to cementitious ratio were strongly relevant for strength prediction with the average percentage influence factor values of 8.8, 13.0, 11.1 and 9.1 respectively. On the other hand, the fineness modulus of fine aggregates can be left out as its contribution in the prediction was close to zero (0.6%). It is worth to mention that the remaining input features had moderate influences on predicted strength as can be seen from Fig. 13.

4. Conclusions

In this study, an artificial neural network strength predictive model was developed to evaluate the compressive and tensile splitting strength of concrete incorporating RHA and RAP based on predetermined attributes of concrete constituent materials. The ANN Model predicted the compressive and tensile splitting strength with prediction error values of 0.648 and 0.072 MPa respectively. The model overpredicted the compressive strength on average by 0.123 MPa, whereas it underpredicted the tensile splitting strength on average by 0.019 MPa. The predicted compressive and tensile splitting strength deviated on average by 2.088 and 2.905% respectively from experimental results. The regression values of the chosen network (L15-15-2) for training, validation and testing were 0.982, 0.990 and 0.985 respectively. The best validation performance was observed at epoch 8. The contents of water, cement, RHA and water to cement ratio played an important role on the model outputs with average percentage

influence factor values of 8.8, 13.0, 11.1 and 9.1 respectively. In general, it was observed that the prediction done using ANN shows a strong degree of coherency with experimentally determined compressive and tensile splitting strengths of concrete.

5. Availability of data

The data used during the present study are available from the corresponding author on reasonable request.

6. Competing interests

The authors confirm that there is no known conflict of interest.

7. Authors' contributions

Stanley Shitote, Abiero Gariy and Mulusew Aderaw conceived of the presented idea; Mulusew Aderaw performed the experiment and collected data; Stanley Shitote and Mulusew Aderaw analyzed the input and output datasets, developed the ANN strength model predictive model and performed simulations. Abiero Gariy helped supervise the project. Mulusew Aderaw, Satanley Shitote and Abiero Gariy wrote the paper.

References

[1] Arthur Nilson, David Darwin, Charles Dolan Design of Concrete Structures, 14th ed., McGraw-Hill, New York, 2010.
[2] C. Meyer, The greening of the concrete industry, Cem. Concr. Compos. 31 (8) (2009) 601–605.
[3] A.W. Kosmatka, Design and Control of Concrete Mixtures, 15th ed., Portland Cement Association, 2011.
[4] B. Suhendro, Toward green concrete for better sustainable environment, Procedia Eng. 95 (Scescm) (2014) 305–320.
[5] E. Benhelal, G. Zahedi, E. Shamsaei, A. Bahadori, Global strategies and potentials to curb CO 2 emissions in cement industry, J. Clean. Prod. 51 (2013) 142–161.
[6] R. Khan, A. Jabbar, I. Ahmad, W. Khan, A. Naeem, J. Mirza, Reduction in environmental problems using rice-husk ash in concrete, Constr. Build. Mater. 30 (2012) 360–365.
[7] H. Naderpour, A. Hossein, P. Fakharian, Compressive strength prediction of environmentally friendly concrete using arti fi cial neural networks, J. Build. Eng. 16 (2018) (2017) 213–219, https://doi.org/10.1016/j.jobe.2018.01.007.
[8] M. Adom-asamoah, Comparative study of the physical properties of palm kernel shell concrete and normal concrete in Ghana, J. Sci. Multidiscip. Res. (2013).
[9] L.T. Lun, Effects of rice husk ash produced from different temperatures on the performance of concrete, Faculty of Engineering and Green Technology Universiti Tunku Abdul Rahman, 2015.
[10] Z.H. Duan, S.C. Kou, C.S. Poon, Prediction of compressive strength of recycled aggregate concrete using artificial neural networks, Constr. Build. Mater. 40 (2013) 1200–1206.
[11] Modarres, Hosseini, Mechanical properties of roller compacted concrete containing rice husk ash with original and recycled asphalt pavement material, J Mater. Des. 64 (2014) 227–236.
[12] W.O. Awetehagn Tuaum, Stanley Shitote, Incorporating recycled glass aggregate, Buildings 1 (2018).

[13] E. Aprianti, P. Shafigh, S. Bahri, J. Nodeh, Supplementary cementitious materials origin from agricultural wastes – A review, Constr. Build. Mater. 74 (2015) 176–187.

[14] K. Yang, Y. Jung, M. Cho, S. Tae, Effect of supplementary cementitious materials on reduction of CO_2 emissions from concrete, J. Clean. Prod. 2 (2014) 1–10.

[15] B. Lothenbach, K. Scrivener, R.D. Hooton, Cement and Concrete Research Supplementary cementitious materials, Cem. Concr. Res. 41 (12) (2011) 1244–1256.

[16] R. Snellings, A. Salze, K.L. Scrivener, Cement and Concrete Research Use of X-ray diffraction to quantify amorphous supplementary cementitious materials in anhydrous and hydrated blended cements, Cem. Concr. Res. 64 (2014) 89–98.

[17] A. Elahi, P.A.M. Basheer, S.V. Nanukuttan, Q.U.Z. Khan, Mechanical and durability properties of high performance concretes containing supplementary cementitious materials, Constr. Build. Mater. 24 (3) (2010) 292–299.

[18] M.A.M. Johari, J.J. Brooks, S. Kabir, P. Rivard, Influence of supplementary cementitious materials on engineering properties of high strength concrete, Constr. Build. Mater. 25 (5) (2011) 2639–2648.

[19] P. Chopra, R.K. Sharma, M. Kumar, Prediction of compressive strength of concrete using artificial neural network and genetic programming, Hindawi Publ. Corp. Adv. Mater. Sci. Eng. vol (2016, 2016.).

[20] P. Chopra, Regression models for the prediction of compressive strength of concrete with & without fly ash, Int. J. Latest Trends Eng. Technol. (IJLTET 3 (4) (2014) 400–406.

[21] K. Yan, H. Xu, G. Shen, P. Liu, Prediction of splitting tensile strength from cylinder compressive strength of concrete by support vector machine, Adv. Eng. Software Mater. Sci. Eng. 2013 (2013).

[22] N. Siraj, Prediction of Compressive Strength of Concrete using Artificial Neural Network, Fuzzy System Model and Thermodynamic Methods, Addis Ababa University Institute of Technology, 2015.

[23] J. Noorzaei, S.J.S. Hakim, M.S. Jaafar, W.A.M. Thanoon, Development of artificial neural networks for predicting concrete compressive strength, Int. J. Eng. Technol. 4 (2) (2007) 141–153.

[24] F. O. K, C. de Silva, Soft Computing and Intelligent Systems Design. Pearson Education Limited, 2004.

[25] Ming Zhou, Intelligent Systems Technology and Applications, CRC Press LLC, Washington, D.C., 2003.

[26] C.-S.P. Zhen-Hua Duan, Shi-Cong Kou, Prediction of compressive strength of recycled aggregate concrete using artificial neural networks, Constr. Build. Mater. (2013).

[27] H. Naderpour, A. Kheyroddin, G.G. Amiri, Prediction of FRP-confined compressive strength of concrete using artificial neural networks, Compos. Struct. 92 (12) (2010) 2817–2829.

[28] T. Ling, Prediction of density and compressive strength for rubberized concrete blocks w, Constr. Build. Mater. 25 (11) (2011) 4303–4306.

[29] S.R. Sarhat, E.G. Sherwood, The prediction of compressive strength of ungrouted hollow concrete block masonry, Constr. Build. Mater. 58 (2014) 111–121.

[30] A. Trocoli, A. Dantas, M.B. Leite, K.D.J. Nagahama, Prediction of compressive strength of concrete containing construction and demolition waste using artificial neural networks, Constr. Build. Mater. 38 (2013) 717–722.

[31] J. Sobhani, M. Najimi, A.R. Pourkhorshidi, T. Parhizkar, Prediction of the compressive strength of no-slump concrete: a comparative study of regression, neural network and ANFIS models, Constr. Build. Mater. 24 (5) (2010) 709–718.

[32] S. Jamalaldin, S. Hakim, J. Noorzaei, M.S. Jaafar, M. Jameel, Application of artificial neural networks to predict compressive strength of high strength concrete, Int. J. Phys. Sci. 6 (5) (2011) 975–981.

[33] G. Kalra, E. Joseph, Research review and modeling of concrete compressive strength using artificial neural networks, IJISET – Int. J. Innov. Sci. Eng. Technol. 3 (2) (2016) 672–677.

[34] S.D. Bharathi, R. Manju, J. Premalatha, Prediction of compressive strength for self- compacting concrete (SCC) using artificial intelligence and regression analysis, Int. J. ChemTech Res. 10 (8) (2017) 263–275.

[35] A. Heidari, M. Hashempour, D. Tavakoli, Using of backpropagation neural network in estimating of compressive strength of waste concrete, J. Soft Comput. Civ. Eng. 1 (2017) 54–64.

[36] Strength prediction of green concrete containing reclaimed, no. November, 2017.

[37] G.A. Applications, Neural Network Techniques and Their Engineering Applications, pp. 1–20, 2003.

[38] S. Suba, Prediction of mechanical properties of cement containing class C fly ash by using artificial neural network and regression technique, Acad. J. 4 (4) (2009) 289–297.

[39] G. Shmueli, P.C. Bruce, M.L. Stephens, N.R. Patel, Data Mining for Business Analytics, third ed., John Wliley & Sons Inc, Canada, 2017.

[40] BS EN 933-1, Tests for geometrical properties of aggregates Part 1 : Determination of particle size distribution — Sieving method, 2012.

[41] BS ISO 3310-2, Test sieves — Technical requirements and testing Part 2 : Test sieves of perforated metal plate, 2013.

[42] BS EN 1097-6, BSI Standards Publication Tests for mechanical and Physical Properties of Aggregates Part 6 : Determination of Particle Density and Water Absorption, BSI Standards Limited 2013, Brussels, 2013.

[43] BS EN 206, Concrete Specification, Performance, Production and Conformity, British Standards Institution 2014, 2014.

[44] BS 8500-2, Concrete Complementary British Standard to BS EN 206: constituent materials and concrete, no. 1. BSI Standards Limited 2013, 2012.

[45] BS EN 12390-1, Concrete – Complementary British Standard to BS EN 206-1 – guidance for the specifier, no. 1. BSI Standards Limited 2012, 2012.

[46] BS EN 12390-2, Testing hardened concrete, Part 2: Making and curing specimens for strength tests, BSI Standards Limited 2009, 2009.

[47] BS EN 12390-4, Testing hardened concrete, Part 4: Specification for Compressive strength testing machines, 2000.

[48] Biswajit, Gauravuday, Function Approximation using Back Propagation Algorithm in Artificial Neural Networks, Rourkel National Institute of Technology, 2007.

[49] H.N. Koivo, Neural Networks Basics using MATLAB Neural Network Toolbox, 2008, pp. 1–59.

[50] J.J. Montan, Numeric sensitivity analysis applied to feed forward neural networks, Neural Comput. Appl. 12 (2003) 119–125.

[51] L. Milne, Feature Selection Using Neural Networks with Contribution Measures, in: Australian Conference on Artificial Intelligence, 1995, pp. 1–8.

Experimental Investigation on Engineering Properties of Concrete Incorporating Reclaimed Asphalt Pavement and Rice Husk Ash

Mulusew Aderaw Getahun [1,2,*] [ID] **, Stanley Muse Shitote [3] and Zachary C. Abiero Gariy [4]**

[1]   Civil Engineering Department, Pan African University Institute for Basic Sciences, Technology and Innovation (PAUSTI), 62000 00200 Nairobi, Kenya

[2]   Ethiopian Roads Authority, Addis Ababa 1770, Ethiopia

[3]   Civil Engineering Department, Rongo University, Rongo 103-40404, Kenya; sshitote@rongovarsity.ac.ke

[4]   Civil Engineering Department, Jomo Kenyatta University of Agriculture and Technology (JKUAT), Nairobi 5505, 00100, Kenya; zagariy@eng.jkuat.ac.ke

*   Correspondence: mulusew06@gmail.com; Tel.: +251-912-914-229

Abstract: Waste generation from agricultural and construction industries is growing at an upsetting rate that causes a heavy burden on landfill facilities. On the other hand, the construction industry is exhausting natural resources thereby posing environmental problems. This study investigates the potential use of agro-industrial waste such as rice husk ash (RHA) and construction waste like reclaimed asphalt pavement (RAP) as promising construction materials. The durability and physical and mechanical properties of concrete were assessed by partially replacing cement and virgin aggregates with RHA and RAP, up to 20% and 50%, respectively. A total of 22 mixes were studied, twelve of which were devoted to studying the collective effects of RHA and RAP on the engineering properties of concrete. Based on experimental results, RHA and RAP decreased slump, compacting factor, density, water absorption and sorptivity. RHA increased compressive and tensile splitting strength, whereas RAP decreased compressive and tensile splitting strength. Comparable strength and favorable sorptivity values were obtained when 15% RHA was combined with up to 20% RAP in the concrete mix. Thus, utilizing RHA and RAP as concrete ingredients can contribute to solid waste management, engineering and economic benefits.

Keywords: slump; compacting factor; density; water absorption; sorptivity; durability; compressive strength; tensile splitting strength; volumes of permeable void spaces

1. Introduction

The construction industry consumes about 40% of the global energy; is the largest global consumer of raw materials; and is responsible for 25–40% of the world's total CO_2 emissions and 28% of solid waste in the form of construction debris [1]. Over 10 billion tons of Portland cement concrete (PCC) is produced annually worldwide due to its versatility, durability and sustainability [2,3]. However, its production consumes a substantial amount of energy and raw materials. The cement production alone is both energy and resource intensive. It was attested that every ton of cement production consumes about 4 GJ of energy and 1.7 tons of raw materials and releases approximately 0.73–0.99 ton of CO_2 [2,4–7]. Moreover, PCC production consumes more than 8 billion tons of aggregates each year [6]. Consequently, an increasing demand for concrete will continue reducing natural stone deposits significantly thereby poses a threat on the environment [7–9].

Concurrently, a substantial quantity of construction and agro-industrial solid wastes disposal is posing a huge threat to the environment [10–12]. For example, road maintenance and rehabilitation

activities have been generating a large amount of valuable asphalt pavement materials that are either discarded along the generation point or hauled off to the disposal site [13–15].

Similarly, according to the FAO 2017 [16] report, the global paddy production in 2017 was forecasted to amount to 756.7 million tons. Assuming annual rice production remains the same, 254.5 million tons of rice husks is available for disposal every year worldwide. Thus, agro-industrial solid waste disposal is another serious concern unless we find a preferred alternative use.

In order to curb these concerns, the cement and concrete industry could be an ideal home for construction and industrial wastes. Recently, waste materials such as crushed concrete, asphalt pavement and crushed glasses are some of the recycled materials which have been used as a coarse and/or fine aggregate in concrete production [17,18]. In addition, numerous researches devoted to find alternatives for cement replacement [19–23]. Thus, utilizing RAP and rice RHA as aggregate and cement partial replacements, respectively, is in harmony with this approach.

The concern on how to use RAP has gained a remarkable curiosity in the United States due to the increasing demand for sustainable construction materials use [24]. But, in underdeveloped and developing countries where recycling materials is not a culture, a tremendous amount of RAP and RHA materials are usually discarded in landfills [13].

Previous studies [25–28] revealed and consistently reported that utilizing RAP in PCC caused reductions in compressive, flexural, and tensile splitting strength compared to PCC containing virgin aggregates. The findings from past studies showed that the decrease in strength of PCC containing RAP was largely instigated by the effects of porosity in the interfacial transition zone (ITZ) and preferential asphalt cohesion failure [29–31] However, previous studies [27–30] exhibited that concrete containing RAP had better ductility, toughness and fracture properties compared to normal concrete. Huang et al. [26] reported that RAP could initiate crack propagation and lead to the formation of a prolonged crack pattern allied to the higher dissipation of energy. Hence, there is a need to improve the strength of concrete containing RAP in order to maximize the utilization of RAP materials in construction applications.

RHA was found to enhance the concrete properties by filler and pozzolanic effects [12,32]. The enhancement in strength is believed to be an advantage from the high silica content of RHA, which, in itself, possesses little cementitious value, but when calcium hydroxide reacts with RHA in the presence of water, a cementitious complex is formed [33]. The hydration of tricalcium silicate (C_3S) gives 61% calcium-silicate-hydrate (C-S-H) and 39% calcium hydroxide; the hydration of dicalcium silicate (C_2S) results in 82% C-S-H and 18% calcium hydroxide, where up to 15% of the weight of Portland cement is hydrated lime [34]. Calcium hydroxide has no contribution to concrete strength, but rather has detrimental effects on the durability of concrete. Thus, RHA can provide an opportunity to alter the free lime (Calcium hydroxide) to a C-S-H gel that makes the concrete strong [35].

Therefore, the main objective of this study was to investigate the collective effects of RHA and RAP on the physical and mechanical properties of concrete. The engineering properties of RHA-inclusive concrete were assessed in the first phase. Then, the effects of RAP on wet and hardened concrete properties were investigated. Finally, the combined effects of RHA and RAP on engineering properties of concrete were assessed. Thus, utilizing RAP in combination with RHA for concrete production can contribute to engineering benefits, economic savings, solid waste management and environmental protection.

2. Material and Methods

2.1. Materials

Materials used for this study were fine reclaimed asphalt pavement (FRAP), course reclaimed asphalt pavement (CRAP), fine virgin aggregate (FVA), course virgin aggregate (CVA), ordinary Portland cement (OPC) type I, rice husk ash (RHA), water, Sika ViscoCrete 3088 superplasticizer (SVCSP) and Sikament NNG superplasticizer (SNNGSP). Figure 1 depicts aggregates (CRAP, CVA,

FRAP, and FVA) and cementitious materials (cement and RHA). All materials were obtained from different parts of Kenya. FVA (river sand) and VCA were purchased from Masinga and Molongo districts of Kenya respectively. The RAP was obtained from an old distressed flexible pavement, Ruaka-Banana-Limuru Road (D407), sampled at the section near Tigoni, Kiambu County of Kenya. The road was constructed about 21 years ago without major rehabilitation. RHA was collected from the dump site of Mwea Rice Milling Factory. Cement and superplasticizers were bought from Bamburi Cement and Sika Kenya Limited respectively. Tap water was used for mixing.

Figure 1. Materials.

2.2. Methods

The methods adopted and followed for this study are discussed in the subsequent section. The most important test methods are summarized in Table 1.

Table 1. Test methods adopted.

Test on Constituent Materials		Tests on Fresh and Hardened Concrete	
Test Performed	Standard Used	Test Performed	Standard Used
Sieve analysis	BS EN 933-1	Slump	BS EN 12350-2
Aggregate specific gravity (SG)	BS EN 1097-6	Compacting factor	BS 1881-103
Fineness modulus	ASTM C136	Fresh density	BS EN 12350-6
cement and RHA SG	ASTM C188	Compressive strength	BS EN 12390-3
Aggregate water absorption	BS EN 1097-6	Tensile strength	BS EN 12390-6
Aggregates density	ASTM C29	Water absorption	ASTM C642
Voids in aggregates	ASTM C29	Sorptivity	ASTM C1585
ACV	IS 2386-IV	Permeable voids	ASTM C642
AIV	IS 2386-IV	Hardened density	ASTM C642

2.2.1. Test Methods for Material Characterization

Aggregate sampling was carried out in accordance with BS EN 932-1 (1997) [36] requirements to get representative samples for the batch. Grading of the aggregates was determined in line with BS EN 933-1 (2012) [37] procedures using test sieves of the sizes complying with BS ISO 3310-2 (2013) [38]. The RAP material was obtained through ripping and milling of old existing pavement, and then crushed manually and finally sieved using 5 mm sieve in order to separate into FRAP (grain size less than 5 mm) and CRAP (grain size greater than 5 mm). RHA was sieved using 0.10 mm sieve. The specific gravity and water absorption of coarse and fine aggregates were determined as per BS EN 1097-6 (2013) [39]. Bulk density and voids in aggregates were determined in line with the procedures defined in ASTM (2003) [40]. Aggregate crushing and impact tests were performed according to the procedures specified in IS 2386: Part IV (2002) [41].

2.2.2. Mix Design and Mixing Procedures

The mix design for 25 MPa Portland cement concrete (PCC) was done in accordance with BS EN 206 (2014) [42] and BS EN 8500-2 (2012) [43]. A total of 22 mixtures were prepared. Table 2 portrays the particulars of studied mixture proportions. In all the mixtures, 254 kg/m^3 of water and water

to cementitious material ratio of 0.65 were kept constant. The first phase of the study was replacing cement by 5, 10, 15 and 20% RHA (by weight of cement) to assess the effect of RHA on wet and hardened properties of concrete. In the second phase, FVA and CVA were replaced by 10, 20, 30, 40, and 50% FRAP and CRAP (by weights of FVA and CVA) respectively to ascertain the influence of RAP on the properties of concrete. The third phase was to ascertain the collective effects of RHA and RAP on engineering properties of concrete. SNNGSP was used at 0.5, 0.85, 2, and 2.75% (by weight of cementitious material) for 5, 10, 15, and 20% RHA content respectively. SVCSP (more powerful than SNNGSP) was used at 0.5, 0.7, 0.9, and 1.1% (by weight of cementitious material) for RHA and RAP combined mixtures. Manual mixing was performed as per BS EN 1881-125 (2013) [44] with a control mechanism to prevent the loss of cementitious materials and water quantified during mixture proportioning. The chemical analysis of cement and RHA were conducted as per BS EN 196-2 (2013) [45] test method. The specific gravities of cement and RHA were done in accordance with ASTM C188 (2016) [46].

Table 2. Mix proportions for 25 MPa concrete comprising RHA and RAP.

Mix Description	Cement (kg/m^3)	RHA (kg/m^3)	FVA (kg/m^3)	FRAP (kg/m^3)	CVA (kg/m^3)	CRAP (kg/m^3)
Control	390	0	712	0	1593	0
(5–20)% RHA	(312–371)	(20–78)	712	0	1593	0
(10–50)% RAP	390	0	(356–641)	(71–356)	(796–1434)	(159–796)
5% RHA + (10–30)% RAP	371	20	(499–641)	(71–214)	(1115–1434)	(159–478)
10% RHA + (10–30)% RAP	351	39	(499–641)	(71–214)	(1115–1434)	(159–478)
15% RHA + (10–30)% RAP	332	59	(499–641)	(71–214)	(1115–1434)	(159–478)
20% RHA + (10–30)% RAP	312	78	(499–641)	(71–214)	(1115–1434)	(159–478)

2.2.3. Test Methods for Fresh Concrete Properties

Fresh concrete properties were assessed by conducting slump, compacting factor, and fresh density tests. Three replicate specimens were prepared for each test. Sampling for testing was done in accordance with procedures stipulated in BS EN 12350-1 (2009) [47]. Slump, compacting factor and fresh density was determined in accordance the procedures specified in BS EN 12350-2 (2009) [48], BS 1881-103 (1993) [49], and BS EN 12350-6 (2009) [50] respectively.

2.2.4. Test Methods for Hardened Concrete Properties

Cubes of dimensions 100 mm × 100 mm × 100 mm and cylinders with a diameter of 100 mm and 200 mm long conforming to BS EN 12390-1 (2012) [51] requirements were used to make concrete specimens for compressive and tensile splitting strength test respectively. A total of 132 cube and 66 cylinder specimens were made and cured in accordance with the methods specified in BS EN 12390-2 (2009) [52] for 7 and 28 days compressive and 28 days tensile splitting strength test respectively. Three replicate specimens were prepared for each test. Compressive and tensile splitting strength of concrete were determined according to BS EN 12390-3 (2009) [53] and BS EN 12390-6 (2009) [54] test method respectively. Specimens were loaded to failure in automatic computerized testing machine conforming to BS EN 12390-4 (2000) [55].

Density, water absorption and void spaces in concrete were determined consistent with ASTM C642 (2013) [56]. Three replicate specimens were prepared for each test. A total of 66 cubes of dimensions 100 mm × 100 mm × 100 mm were made and cured for 28 days. The samples were dried in an oven for 72 h at a temperature of 105 °C until the change in mass was less than 0.5%. Then, the samples were put in the water at an average temperature of 21.5 °C for about 72 h until the increase in saturated surface dried mass was less than 0.5%. Finally, the specimens were placed in a receptacle, covered with tap water, and boiled for 5 h and then cooled by natural loss of heat for 15 h to a final average temperature of 22.5 °C.

Sorptivity by the concrete specimens was determined in accordance with ASTM C1585 (2013) [57] test methods. Three replicate specimens were prepared for each test. A total of 66 cubes of dimensions 100 mm × 100 mm × 100 mm were made and cured for 28 days for the sorptivity test. The specimens were dried in an oven at 110 °C temperature for 24 h and then remained in an oven at a temperature of 50 °C for 3 days. After 3 days, each specimen was placed inside a container and stored at an average temperature of 22 °C for 15 days before the start of the absorption procedure. The specimens were removed from the storage container and the 5 faces of the specimens were sealed properly to deter entrance of moisture while the opposite face left open and exposed to water. The initial weight of the specimens was recorded after sealing and submerged in water about 3.5 mm above the bottom face. The weight gain was determined for each test specimens at interval of time 5, 10, 30 min, 1, 2, 3, 4, 5, and 6 h.

3. Results and Discussion

3.1. Material Characterization

Virgin aggregates (VA) and RAP materials were characterized in terms of gradation, fineness modulus, water absorption, specific gravity, bulk density, void content, ACV, and AIV.

Physical and Mechanical Properties of Materials

The specific gravity, water absorption, bulk density, aggregate crushing value (ACV), aggregate impact value (AIV) of aggregates, among others, are tabulated in Table 3.

Table 3. Physical and mechanical properties of materials.

Property	OPC	RHA	FVA	FRAP	CVA	CRAP
Fineness modulus	-	-	2.65	3.61	-	-
Silt Content (%)	-	-	5.19	0.81	-	-
Bulk specific gravity	3.12	2.03	2.43	2.32	2.62	2.41
Bulk specific gravity, SSD basis	-	-	2.52	2.37	2.68	2.45
Apparent specific gravity	-	-	2.68	2.46	2.80	2.51
Water Absorption (%)	-	-	3.95	2.42	2.41	1.63
Loose bulk density (kg/m^3)	1398	359	1456	1318	1421	1300
Rodded bulk density (kg/m^3)	1435	470	1577	1407	1584	1326
Voids in loose aggregates (%)	-	-	39.33	43.09	45.75	43.97
Voids in Rodded aggregates (%)	-	-	34.31	39.25	39.52	42.83
Maximum particle size (mm)	0.09	0.10	5	5	20	20
Aggregate crushing values (%)	-	-	-	-	18.73	15.92
Aggregate Impact values (%)	-	-	-	-	15.51	9.83

Gradation results of coarse and fine aggregates are depicted in Figures 2 and 3 respectively. As can be seen from the figures, the grading of CVA and FVA met the grading requirements of BS 882 (1992) [58].
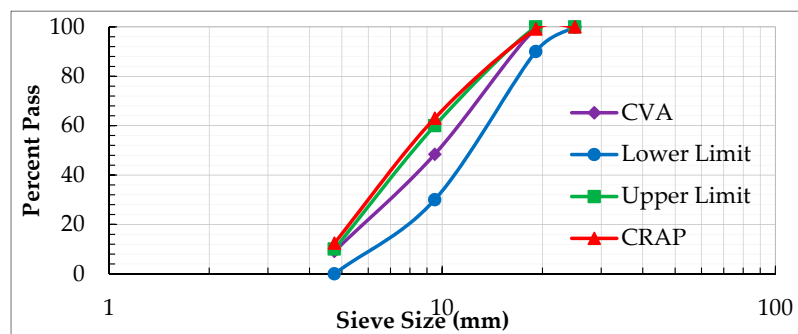

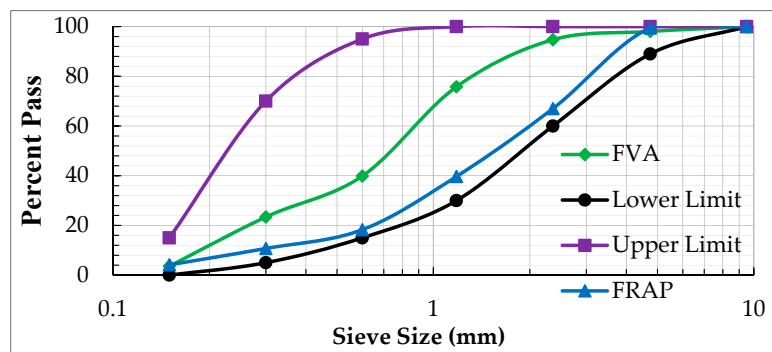**Figure 2.** Coarse aggregate particle size distribution as per BS 882 specifications.

Figure 3. Fine aggregate particle size distribution as per BS 882 specifications.

The grading of CRAP was slightly outside the limits and while that of FRAP was within the limits specified in BS 882. It is apparent from the figure that CRAP was finer than CVA whereas, FRAP was coarser than FVA. Similar findings were reported by previous study [28]. The fineness of CRAP and coarseness of FRA might be attributed to the fragmentation of CRAP materials during crushing and agglomeration of particles respectively and their sources as well. All coarse aggregates used in this study had 19.1 mm nominal maximum aggregate sizes. The fine aggregates particle sizes were between 0.15 and 5 mm. FVA and FRAP had fineness modulus of 2.65 and 3.61 respectively.

RAP materials had lower specific gravity than that of virgin aggregates. This is consistent with the findings by [25]. The lower specific gravity of RAP may be attributed to the substantial amounts of low-density asphalt-mortar coatings on the RAP surfaces and its source as well. The water absorption of RAP was found to be lower than that of VA. The reason might be attributed to the asphalt coating around both coarse and fine RAP that could hinder the maximum possible amount of water which could have been absorbed by the aggregates. RAP materials had lower loose and rodded bulk density than that of virgin aggregates. RAP materials also showed higher void space than that of virgin aggregates which may demand a higher amount of cement paste to fill the total surface area in order to produce quality concrete [35].

The ACV test done on the CRAP exhibited the abnormal result. The test specimen compressed into a single solid mass under loading. This might be due to the presence of asphalt film around RAP might bind the crushed aggregates into a single solid dense mass. The ACV and AIV values of CVA and CRAP were below the maximum limit stipulated in IS 383 (2002) [59]. CRAP had lower ACV and AIV value than that of CVA.

The specific gravity of RHA was less than that of OPC by 35%. The bulk density of RHA was also about 33% of that of OPC. The lower the specific gravity and bulk density of RHA may result in a reduction of concrete density. The maximum particle size of OPC and RHA were 90 and 100 μm respectively. Table 4 depicts the chemical composition of OPC, RHA, FRAP, and FVA.

Table 4. Chemical composition of cement, RHA, FRAP, and FVA.

Chemical Compound (%)	Cement	RHA	FRAP	FVA
CaO	63.38	0.86	2.00	1.03
SiO_2	20.62	92.97	58.85	80.00
Al_2O_3	5.06	0.93	15.6	11.00
MgO	0.82	0.48	0.04	2.00
Na_2O	0.16	2.43	6.20	3.20
K_2O	0.53	2.54	4.30	2.50
TiO_2	-	-	0.85	0.16
MnO	-	-	0.29	0.02
Fe_2O_3	3.23	0.88	5.44	1.00
C_3A	7.90	-	-	-
SO_3	2.76	4.84	-	-
Loss on ignition (LOI)	2.91	7.40	10.00	0.90

The sum of the silicon dioxide (SiO_2), aluminium oxide (Al_2O_3) and iron oxide (Fe_2O_3) contents of RHA was 94.8%; as a result, RHA fulfilled the 70% minimum requirement of BS EN 450-1 (2012) [60] to be used as a good pozzolana. The free calcium oxide (CaO) content was less than the upper bound (1.5%) specified in BS EN 450-1 (2012). This indicates the ability of the RHA to convert the free lime (Calcium hydroxide) to a C-S-H gel [60] that makes the concrete strong. The loss on ignition (LOI) of RHA was greater than that of cement but satisfied the limits specified in BS EN 450-1 (2012) [60]. LOI denotes the amount of unburnt carbon residue in the RHA that is responsible for an increase in water demand [32] which may have an influence on the properties of fresh concrete i.e., could result in low workability. The physical and chemical properties of superplasticizers used in the study are presented in Table 5.

Table 5. Properties of superplasticizers.

Property	Superplasticizer	
	Sikament NNG	**Sika ViscoCrete 3088**
Appearance/color	Dark brown liquid	Yellowish liquid
Density (kg/L)	1.2	1.06
pH value	8	5.5
Chemical base	Naphthalene formaldehyde sulphonate	Aqueous solution of modified polycarboxylate
Dosage	0.5–3.0% by weight of cement	0.2–2% by weight of cement

3.2. Fresh and Hardened Properties of Concrete

3.2.1. Fresh Properties of Concrete

Tables 6–8 show slump, compaction factor (CF) and density of fresh concrete.

- Slump

From trial mixes, it was observed that RHA caused a dramatic decrease in slump as compared to the control mix. When Sikament NNG SP was added, the slump increased by 23.33% from 60 to 74 mm at 5% RHA and 0.5% SP content. Surprisingly, it was also discovered that as the content of RHA increased, the slump decreased considerably despite increasing the dosages of SP. The slump decreased by 20, 33.33, and 75% from 60 mm to 48, 40, and 15 mm at 10, 15, and 20% RHA content with the addition of 0.85, 2, and 2.75% SP respectively. The high demand for water and the resulted lower slump might be attributed to the large specific surface area and high unburnt carbon content of RHA.

Like that of RHA, the partial replacement of virgin aggregate by RAP resulted in a substantial decrease of slump as compared to the control mix. The slump decreased by 33, 47, 62, 67, and 78% from 60 mm to 40, 32, 23, 20, and 13 mm at 10, 20, 30, 40, and 50% RAP content respectively. The reduction in slump might be attributed to absorption of the mixing water by the fine dust layers around the RAP periphery and water might also be controlled by RAP particle and was not able to move freely and thus, play no role to workability.

The inclusion of both RHA and RAP in the mix found to decrease the slump significantly as expected. However, there was a slight (3%) improvement in the slump when 0.5% Sika ViscoCrete 3088 SP was added to the concrete mix containing (5RHA + 10RAP) % as shown in Table 8. The slump decreased steadily as the RHA and RAP content increased regardless of increasing the SP dosages. This may be attributed to the combined effects of RHA and RAP as already discussed.

Table 6. Fresh properties of RHA concrete mixes.

Fresh Properties	Mix Designation (RHA)%				
	Control	(5)	(10)	(15)	(20)
Slump (mm)	60	74	48	40	15
Compaction Factor (CF)	0.935	0.944	0.912	0.908	0.758
Fresh Density (g/cm^3)	2.480	2.441	2.408	2.399	2.386

Table 7. Fresh properties of RAP concrete mixes.

Fresh Properties	Mix Designation (RAP)%					
	Control	(10)	(20)	(30)	(40)	(50)
Slump (mm)	60	40	32	23	20	13
Compaction Factor (CF)	0.935	0.931	0.922	0.921	0.902	0.892
Fresh Density (g/cm^3)	2.480	2.442	2.414	2.395	2.367	2.339

Table 8. Fresh properties of both RHA and RAP concrete mixes.

Fresh Properties	Mix Designation (RHA + RAP) %					
	(5 + 10)	(5 + 20)	(5 + 30)	(10 + 20)	(10 + 30)	(10 + 30)
Slump (mm)	62.0	58.0	53.5	49.0	45.0	40.5
Compaction Factor (CF)	0.953	0.948	0.943	0.937	0.932	0.927
Fresh Density (g/cm^3)	2.441	2.427	2.418	2.421	2.411	2.401
Fresh Properties	**(15 + 10)**	**(15 + 20)**	**(15 + 30)**	**(20 + 10)**	**(20 + 20)**	**(20 + 30)**
Slump (mm)	45.0	41.0	36.5	32.5	28.5	24.0
Compaction Factor (CF)	0.934	0.930	0.924	0.860	0.855	0.850
Fresh Density (g/cm^3)	2.421	2.407	2.397	2.414	2.400	2.391

- Compaction Factor (CF)

The CF values of the concrete ranged from 0.758 to 0.953 as shown in Tables 6–8; these values are within the ranges specified in BS 1881-103 [49]. The CF of RHA-inclusive concrete increased by 1% at 5% RHA content, whereas CF decreased by 19% as the RHA content increased to 20%. Figure 4a and Equation (1) (obtained by regression) show the relationship between slump and compaction factor. R^2 and standard error of estimate (SEE) of the model were 0.958 and 0.012 respectively.

Similarly, the CF values of RAP-inclusive concrete decreased by 5% from 0.935 to 0.892 at 50% RAP content relative to the control mix. Figure 4b and Equation (2) (obtained by regression) illustrate the relationship between slump and compaction factor. R^2 and SEE of the model were 0.965 and 0.002 respectively.

(**a**) RHA concrete　　　　　　　　　　(**b**) RAP concrete
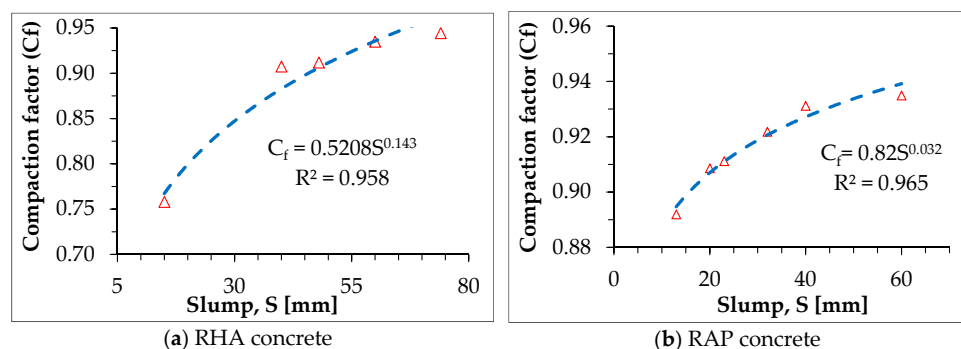
Figure 4. Relationship between slump and compaction factor for RHA and RAP concrete.

$$C_f = 0.52 \times S^{0.143} \tag{1}$$

where: C_f is compacting factor; and S is the slump in mm for fresh RHA concrete

$$C_f = 0.82 \times S^{0.032} \tag{2}$$

where: C_f is the compacting factor; and S is the slump in mm for fresh RAP concrete

　　　A slight increase was observed in CF values at 5% RHA + (10–30)% RAP content, whereas CF decreased marginally for the remaining mixes. Figure 5 (obtained by regression) depicts the relationship between slump and compaction factor for RHA- and RAP-inclusive concrete. R^2 and SEE of the model were 0.894 and 0.013 respectively.
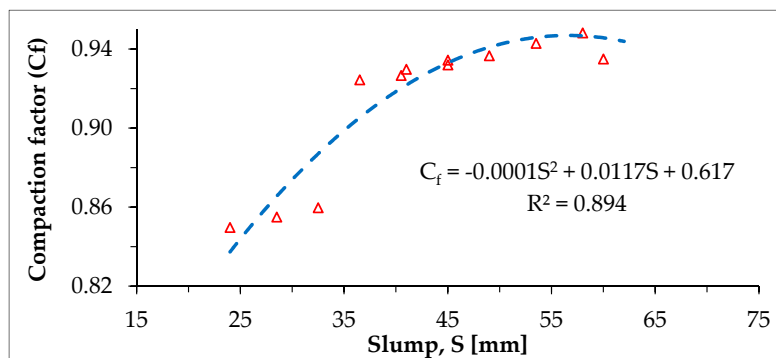
Figure 5. Relationship between slump and compaction factor.

- Fresh Density

　　　The fresh density of RHA-inclusive PCC decreased by 3.8% from 2480 to 2386 kg/m^3 as the RHA content in the mix increased from 0 to 20%. The reduction in fresh density might be due to the fact that the particle density of RHA (2.03) was lower than that of cement particle density (3.12). The relationship between fresh density and RHA content (obtained by regression) is depicted in Figure 6a. R^2 and SEE of the model were 0.990 and 0.008 respectively.

　　　The mix containing RAP exhibited relatively lower fresh density compared to the mix containing virgin aggregates. The fresh density of RAP-inclusive mix decreased by 5.7% from 2480 to 2339 kg/m^3 as the RAP content in the mix increased from 0 to 50%. The reduction in density might be attributed to the fact that specific gravities of both FRAP and CRAP were lower than those of both FVA and CVA respectively. Figure 6b (obtained by regression) gives the relationship between fresh density and RAP Content. R^2 and SEE of the model were 0.993 and 0.005 respectively.

(**a**) RHA concrete　　　　　　　　　　　　　(**b**) RAP concrete
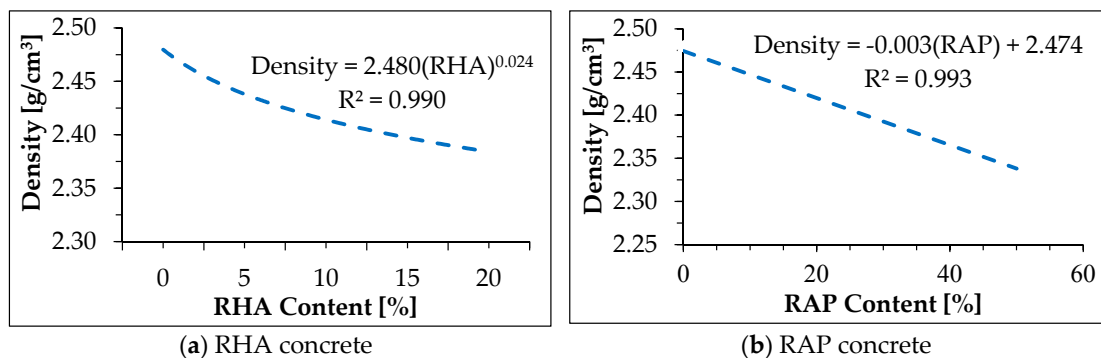
Figure 6. Fresh density for RHA and RAP concrete.

The fresh density for mixes containing both RHA and RAP is graphically depicted in Figure 7. It was observed that the mixes containing both RHA and RAP had lower fresh density compared to the control mix. The mix incorporating 20% RHA + 30% RAP showed 3.6% reduction in fresh density relative to that of the control mix. The reduction in fresh density might be attributed to the collective effects pertaining to RHA and RAP as has been explained.
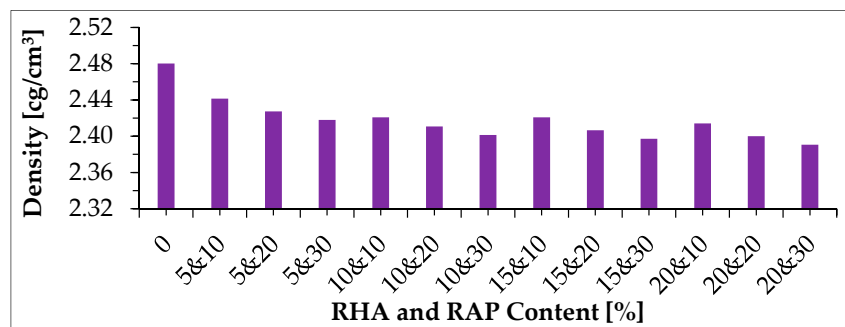

Figure 7. Fresh density for both RHA- and RAP-inclusive concrete.

3.2.2. Hardened Properties of Concrete

Table 9 shows the compressive strength (CS), tensile splitting strength (TSS), bulk dry density, water absorption (w), permeable void spaces (v), and sorptivity (k) of the concrete.

Table 9. Hardened properties of concrete.

Mix Description	CS (MPa)		TSS (MPa)	w (%)	v (%)	K (mm/h$^{1/2}$)
	7 Days	28 Days	28 Days			
Control	17.34 (0.41)	26.72 (0.42)	2.13 (0.13)	7.24 (0.18)	17.33 (0.01)	1.96 (0.02)
RHA5%	19.42 (0.61)	27.90 (0.75)	2.19 (0.20)	7.19 (0.30)	17.09 (0.29)	1.92 (0.06)
RHA10%	20.13 (0.71)	29.60 (0.73)	2.26 (0.06)	7.16 (0.18)	17.02 (0.60)	1.90 (0.25)
RHA15%	21.23 (0.41)	30.05 (0.79)	2.29 (0.01)	7.15 (0.11)	16.90 (0.40)	1.80 (0.78)
RHA20%	20.90 (0.80)	29.13 (0.32)	2.25 (0.09)	7.15 (0.01)	16.77 (0.03)	1.75 (0.11)
RAP10%	16.75 (0.20)	20.87 (0.90)	1.87 (0.06)	6.86 (0.30)	16.86 (0.18)	1.82 (0.20)
RAP20%	16.14 (0.40)	19.56 (0.0.5)	1.69 (0.07)	6.74 (0.09)	16.61 (0.08)	1.30 (0.02)
RAP30%	14.51 (0.40)	17.86 (0.08)	1.50 (0.01)	6.65 (0.19)	16.28 (0.64)	1.16 (0.13)
RAP40%	12.73 (0.60)	16.36 (0.07)	1.39 (0.10)	6.54 (0.20)	15.98 (0.47)	0.91 (0.03)
RAP50%	11.08 (0.30)	14.87 (0.12)	1.26 (0.04)	6.45 (0.30)	15.68 (0.65)	0.69 (0.01)
[5RHA + 10RAP]%	18.37 (0.75)	23.00 (0.68)	2.05 (0.03)	6.69 (0.15)	16.94 (0.16)	1.88 (0.27)
[5RHA + 20RAP]%	16.90 (0.38)	21.42 (0.47)	1.85 (0.10)	6.65 (0.04)	16.79 (0.05)	1.81 (0.08)
[5RHA + 30RAP]%	15.00 (0.84)	19.42 (0.54)	1.77 (0.04)	6.62 (0.08)	16.53 (0.08)	1.69 (0.05)
[10RHA + 10RAP]%	19.66 (0.84)	25.12 (0.66)	2.12 (0.06)	6.68 (0.01)	16.92 (0.11)	1.80 (0.55)
[10RHA + 20RAP]%	17.00 (0.97)	23.62 (0.07)	2.09 (0.01)	6.49 (0.18)	16.72 (0.24)	1.65 (0.18)
[10RHA + 30RAP]%	16.65 (0.38)	20.4 4(0.61)	1.80 (0.03)	6.20 (0.10)	16.64 (0.06)	1.41 (0.17)
[15RHA + 10RAP]%	20.02 (0.55)	27.62 (0.54)	2.22 (0.25)	6.33 (0.06)	16.78 (0.02)	1.87 (0.35)
[15RHA + 20RAP]%	19.54 (0.24)	25.01 (0.56)	2.10(0.03)	6.32 (0.05)	16.76 (0.10)	1.61 (0.07)
[15RHA + 30RAP]%	17.14 (0.13)	21.69 (0.12)	1.89 (0.01)	6.30 (0.07)	16.60 (0.17)	1.47 (0.29)
[20RHA + 10RAP]%	18.95 (0.50)	25.48 (0.14)	2.15 (0.05)	6.30 (0.13)	16.81 (0.45)	1.92 (0.46)
[20RHA + 20RAP]%	17.30 (1.04)	22.19 (0.92)	1.99 (0.01)	6.25 (0.08)	16.88 (0.52)	1.89 (0.04)
[20RHA + 30RAP]%	16.38 (0.43)	20.20 (0.93)	1.79 (0.06)	6.25 (0.11)	16.48 (0.03)	1.65 (0.06)

Average value for three replicate specimens and standard deviation (in parentheses).

● Compressive Strength (CS)

CS test results of PCC mixtures containing RHA are depicted in Figure 8a. RHA enhanced the 7-days CS by 12.0, 16.1, 22.4, and 20.5% at 5, 10, 15, and 20% RHA content respectively relative to the control mix. Similarly, the 28-days CS was also enhanced by 4.4, 10.8, 12.5, and 9.0%. In this study, the highest 7 and 28-days CS gain was observed at 15% RHA content.

The 7 and 28 days CS test results of RAP inclusive concrete are depicted in Figure 8b. A dramatic reduction in CS was observed with an increment of RAP content in the concrete mixtures. The 7 and

28-days CS decreased by 36.1 and 44.3%, relative to the control mix, respectively, at 50% RAP content. This is consistent with the results found in previous studies [23,28,29]. The reduction in CS might be attributed to the collective effect of higher porosity and asphalt cohesion failure, which occurs instead of the adhesive failure of the cement-asphalt interface or cohesive failure of the ITZ [26,27].
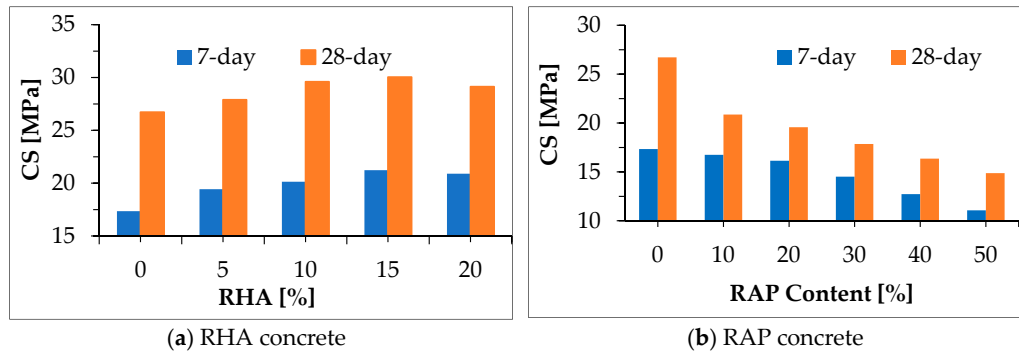

| (**a**) RHA concrete | (**b**) RAP concrete |

Figure 8. Compressive strength for RHA and RAP concrete.

The relationship between RHA content and the 28-days CS given in Figure 9a (obtained by regression). The regression model had R^2 and SEE values of 0.950 and 0.444 respectively. The CS decreased linearly with RAP content as shown in Figure 9b. A similar trend was found by previous study [61]. From the regression analysis, linear form relationship, Equation (3) was found. R^2 and SEE values of the model were 0.902 and 1.476 respectively.

$$f_c = f_{co} - 0.21 \times RAP \tag{3}$$

where: f_c is the 28-days CS of the RAP-inclusive concrete in MPa; f_{co} is the 28-days CS of the mix with no RAP content in MPa; and RAP is the reclaimed asphalt pavement content in %.

| (**a**) RHA concrete | (**b**) RAP concrete |
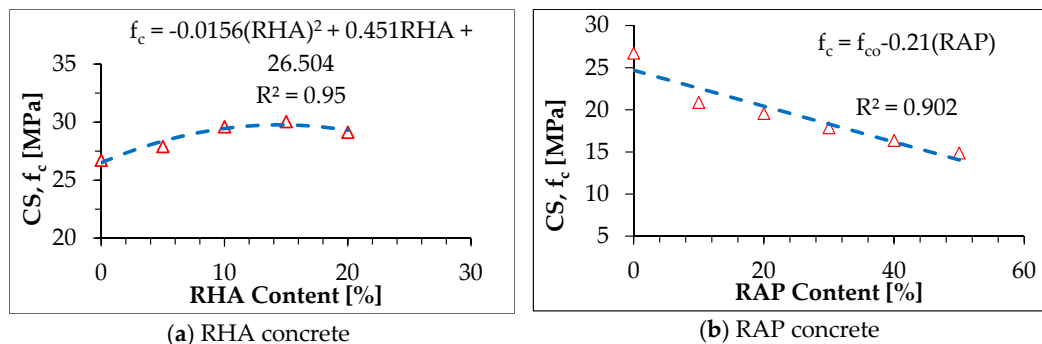
Figure 9. Relationship between RHA and RAP content and CS.

Figure 10 portrays the compressive strength of both RHA- and RAP-inclusive concrete at 7 and 28-days. The partial replacement of cement by RHA improved the CS of RAP-inclusive concrete moderately. This might be credited to the development of additional C-S-H gel due to the high reactive silica content of RHA and/or filler effect. Mixtures incorporating (10RHA + 10RAP)%, (15RHA + 10RAP)%, (15RHA + 20RAP)% and (20RHA + 10RAP)% showed comparable strength. The maximum strength (27.62 MPa) obtained at 15% RHA and 10% RAP combination. Thus, it is evident that treatment of RAP by RHA possibly will be an effective way to enhance the mechanical properties of RAP incorporating concrete.
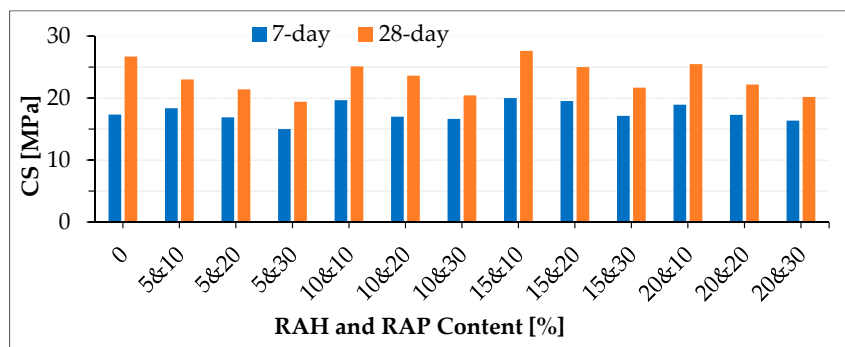
Figure 10. Compressive strength for both RHA and RAP inclusive concrete.

- Tensile Splitting Strength (TSS)

The 28-days TSS of the mixtures containing RHA is represented in Figure 11a. There was a gradual increment in TSS with increasing the RHA content up to 15%. The TSS peaked at 15% RHA and then decreased beyond 15% RHA. However, still 20% RHA inclusive concrete showed better strength than the control mix. The increment in strength was 2.8, 6.1, 7.5, and 5.6% at 5, 10, 15, and 20% RHA content respectively, relative to the control mix. TSS increased in a second-order polynomial with RHA content as depicted in Figure 11a (R^2 = 0.96 and SEE = 0.018). The trend for TSS was similar to that of CS. The increment in TSS might be ascribed to the development extra of C-S-H gel due to the active silica content of RHA.

TSS decreased linearly with increasing the RAP content as can be seen in Figure 11b (R^2 = 0.98 and SEE = 0.052). TSS decreased by 12.2, 20.7, 29.6, 34.7, and 40.8% for 10, 20, 30, 40, and 50% RAP respectively. The decrement pattern for TSS was similar to that of the CS. However, the rate of strength reduction in the TSS mixtures was lower compared to the CS's. This is consistent with previous study [26].

(**a**) RHA concrete   (**b**) RAP concrete
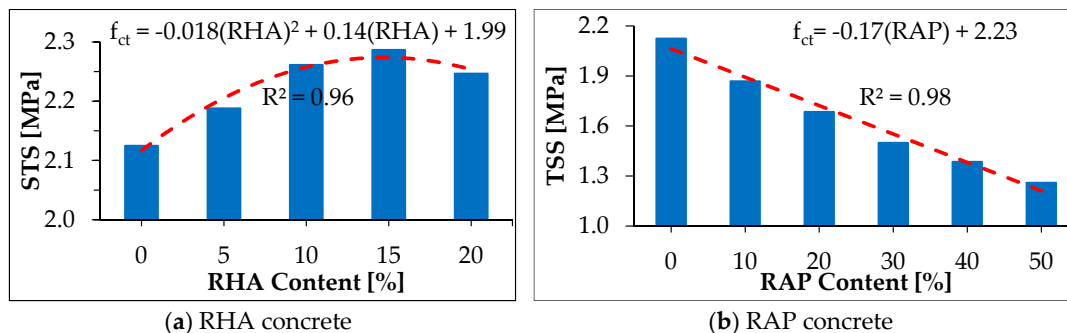
Figure 11. Splitting strength for RHA and RAP concrete.

From regression analysis, a power form relationship was found between the 28 days TSS and CS of RHA inclusive concrete as shown in Equation (4) and Figure 12a (R^2 =0.99 and SEE= 0.004).

$$f_{ct} = 0.28 \times f_c^{0.6} \tag{4}$$

where: f_c and f_{ct} are the 28-days CS and TSS of the RHA inclusive concrete respectively, in MPa.

The exponential form relationship was found between the 28 days TSS and CS of RAP inclusive concrete as presented in Figure 12b (R^2 = 0.97 and SEE = 0.0526). Equations (5) and (6) were obtained by regression.

$$f_{ct} = -0.17 \times RAP + 2.23 \tag{5}$$

$$f_{ct} = 0.105 \times f_c^{0.93} \tag{6}$$

where: f_c and f_{ct} are the 28-days CS and TSS of the RAP inclusive concrete respectively, in MPa.

(**a**) RHA concrete   (**b**) RAP concrete
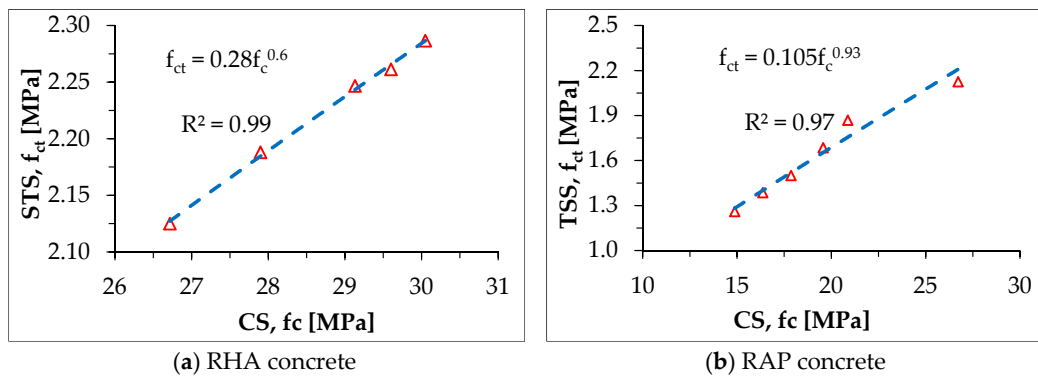
Figure 12. Relationship between CS and TSS for RHA and RAP concrete.

The experimental results of TSS of both RHA and RAP inclusive PCC and its relationship with CS are depicted in Figures 13 and 14 respectively. TSS was improved by 4.7% at 15% RHA and 10% RAP content compared to the control specimen's result which was similar to the CS results. TSS and CS were positively correlated ($R^2 = 0.928$ and SEE = 0.065) with a power function as shown in Equation (7).

$$f_{ct} = 0.235 \times f_c^{0.68} \tag{7}$$
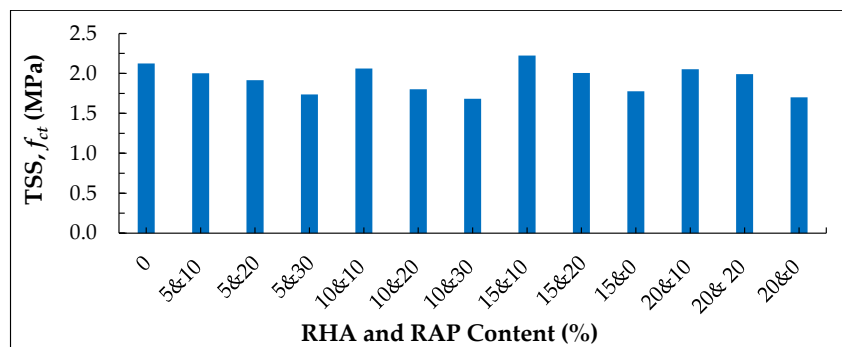
Figure 13. Tensile splitting strength for RHA and RAP inclusive concrete.
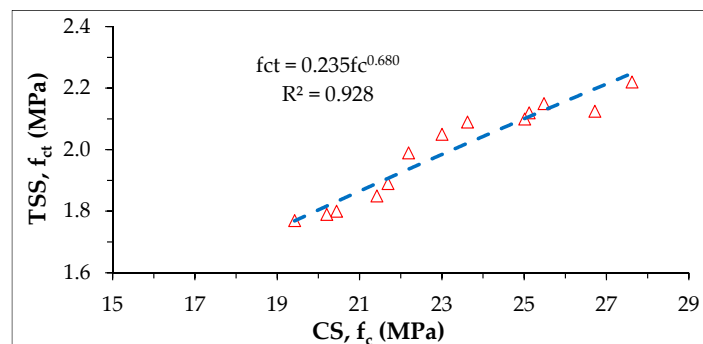
Figure 14. Relationship between TSS and CS for RHA and RAP inclusive concrete.

- Water Absorption

    The water absorption after immersion (w_i) and after immersion and boiling ($w_{i\&b}$) decreased with increasing RHA content as shown in Figure 15a. The minimum relative percentage of reduction in water absorptions were 0.7 and 1.2% for w_i and $w_{i\&b}$ respectively at 5% RHA content, whereas the maximum relative percentage of reduction in water absorption were 1.3, and 2.0% for w_i, and $w_{i\&b}$ respectively at 20% RHA content. This reduction could be due to the fact that the finer HHA particles might have filled the pore spaces of the concrete. The water absorption is correlated to RHA content in a power function as shown in Equations (8) and (9). The $w_{i\&b}$ values are slightly higher than those of w_i.

    The water absorption of RAP inclusive concrete decreased with increasing RAP content, as can be seen from Figure 15b. The minimum w_i and $w_{i\&b}$ were 6.4, and 6.9%, with relative percentage reduction of 10.94 and 6.20% respectively at 50% RAP content. The reductions in water absorption might be due to the lower water absorption of RAP aggregates compared to that of virgin aggregate. The other possible reason might be due to the melted asphalt and dust layer engulfed around the aggregate could fill void spaces in the concrete [62]. The water absorption is related to RAP content in a power function as shown in Equations (10) and (11). The $w_{i\&b}$ values were somewhat higher than those of w_i.
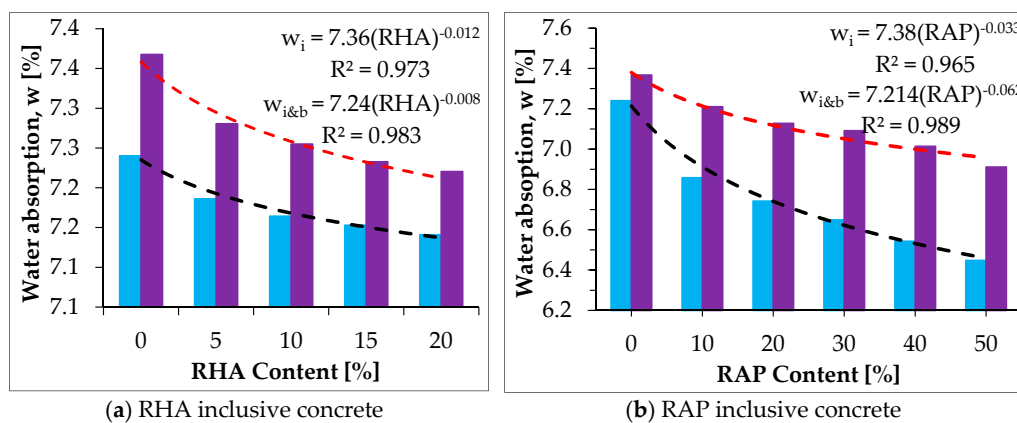
Figure 15. Water absorption by RHA and RAP concrete.

$$w_i = 7.36 \times \mathrm{RHA}^{-0.012} \tag{8}$$

$$w_{i\&b} = 7.24 \times \mathrm{RHA}^{-0.008} \tag{9}$$

$$w_i = 7.38 \times \mathrm{RAP}^{-0.033} \tag{10}$$

$$w_{i\&b} = 7.214 \times \mathrm{RAP}^{-0.062} \tag{11}$$

where: w_i is the water absorption after immersion in %; $w_{i\&b}$ is the water absorption after immersion and boiling; RHA and is the rice husk ash content in %; and RAP is reclaimed asphalt pavement content in %.

    The water absorption of RHA and RAP inclusive concrete at 28 days are depicted in Figure 16. Both w_i and $w_{i\&b}$ decreased as RHA and RAP content increased. The relative percentage reduction of $w_{i\&b}$ (13.7%) was lower than both that of RHA inclusive concrete (1.30%) and RAP inclusive concrete (10.94%). The least w_i, and $w_{i\&b}$ found were 6.25, and 7.06% respectively at 20% RHA and 30% RAP combination. The maximum relative percentage of reduction in absorption were 13.7 and 4.2% for the respective least absorptions. The reduction of water absorption might be due to the collective effect of RHA and RAP discussed above.
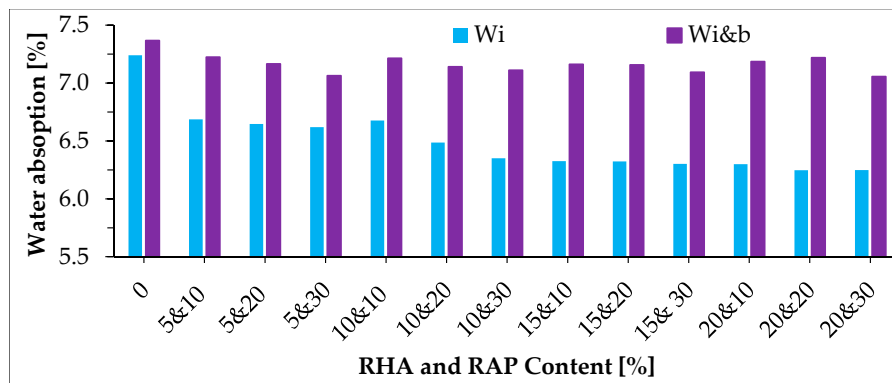
Figure 16. Water absorption by both RHA- and RAP-inclusive concrete.

- Volume of Permeable Void Spaces in Hardened Concrete

The volume of permeable void spaces in hardened RHA inclusive concrete decreased slightly with increment of RHA. The voids decreased by 3.22% from 17.32 to 16.77% as the RHA content increased from 0 to 20%. The reduction in void space might be attributed to the finer siliceous particles which could fill a portion of void spaces that exist in the concrete matrix. As can be seen from Figure 17a and Equation (12), a power function was found as a good fit (R^2 = 0.970 and SEE = 0.026) to correlate RHA content with the voids.

Figure 17b depicts the volume of permeable void spaces in RAP inclusive concrete. It is clear from the figure that voids decreased exponentially with an increment of RAP content. The voids decreased by 9.47% from 17.32 to 15.68% as the RAP content increased from 0 to 50%. The reduction in void space could be due to the lower water absorption of RAP aggregates compared to that of virgin aggregates and oozed out asphalt film which could fill a portion of voids spaces in concrete. As can be seen from Equation (13), an exponential function was obtained from regression analysis to correlate RAP content with the voids (R^2 = 0.995 and SEE = 0.024).

(**a**) RHA inclusive concrete

(**b**) RAP inclusive concrete
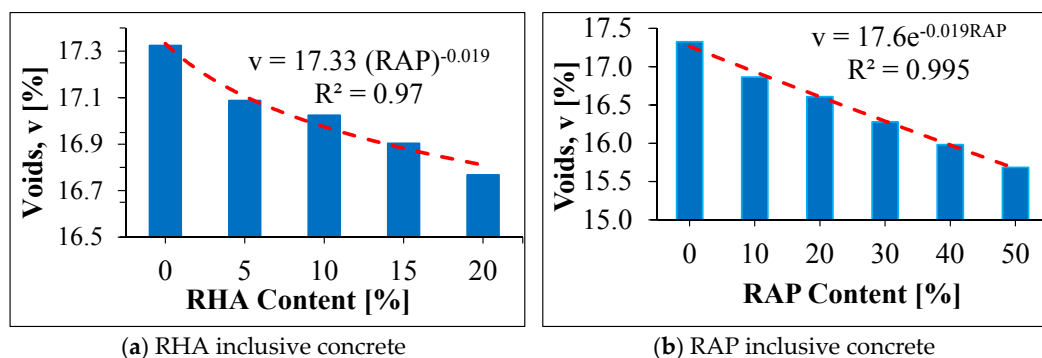
Figure 17. Voids in RHA and RAP concrete.

$$v = 17.33 \times \text{RHA}^{-0.019} \tag{12}$$

$$v = 17.36 \times e^{-0.019 \times \text{RAP}} \tag{13}$$

where: v is the volume of permeable void spaces in %; and RHA is the rice husk ash content in %; and RAP is the reclaimed asphalt pavement content in %.

A relationship between voids and water absorption for RHA concrete was determined as shown in Figure 18a and Equations (14) and (15). According to the correlation found, water absorption

decreased exponentially as the void in concrete decreased. Water absorption by RAP concrete decreased exponentially with voids in concrete as shown in Figure 18b, and Equations (16) and (17).
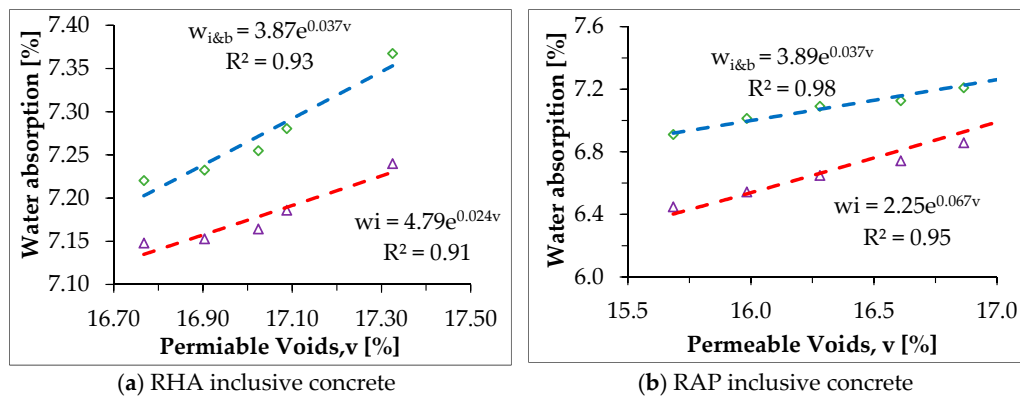

(a) RHA inclusive concrete

(b) RAP inclusive concrete

Figure 18. Relationship between water absorption and voids for RHA and RAP concrete.

$$w_i = 4.79 \times e^{0.024 \times v} \tag{14}$$

$$w_{i\&b} = 3.87 \times e^{0.027 \times v} \tag{15}$$

$$w_i = 2.25 \times e^{0.067 \times v} \tag{16}$$

$$w_{i\&b} = 3.89 \times e^{0.037 \times v} \tag{17}$$

where: w_i is absorption after immersion in %; $w_{i\&b}$ is absorption after immersion and boiling; and v is the volume of permeable void spaces in %.

The volume of permeable void spaces in both RHA and RAP inclusive PCC is portrayed in Figure 19. As expected, the relative percentage of reduction of voids (4.86%) in both RHA and RAP inclusive PCC is higher than that of RHA inclusive PCC (3.22%) but lower than that of RAP inclusive PCC (9.47) by 1.64 and 4.61% respectively.
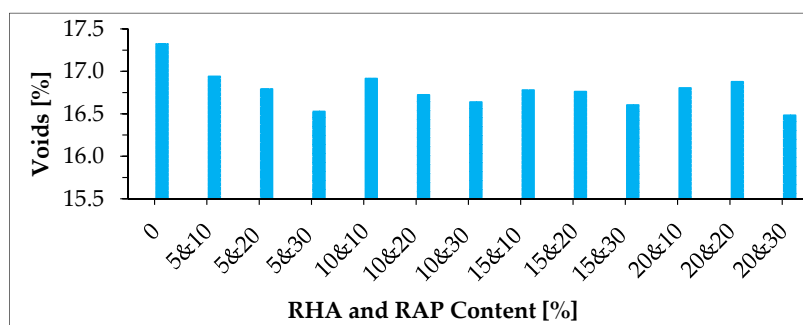
Figure 19. Void spaces in both RHA- and RAP-inclusive concrete.

- Sorptivity

The sorptivity by RHA concrete, shown in Table 10, was obtained from the slope of the line that is the best fit to the cumulative amount of water absorption (I) plotted against the square root of time ($t^{1/2}$), depicted in Figures A1 and A2 shows the cumulative amount of water absorption from which the sorptivity of RAP inclusive concrete was determined and tabulated in Table 11.
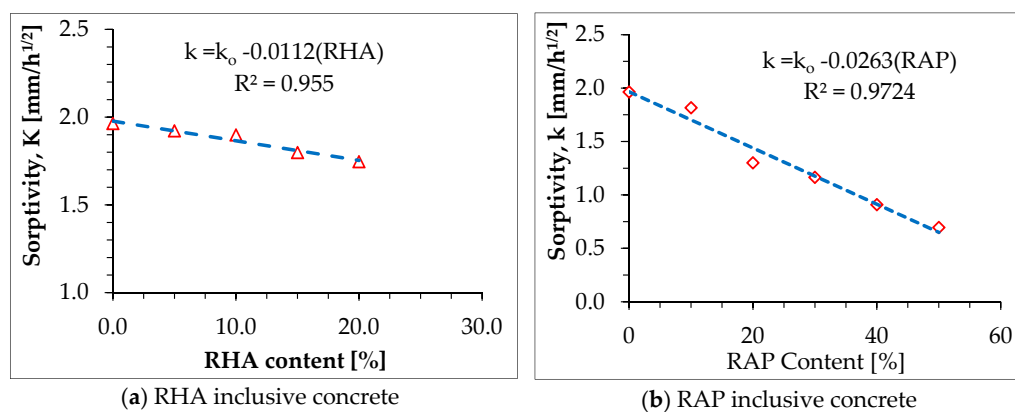
Table 10. Sorptivity by RHA inclusive concrete.

RHA Content (%)	(0)	(5)	(10)	(15)	(20)
Sorptivity, K (mm/h$^{1/2}$)	1.964	1.922	1.899	1.799	1.746
Determination Coefficient (R^2)	0.969	0.976	0.974	0.982	0.977
Correlation Coefficient (R)	0.984	0.988	0.987	0.991	0.988

Table 11. Sorptivity by RAP inclusive concrete.

RAP Content (%)	(0)	(10)	(20)	(30)	(40)	(50)
Sorptivity (mm/h$^{1/2}$)	1.964	1.816	1.301	1.164	0.908	0.694
Determination Coefficient (R^2)	0.969	0.971	0.989	0.983	0.985	0.993
Correlation Coefficient (R)	0.984	0.985	0.994	0.992	0.993	0.997

The effect of RHA content on the sorptivity of concrete is depicted in Figure 20a. As can be seen from Equation (18), the sorptivity decreased linearly as the RHA content increased. The sorptivity decreased by 11.1% from 1.964 to 1.746 mm/h$^{1/2}$ when RHA content increased from 0 to 20%. The reduction in sorptivity might be due to the fact that finer RHA particles filled up air voids exist in the concrete matrix, as a result of which the rate of ingress of water was inhibited. The influence of RAP content on the sorptivity of concrete is also portrayed in Figure 20b. Sorptivity decreased significantly as the content of RAP increased. A linear relationship was found between RAP content and sorptivity, and Equation (19) represents the same. Similar findings were reported in the previous studies [13,27]. The main reason being given for the reduction in sorptivity was the melted asphalt layer surrounding the RAP aggregates. In addition, the authors of this paper believed that the reduction in sorptivity might also be ascribed to the lower water absorption by the RAP aggregates compared to that of the virgin aggregates.

(**a**) RHA inclusive concrete   (**b**) RAP inclusive concrete

Figure 20. Relationship between sorptivity and RHA, and RAP contents.

$$k = k_o - 0.0112 \times \text{RHA} \tag{18}$$

where: k and k_o are the sorptivity by RHA inclusive concrete and concrete without RHA respectively in mm/h$^{1/2}$; and RHA is the rice husk ash content in %.

$$k = k_o - 0.0236 \times \text{RAP} \tag{19}$$

where: k and k_o are the sorptivity by RAP inclusive concrete and concrete without RAP, respectively, in mm/h$^{1/2}$; and RAP is the reclaimed asphalt pavement content, in %.

Figures A3–A6 depict the cumulative amount of water absorption (I) plotted against the square root of time ($t^{1/2}$), from which the sorptivity by both RHA and RAP inclusive concrete was determined and tabulated in Table 12.

Table 12. Sorptivity by both RHA- and RAP-inclusive concrete.

RHA and RAP Content	Sorptivity (mm/h$^{1/2}$)	Determination Coefficient (R^2)	Correlation Coefficient (R)
Control	1.964	0.9688	0.984
5% RHA + 10% RAP	1.883	0.971	0.985
5% RHA+ 20% RAP	1.808	0.975	0.987
5% RHA+ 30% RAP	1.688	0.978	0.989
10% RHA+ 10% RAP	1.801	0.972	0.986
10% RHA+ 20% RAP	1.653	0.98	0.990
10% RHA+ 30% RAP	1.411	0.986	0.993
15% RHA+ 10% RAP	1.867	0.977	0.988
15% RHA+ 20% RAP	1.610	0.983	0.991
15% RHA+ 30% RAP	1.474	0.973	0.986
20% RHA+ 10% RAP	1.919	0.983	0.991
20% RHA+ 20% RAP	1.891	0.988	0.994
20% RHA+ 30% RAP	1.646	0.982	0.991

It is evident from experimental results that the sorptivity by RHA and RAP inclusive concrete was decreased as expected. The reduction in sorptivity ranged from 2.29 to 28.16% relative to the control specimens. The reduction in sorptivity could be due to the combined influences of RHA and RAP as already discussed.

Although sorptivity value alone does not suffice to envisage the service life of a structure [63], according to the research conducted by Hinczak, Conroy, and Lewis, cited in the study [64], a concrete is said to be durable if sorptivity is less than 6 mm/h$^{1/2}$. The experimental results of this study revealed that all concrete specimens had sorptivity values under the limit specified i.e., considered as durable concrete holding other factors constant.

4. Conclusions

The effects of RHA and RAP on the engineering properties of concrete were studied. Based on the experimental results obtained and the analysis and discussion made, the following conclusions can be drawn:

1. The water demand of the mix increased as the RHA and RAP content increased; as a result, the slump and compaction factor of the fresh concrete decreased significantly.
2. The density of concrete decreased with increasing RHA and RAP content in the concrete mix.
3. RHA-inclusive concrete exhibited an increase in both compressive and tensile splitting strength. The maximum possible strength was obtained when cement was replaced by 15% RHA.
4. Compressive and tensile splitting strength decreased drastically as the RAP content increased beyond 20%.
5. Comparable strength and favorable sorptivity values were obtained when 15% RHA was combined with up to 20% RAP in the concrete mix.
6. Specimens containing both RHA and RAP exhibited lower water absorption, permeable void space and sorptivity values compared to that of the control specimens. This indicates that RHA and RAP inclusive concrete might perform better when subjected to aggressive environment.

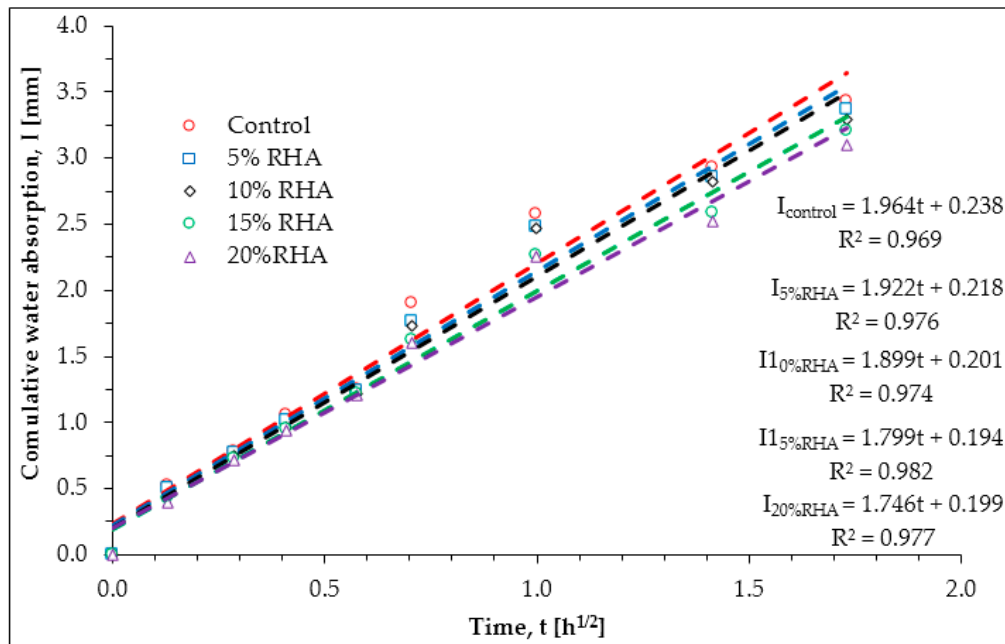## Appendix Cumulative Water Absorption

Figure A1. Cumulative water absorption by RHA Concrete.
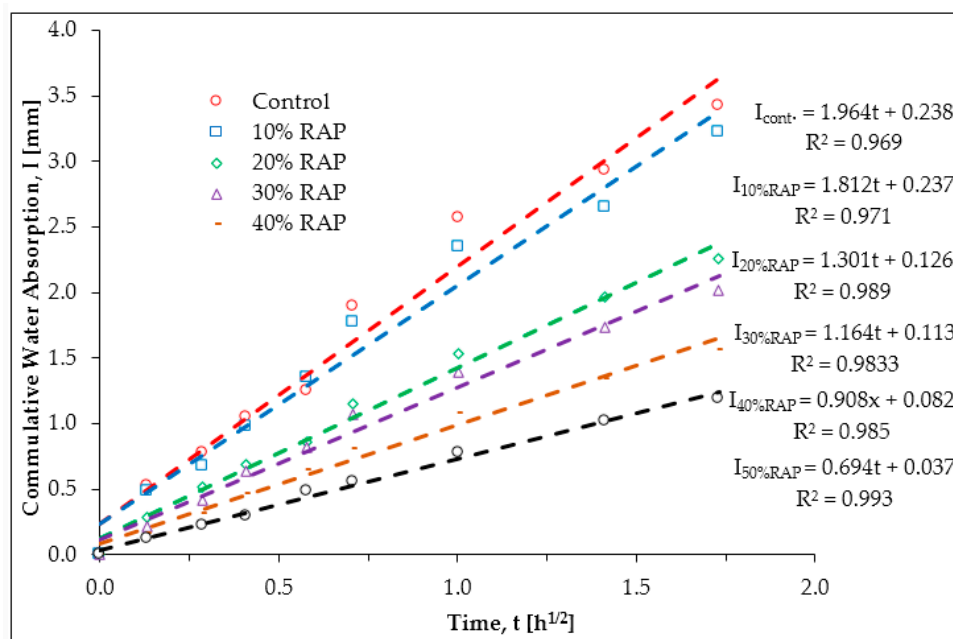

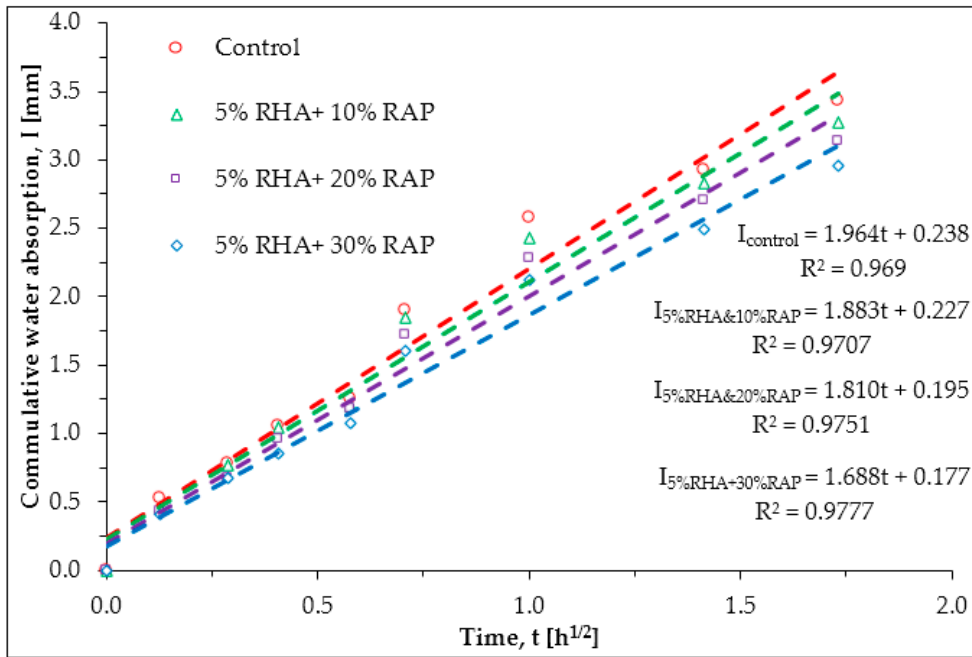**Figure A2.** Cumulative water absorption by RAP Concrete.

Figure A3. Cumulative water absorption by 5% RHA and (10–30) % RAP-inclusive concrete.
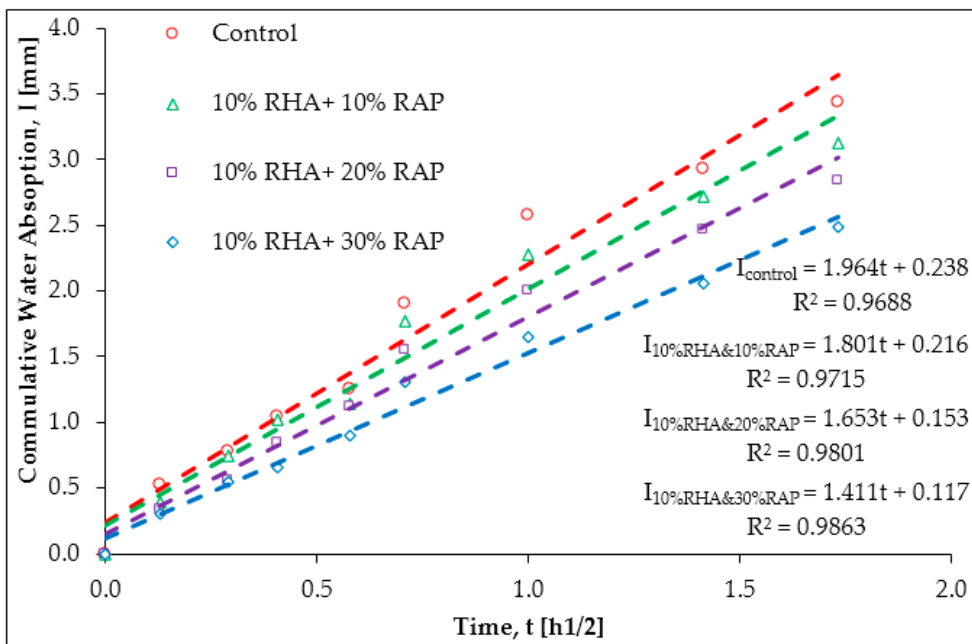

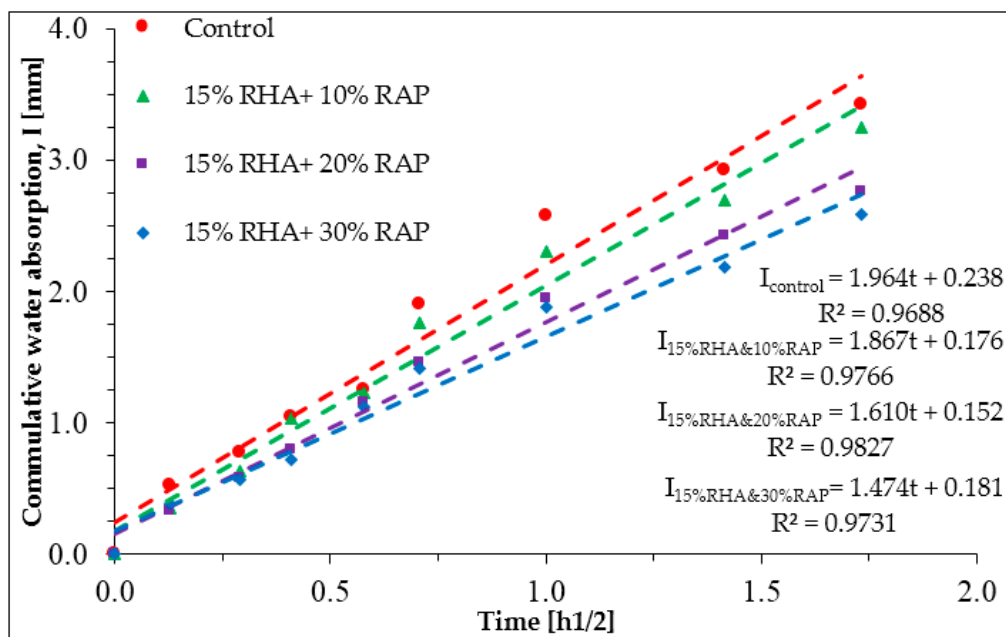**Figure A4.** Cumulative water absorption by 10% RHA and (10–30) % RAP-inclusive concrete.

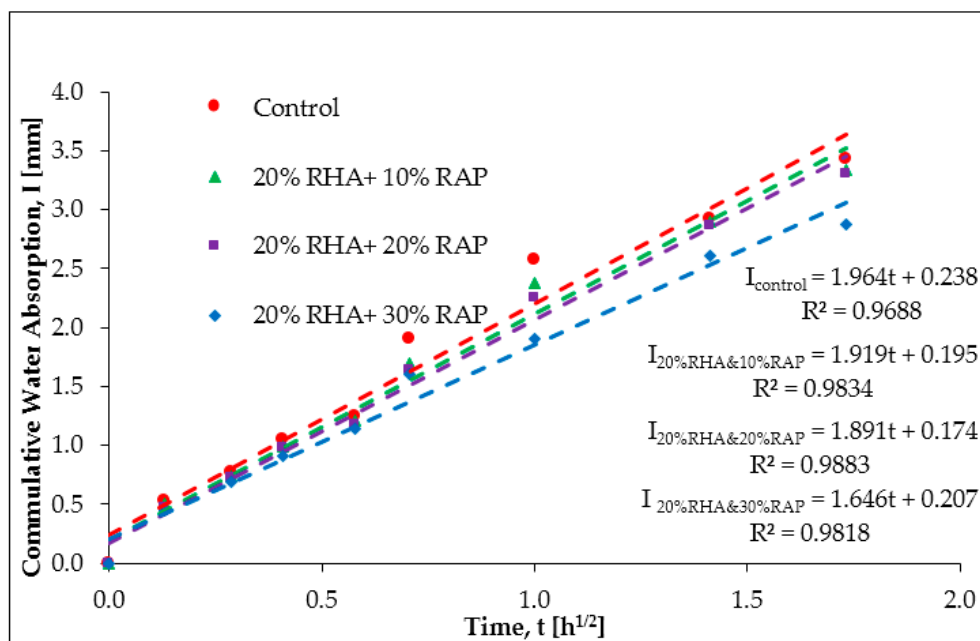**Figure A5.** Cumulative water absorption by 15% RHA and (10–30) % RAP-inclusive concrete.

Figure A6. Cumulative water absorption by 20% RHA and (10–30) % RAP-inclusive concrete.

References

1. World Economic Forum. *Shaping the Future of Construction: A Breakthrough in Mindset and Technology*; World Economic Forum: Cologny, Switzerland, 2016.
2. Meyer, C. The greening of the concrete industry. *Cem. Concr. Compos.* **2009**, *31*, 601–605. [CrossRef]
3. Kosmatka, A.W. *Design and Control of Concrete Mixtures*, 5th ed.; Portland Cement Association: New York, NY, USA, 2011.
4. Suhendro, B. Toward green concrete for better sustainable environment. *Procedia Eng.* **2014**, *95*, 305–320. [CrossRef]

5. Benhelal, E.; Zahedi, G.; Shamsaei, E.; Bahadori, A. Global strategies and potentials to curb CO_2 emissions in cement industry. *J. Clean. Prod.* **2013**, *51*, 142–161. [CrossRef]

6. Khan, R.; Jabbar, A.; Ahmad, I.; Khan, W.; Naeem, A.; Mirza, J. Reduction in environmental problems using rice-husk ash in concrete. *Constr. Build. Mater.* **2012**, *30*, 360–365. [CrossRef]

7. Pin, K.; Behnood, A.; Ash, F. Effects of deicers on the performance of concrete pavements containing air-cooled blast furnace slag and supplementary cementitious materials. *Cem. Concr. Compos.* **2018**, *90*, 27–41.

8. Adom-Asamoah, M. *Comparative Study of the Physical Properties of Palm Kernel Shell Concrete and Normal Concrete in Ghana*; University of Johannesburg: Johannesburg, South Africa, 2013.

9. Lun, L.T. *Effects of Rice Husk Ash Produced from Different Temperatures on the Performance of Concrete*; Faculty of Engineering and Green Technology Universiti Tunku Abdul Rahman: Petaling Jaya, Malaysia, 2015.

10. Ismail, S.; Wai, K.; Ramli, M. Sustainable aggregates: The potential and challenge for natural resources conservation. *Procedia Soc. Behav. Sci.* **2013**, *101*, 100–109. [CrossRef]

11. Aprianti, E.; Shafigh, P.; Bahri, S.; Nodeh, J. Supplementary cementitious materials origin from agricultural wastes—A review. *Constr. Build. Mater.* **2015**, *74*, 176–187. [CrossRef]

12. Alex, J.; Dhanalakshmi, J.; Ambedkar, B. Experimental investigation on rice husk ash as cement replacement on concrete production. *Constr. Build. Mater.* **2016**, *127*, 353–362. [CrossRef]

13. Bida, S.M.; Danraka, M.N.; Ma'ali, J.M. Performance of Reclaimed Asphalt Pavement (RAP) as a Replacement of Fine Aggregate in Concrete. *Int. J. Sci. Res.* **2016**, *5*, 2015–2017.

14. Singh, S.; Ransinchung, G.D.R.N.; Debbarma, S.; Kumar, P. Utilization of reclaimed asphalt pavement aggregates containing waste from Sugarcane Mill for production of concrete mixes. *J. Clean. Prod.* **2018**, *174*, 42–52. [CrossRef]

15. Behnood, A.; Modiri, M.; Gozali, F.; Ameri, M. Effects of copper slag and recycled concrete aggregate on the properties of CIR mixes with bitumen emulsion, rice husk ash, Portland cement and fly ash. *Constr. Build. Mater.* **2015**, *96*, 172–180. [CrossRef]

16. Food and Agriculture Organization. *FAO Rice Market Monitor*; FAO: Rome, Italy, 2017.

17. Tuaum, W.O.A.; Shitote, S. Incorporating Recycled Glass Aggregate. *Buildings* **2018**, unpublished.

18. Szilagyi, F.H.; Dico, C. Concrete production with recycled materials in the sustainable development context. *J. Environ. Res. Prot.* **2016**, *13*, 19–25.

19. American Society of Civil Engineers. *Sustainable Construction Materials*; American Society of Civil Engineers: Reston, VA, USA, 2012.

20. Modarres, A.; Hosseini, Z. Mechanical properties of roller compacted concrete containing rice husk ash with original and recycled asphalt pavement material. *J. Mater. Des.* **2014**, *64*, 227–236. [CrossRef]

21. Johari, M.A.M.; Brooks, J.J.; Kabir, S.; Rivard, P. Influence of supplementary cementitious materials on engineering properties of high strength concrete. *Constr. Build. Mater.* **2011**, *25*, 2639–2648. [CrossRef]

22. Elahi, A.; Basheer, P.A.M.; Nanukuttan, S.V.; Khan, Q.U.Z. Mechanical and durability properties of high performance concretes containing supplementary cementitious materials. *Constr. Build. Mater.* **2010**, *24*, 292–299. [CrossRef]

23. Snellings, R.; Salze, A.; Scrivener, K.L. Cement and Concrete Research Use of X-ray diffraction to quantify amorphous supplementary cementitious materials in anhydrous and hydrated blended cements. *Cem. Concr. Res.* **2014**, *64*, 89–98. [CrossRef]

24. Lothenbach, B.; Scrivener, K.; Hooton, R.D. Cement and Concrete Research Supplementary cementitious materials. *Cem. Concr. Res.* **2011**, *41*, 1244–1256. [CrossRef]

25. Shi, X.; Mukhopadhyay, A.; Liu, K.W. Mix design formulation and evaluation of portland cement concrete paving mixtures containing reclaimed asphalt pavement. *Constr. Build. Mater.* **2017**, *152*, 756–768. [CrossRef]

26. Huang, B.; Shu, X.; Li, G. Laboratory investigation of portland cement concrete containing recycled asphalt pavements. *Cem. Concr. Res.* **2013**, *35*, 2008–2013. [CrossRef]

27. Ibrahim, A.; Mahmoud, E.; Khodair, Y.; Patibandla, V.C. Fresh, Mechanical, and Durability Characteristics of Self-Consolidating Concrete Incorporating Recycled Asphalt Pavements. *J. Mater. Civ. Eng.* **2014**, *26*, 668–676. [CrossRef]

28. Abraham, S.M.; Ransinchung, G.D.R.N. Strength and permeation characteristics of cement mortar with Reclaimed Asphalt Pavement Aggregates. *Constr. Build. Mater.* **2018**, *167*, 700–706. [CrossRef]

29. Brand, A.S.; Roesler, J.R. Bonding in cementitious materials with asphalt-coated particles: Part I—The interfacial transition zone. *Constr. Build. Mater.* **2017**, *130*, 171–181. [CrossRef]

30. Brand, A.S.; Roesler, J.R. Bonding in cementitious materials with asphalt-coated particles: Part II—Cement-asphalt chemical interactions. *Constr. Build. Mater.* **2017**, *130*, 182–192. [CrossRef]

31. Berry, M.; Stephens, J.; Bermel, B.; Hagel, A.; Schroeder, D. *Feasibility of Reclaimed Asphalt Pavement as Aggregate in Portland Cement Concrete*; Montana Department of Transportation: Helena, MT, USA, 2013.

32. Chao-lung, H.; le Anh-tuan, B.; Chun-tsun, C. Effect of rice husk ash on the strength and durability characteristics of concrete. *Constr. Build. Mater.* **2011**, *25*, 3768–3772. [CrossRef]

33. *ASTM C595. Standard Specification for Blended Hydraulic Cements 14*; ASTM International: West Conshohocken, PA, USA, 2003.

34. Mamlouk, M.S.; Zaniewski, J.P. *Materials for Civil and Construction Engineers*, 3rd ed.; Pearson Education Ltd.: Hoboken, NJ, USA, 2011.

35. Jamil, M.; Kaish, A.B.M.A.; Raman, S.N.; Zain, M.F.M. Pozzolanic contribution of rice husk ash in cementitious system. *Constr. Build. Mater.* **2013**, *47*, 588–593. [CrossRef]

36. *BS EN 932-1. Tests for General Properties of Aggregates: Part 1. Methods for Sampling*; Concrete Society: Farmington Hills, MI, USA, 1997.

37. *BS EN 933-1. Tests for Geometrical Properties of Aggregates Part 1: Determination of Particle Size Distribution—Sieving Method*; Concrete Society: Farmington Hills, MI, USA, 2012.

38. *BS ISO 3310-2. Test Sieves—Technical Requirements and Testing Part 2: Test Sieves of Perforated Metal Plate*; ISO: Geneva, Switzerland, 2013.

39. *BS EN 1097-6. Tests for Mechanical and Physical Properties of Aggregates Part 6: Determination of Particle Density and Water Absorption*; BSI Standards Ltd.: Brussels, Belgium, 2013.

40. *ASTM C29/C29M. Standard Test Method for Bulk Density ("Unit Weight") and Voids in Aggregate*; ASTM International: West Conshohocken, PA, USA, 2003.

41. *IS 2386: Part IV. Methods of Test for Aggregates for Concrete: Part IV Mechanical Properties*; Concrete Society: Farmington Hills, MI, USA, 2002.

42. *BS EN 206. Concrete Specification, Performance, Production and Conformity*; British Standards Institution: London, UK, 2014.

43. *BS 8500-2. Concrete Complementary British Standard to BS EN 206: Constituent Materials and Concrete*; BSI Standards Ltd.: London, UK, 2012.

44. *BS 1881-125. Testing Concrete—Part 125: Methods for Mixing and Sampling Fresh Concrete*; British Standards Institution: London, UK, 2013.

45. *BS EN 196-2. Method of Testing Cement, Part 2: Chemical Analysis of Cement*; BSI Standards Ltd.: London, UK, 2013.

46. *ASTM C188. Standard Test Method for Density of Hydraulic Cement*; ASTM International: West Conshohocken, PA, USA, 2016; Volume I, pp. 1–3.

47. *BS EN 12350-1. Testing fresh concrete, Part 1: Sampling Fresh Concrete*; BSI Standards Ltd.: London, UK, 2009.

48. *BS EN 12350-2. Testing Fresh Concrete, Part 2: Slump Test*; BSI Standards Ltd.: London, UK, 2009.

49. *BS 1881-103. Testing Concrete, Part 103: Method for Determination of Compacting Factor*; BSI Standards Ltd.: London, UK, 1993.

50. *BS EN 12350-6. Testing Fresh Concrete, Part 6: Fresh Density*; BSI Standards Ltd.: London, UK, 2009.

51. *BS EN 12390-1. Concrete—Complementary British Standard to BS EN 206-1—Guidance for the Specifier*; BSI Standards Ltd.: London, UK, 2012.

52. *BS EN 12390-2. Testing Hardened Concrete, Part 2: Making and Curing Specimens for Strength Tests*; BSI Standards Ltd.: London, UK, 2009.

53. *BS EN 12390-3. Testing Hardened Concrete, Part3: Compressive Strength of Test Specimens*; BSI Standards Ltd.: London, UK, 2009.

54. *BS EN 12390-6. Testing Hardened Concrete, Part 6: Tensile Splitting Strength of Test Specimens*; BSI Standards Ltd.: London, UK, 2009.

55. *BS EN 12390-4. Testing Hardened Concrete, Part 4: Specification for Compressive Strength Testing Machines*; BSI Standards Ltd.: London, UK, 2000.

56. *ASTM C642. Standard Test Method for Density, Absorption, and Voids in Hardened Concrete*; ASTM International: West Conshohocken, PA, USA, 2013.

57. *ASTM C1585. Standard Test Method for Measurement of Rate of Absorption of Water by Hydraulic Cement Concretes*; ASTM International: West Conshohocken, PA, USA, 2013.

58. *BS 882. Specification for Aggregates from Natural Sources For Concrete*; BSI Standards Ltd.: London, UK, 1992.

59. *IS 383. Specification for Coarse and Fine Aggregates from Natural Sources for Concrete*; BSI Standards Ltd.: London, UK, 2002.

60. *BS EN 450-1. Fly Ash for Concrete, Part 1: Definition, Specifications and Conformity Criteria*; BSI Standards Ltd.: London, UK, 2012.

61. El, S.; Ben, E.; El, S.; Khay, E.; Achour, T.; Loulizi, A. Modelling of the adhesion between reclaimed asphalt pavement aggregates and hydrated cement paste. *Constr. Build. Mater.* **2017**, *152*, 839–846.

62. Singh, S.; Ransinchung, G.D.; Kumar, P. An economical processing technique to improve RAP inclusive concrete properties. *Constr. Build. Mater.* **2017**, *148*, 734–747. [CrossRef]

63. Martys, N.S.; Ferraris, C.E. Pii sooos-8846(97)00052-5 capillary transport in mortars and concrete. *Cem. Concr. Res.* **1997**, *27*, 747–760. [CrossRef]

64. Menéndez, G.; Irassar, V.L.B.E.F. Hormigones con cementos compuestos ternarios. Parte II: Mecanismos de transporte Ternary blend cements concrete. Part II: Transport mechanism. *Constr. Build. Mater.* **2007**, *57*, 31–43.